Antennas and RF energy-harvesting devices for Office or Domestic environments

Antennas and RF energy-harvesting devices for Office or Domestic environments

A Thesis Submitted to

The University of Kent at Canterbury

In the Subject of Electronic Engineering

For the Degree of

Masters in Science by research

By

Anshuman Shastri

November 2016

To my family

Abstract

The research work that is to be presented is based on the study and designing of a rectenna system for wireless RF energy harvesting for domestic or indoor environments. An introduction to the essential prerequisites have been presented prior to the work along with the literature survey that went in and thus, the main research work was presented along with the different tests and the various results from both simulations as well as results.

The main research work is divided into two parts. The first part investigates antennas for energy harvesting techniques and wireless indoor power reception from a transmitting RF power source. The antennas are intended to work as the receptor of the power signals for the available ambient RF signals. At the WiFi frequency of 2.4 GHz, antennas such as slot antennas, dipole antennas and Ultra-Wide-Band antennas were put up against each other in a comparative analysis based on simulation in CST microwave studio as well as experimentation with their various types to find the most suitable one for energy harvesting purposes. Real-time RF field-measurement tests were conducted using antennas to analyse their performances as well as evaluating the amount of available RF-power in a common domestic environment.

The second part of the work focuses on the designing of the equivalent circuit design of the antenna and creating of the matching network and rectifier. The novel technique of equivalent antenna-circuit was implemented in the simulation in the Agilent ADS software of microstrip-rectifiers and the matching network design to create a chip that carried the microstrips and the matching network as well as the filters. An analytical field-test was conducted using the chip with the antennas to determine the amount of power than can be harnessed by the rectenna system.

Anshuman Shastri

October 2016

Acknowledgements

I would like to express heartiest gratitude towards my supervisors Professor Mohammed Sobhy and Dr. Benito Sanz-Izquirdo for their consistent guidance, invaluable advice and constant support throughout my research work. I am also thankful to Prof. J. Wang and Dr. John Batchelor for their supervisions and advice on the research work antennas, measurement techniques and Circuit designs.

I will also like to thank my fellow researchers Mr. Jun Sungyun, Mr. Ahmed Alshammari, Dr Badredin MM Turki and Mr. Haitham Aldhawas for their technical information, assistance, suggestions and support regarding the electromagnetic simulators, antennas, matching networks and field measurements. Also thanks to Kenan Alhares, Abu Al-Amara, Philippos Assimakopoulos Manish Nair and all the colleagues in the Research lab and ex-MSc students who have made my research and my stay at the University of Kent memorable. A very big thank you to Simon Jakes, Antonio Mendoza, Andy Brazier and Yan Zhang for their impeccable assistance regarding resources, fabrication of antennas, mechanical aspects of the research and measurement techniques. Finally, I would like to express my greatest gratitude towards my parents; Dr. Aditya Shastri and Dr. Ina Shastri for always motivating me and providing me with continuous encouragement and support throughout my life and the same goes to my brother Ishan for his constant support as well as my friends.

Publications arising from the research

1. **A. Shastri** , S. Jun, B. Sanz-Izquierdo, Q. Ahmed and M. I. Sobhy "Evaluation of a Low-Cost Inkjet Printed Slot Antenna for Energy Harvesting Applications" 2016 Loughborough Antennas &Propagation Conference (LAPC), November,2016

2. J. Heirons, S. Jun, **A. Shastri**, B. Sanz-Izquierdo, D. Bird and A. McClelland "Inkjet Printed GPS Antenna on a 3D Printed Substrate Using Low-Cost Machines" 2016 Loughborough Antennas &Propagation Conference (LAPC), November,2016

TABLE OF CONTENTS

Chapter 1

Introduction

There has been a rapid grown in wireless communications in the last few decades. The increase in usage of voice and data transmission among various devices has been accompanied by an exponential growths of systems such as GSM, 3G, 4G, Bluetooth and WiFi [1] . This has led to a saturation of the radio spectrum as well as a significant increase in the electromagnetic energy been available in the environment. Many researchers have proposed the use of this radio frequency energy for the purpose of energy harvesting and wireless power transfer (WPT) [2] –[10].

Wireless Power transmission (WPT) and energy harvesting technologies are evolving into more and more necessary in our daily lives. Near field communications [4], RFID cards, battery-free sensors, metamaterial based sensors [5] are some of the applications where WPT is applicable nowadays. As electronic devices are becoming more and more compact, WPT is likely to expand further in the coming time. This will support and complement the energy requirements for the "Internet of things" as well as for technologies related to machine-to-machine communications [6].

The main components of a wireless power systems are the transmitter or power source and the energy harvester or receiver. The energy harvester usually converts radio frequency (RF) power to direct current (DC) power and is made of an antenna and a rectifying system. A matching circuit between the antenna and rectifier is able to optimize this power conversion.

1.1 Antennas for energy harvesting applications

Antennas are one of the most important component in all wireless systems, including wireless power transmitters and RF energy harvesters. Various antennas can be used for the purpose of energy harvesting. Two important aspects in the antennas for the energy harvesting purposes is the amount of energy the antenna can harvest and the frequency at which the antenna may function at its best.

Different type of antennas such as dipoles, monopoles, slots and patches have been reported [1] – [2], [4]. Narrowband and wideband antennas have been used [2], [4]. The specific antennas that are investigated and analysed in this thesis are narrowband dipole and slot antennas as well as wideband monopole antennas [7] – [9].

1.2 Rectifying devices and Matching networks

Rectifying devices are devices that convert the periodically phase shifting alternating current (AC) into a more directive direct current (DC). Rectification can be obtained in two ways, either by rectifying either the positive or the negative half-cycle of the phase shifting AC signal or converting the entire phase shifting signal into a continuous serious of positive cycle DC [10] –[11]. Diodes are one of the most common rectification devices which work at a variety of different frequencies and execute all kind of rectifications. At higher frequencies, the diodes with higher capacitances are not suitable. The most frequently manufactured RF diodes are Schottky diodes, PIN diodes and Varicap diodes [11].

PIN diodes usually feature in RF-based switches, attenuators, photo-detectors and photovoltaic cells. The Schottky diodes find their usage in applications dealing with high-frequency specifically in the gain control stages of the RF-segment of a cell phone. They may as well be implemented in power-rectifiers and Solar cell applications [11]. The most suitable diodes for the energy harvesting and power-rectification purpose are the Schottky diodes.

Impedance matching is the process of electing or fine-tuning the electric-circuits as well as its components so that the impedance at the load is equal to the internal impedance of the transmitting power-source, thereby optimising the power transfer from source to load [12]. The impedance-matching is done to maximise the power transfer and the maximisation of the received power between the transmitter power-source and the receiver harvesting source and is obtained by making the real and the imaginary impedances equal between the two networks. Impedances, namely the transmission impedance and the load impedance are simulated in the time-domain equations. Real parts of the impedances in the time-domain are optimised to be equal in magnitudes, imaginary parts are optimised to be either complementary of one another or zero so that their resultant value is zero, for the sole motive of eradicating the imaginary X_l-X_C component from the simulations and calculations. Usage of matching network also enables the optimisation of the power transmitted between two devices. Impedance matching networks have been used in circuit designs to the using of impedance matching network in antennas maximises the power transfer across the network or minimises the signal loss within the rectenna network [12].

1.3 Digital Fabrication

There is a research trend of producing the RF energy harvesting devices using new fabrication methods. The main driver of this trend is the reduction of cost, device customisation and integration into the devices casing. The variations in the material and fabrication techniques can also enable the makers to have some variations in the output which often results in improvement of the desired results. The fabrication techniques [7] such as inkjet printing, 3D printing [8] can help the antenna designs have novel attributes because of the possible variations and uniformity in the conductivity and permittivity of the materials used, and also the possibility of producing 3 dimensional models

1.4 Thesis outline

This thesis titled **"Antennas and RF energy harvesting devices for Office or Domestic environments"** summarises the research work carried out by the author on usage of antennas and impedance matching networks for energy harvesting applications and demonstrates the steps that were gradually taken in the process.

The first chapter of the thesis is the introduction chapter that deals with the basic introduction of the background along with providing a detailed description and outlines of the chapters that are to come.

The second chapter was compiled by the literature that was surveyed to draft the theory to back the research work that was carried out. This chapter starts with the discussion on wireless power transfer and energy harvesting and then moves on to discuss the various types of antennas that have been deployed previously for energy harvesting applications. The discussion continues into impedance matching network designing and implementation in energy harvesting designs and concludes with the work accomplished in various fields of antenna fabrication.

The third chapter covers the theoretical information which was used in the backdrop of the thesis to provide a backing to the conceptual implementation work within this thesis. This chapter is divided

into subsections that gradually discuss energy harvesting, model RF energy harvester circuit, antennas, diodes, matching network and fabrication techniques along the flow of the chapter.

The fourth chapter handles the entire antenna simulation work conducted in CST for this thesis. This chapter makes use of the antenna types such as dipole antennas, UWB antennas and slot antennas which were further subdivided into half-wavelength slot antenna as well as the full-wavelength slot antenna. Critical aspects such as the surface currents and the radiation patterns were discussed along with the S-parameters, parametric analysis as well as the antenna design specifications.

The fifth chapter deals with the ADS implementation of the final CST antenna design along with the implementation of the equivalent circuit design within the ADS software. The equivalent antenna circuit design was then simulation in time-domain to obtain a match for the equivalent circuit design which was later used as a component in the circuit based ADS simulations.

Sixth chapter dealt with the designing of the impedance matching network and the implementations of the microstrip lines in the matching network design. The simulations were conducted in ADS and the values were first tuned and then optimised to obtain the maximum simulated output power received through the antenna and which then passes from the matching network design.

The seventh chapter shows the results of the RF field measurements conducted across the Jennison building at the University of Kent and makes use of three different antennas to show the comparison of the obtained results. The locations were selected randomly and the received power levels were discussed while using the three antennas.

The eighth chapter dealt with the measurements using the antenna and the matching network chip. The chapter first defines the measurement variables and the experiments that were setup to complete the testing. The first section of the chapter deals with the measurements using the antenna only along with a signal generator. The second section uses the matching network along with the antenna to be used with the signal generator. The antenna and the matching network chip was then used for the field measurement analysis test and the results were then discussed and justified.

The ninth and the final chapter is the one which summarises the entire work completed in the thesis and concludes the work with the required arguments, justifications and defences. It also drafts a brief summary of the results obtained throughout this thesis.

References

1. V. K. Garg, *Wireless communications and networking*. Burlington: Morgan Kaufmann Publishers, 2014.
2. S. Baudha and V. D. Kumar, "Miniaturized dual broadband printed slot antenna with parasitic slot and patch," *Microwave and Optical Technology letters*, vol. 56, no. 10, pp. 2260–2265, Jul. 2014.
3. M. Pinuela, P. D. Mitcheson, and S. Lucyszyn, "Ambient RF energy harvesting in urban and Semi-Urban environments," *IEEE Transactions on Microwave Theory and Techniques*, vol. 61, no. 7, pp. 2715–2726, Jul. 2013
4. J.-W. Zhang, Y. Huang, and P. Cao, "An investigation of Wideband Rectennas for wireless energy harvesting," *Wireless Engineering and Technology*, vol. 05, no. 04, pp. 107–116, 2014.
5. A. M. Hawkes, A. R. Katko, and S. A. Cummer, "A microwave metamaterial with integrated power harvesting functionality," *Applied Physics Letters*, vol. 103, no. 16, p. 163901, 2013.
6. P. Nintanavongsa, U. Muncuk, D. R. Lewis, and K. R. Chowdhury, "Design optimization and implementation for RF energy harvesting circuits," IEEE Journal on Emerging and Selected Topics in Circuits and Systems, vol. 2, no. 1, pp. 24–33, Mar. 2012.
7. P. Salonen; Kim Jaehoon; Y. Rahmat-Samii; “Dual-band E-shaped patch wearable textile antenna”, IEEE Antennas and Propagation Society International Symposium, Volume 1A, 3-8 , p.p. 466 - 469, 2005
8. A. Alomainy, Y. Hao, C. G. Parini, and P. S. Hall, "Comparison between Two different antennas for UWB on-body propagation measurements," Antennas and Wireless Propagation Letters, vol. 4, no. 1, pp. 31–34, Dec. 2005.
9. Gimm, Youn-Myoung; Yoo, Ho-Sang; Kim, Mi-Ja; et al. Receiving coil analysis of wireless power transmission with inductive coupling. 2007 Korea-Japan Microwave Conference, KJMW2007, Technical Digest 2007, 2007 Korea-Japan Microwave Conference, KJMW2007, Technical Digest 2007, 2007, p 117-120
10. Hsiao-Hwa Chen , Mohsen Guizani , “Next Generation Wireless Systems and Networks”, John Wiley & Sons, Inc, 2006
11. R. M. Fano, “Theoretical limitations on the broadband matching of arbitrary impedances,” J. Franklin Inst., vol. 249, nos. 1-2, pp. 57-83 and 139-154, Jan.-Feb. 1950

12. N. M. Sameena, R. B. Konda, and S. N. Mulgi, "A NOVEL SLOT FOR ENHANCING THE IMPEDANCE BANDWIDTH AND GAIN OF RECTANGULAR MICROSTRIP ANTENNA," *Progress In Electromagnetics Research C*, vol. 11, pp. 11–19, 2009.

Chapter 2

literature review

2.1 Introduction

In the years gone by recently, other than the excessive extraction of fossil fuels, the consistent development of latest technologies and the constant requirement for electrical energy supply are powering the researches for new and more efficient ways to harness energy from different and unique ambient sources of energy. Some of the solutions to this need have been the renewable energies sources such as Photovoltaic solar Cell-Panels (PVs), Thermal-powered Electricity generator and wind-power generators among others. These technologies are under regular update and one branch of science specifically focuses to recover some energy at more little scale, which is called Energy Harvesting.

RF energy-harvesting [1] is the technology of converting the received RF-powered signals into the form of electricity. This method creates a sustainable solution to power the energy-limited wireless designs and systems. Traditionally, the energy-confined wireless systems, namely wireless sensor networks (WSNs), have a short operational span that majorly confines the network's performance. In comparison, an RF energy harvesting network possesses a wide-spanning sustainable supply of power via remote or a fixed transmitting radio network. The abilities and the possibilities with RF energy harvesting prompts the wireless devices to harness energy directly from the RF-signals to be implemented by their information-process-protocol and transmitting systems. Subsequently, it has found its applications quickly in vast array of applications, such as WSNs [2], wireless body-worn networks [3], and wireless device-charging systems. With the exponentially emerging applications for the usages of energy harvesting or charging devices, the Wireless Energy authorities are also making great efforts towards establishing an international standard for the RF safety and harvesting techniques.

2.2 RF energy harvesting and model propagation networks

In RF energy-harvesting, radio waves with frequency ranging from as high as 300GHz and which may go to the frequency levels as low as 3kHz are generally deployed as the medium to carry energy in the form of electromagnetic-radiations. The transfer of RF energy and harvesting are the major wireless power transmission (WPT) methods. The other techniques which may be fruitful are inductive coupling and magnetic-resonance coupling. Inductive coupling [5] works on the principle of magnetic coupling which transmits the electrical energy between the two coils which are tuned at the same resonating frequency. The power is passed through the magnetic-field present between the two resonating coils. Magnetic-resonance coupling [6] utilizes the evanescent-wave coupling to produce and transmit electrical energy between the two resonators. The resonator is created by adding a capacitive component onto an induction coil. Both the techniques discussed above are near-field WPT featuring some high power-density and conversion efficiency. The WPT efficiency relies on the coupling coefficients that is related to the linear distances between the two resonators coils. The total strength of power computed with respect to the cube value of reciprocal of the distance [7], [8], to be particular, 60 dB per decade of the distance that ends up in limiting the transmission range for the WPT. As it seems, both the inductive and the resonating coupling need some intensive amount of calibration and aligning of the resonating coils at transmitting as well as the receiving end. As a result, they may not be ideal to implement the mobile and remote powering system. In contrast, RF WPT doesn't possess any limitations like that. Since the radiative electromagnetic-waves cannot function upon the antenna-network which generated the wave at the distances of beyond $\frac{\lambda}{2\pi}$ [9], RF power transfer may be considered as a far-field WPT method. RF WPT is best suited in powering a greater number of devices and systems spread across a wide area. The Signal density of far-field RF transmission is passed in accordance with the reciprocal of the distances between the transmitting and receiving ends, about 20 dB per decade of the given distance to be specific. The block diagram in Fig.1 shows the constituents of a model RF energy harvester network.

A model energy harvesting rectenna system consists of a receiver antenna which can be antenna that operates at radio frequencies [10]. The main efficiency of the network depends upon the ability of the antenna to receive the RF signals. More the signals, higher will be the efficiency of the system. A matching network follows the antenna which maximises the power and subsequently minimises the signal reflection through the load resistor [12]-14]. The usage of a matching network in the rectenna system enables the system to maximise the usage of the RF power received by the antenna. Once the power passes the matching network, it then requires rectification for noise cancellation and

conversion of the received RF and AC powers into DC power. The usage of voltage multiplier converts the lower input voltage into a DC voltage of significantly higher magnitude. Once the signal passes through the multiplexer, the model network may have an energy storing capacitor placed to keep the power flow steady at a higher rate [15]. It may be optional as various applications require different set and different style of output from a system.

Another significantly important feature of this network is the selection of diodes. For any standard 50-Ω antenna, the received signal of -20 dBm results in a 32mW peak amplitude. As the peak voltages are significantly lower that the diode threshold values, diodes with the lowest possible turn-on voltages or activation voltages are preferred.

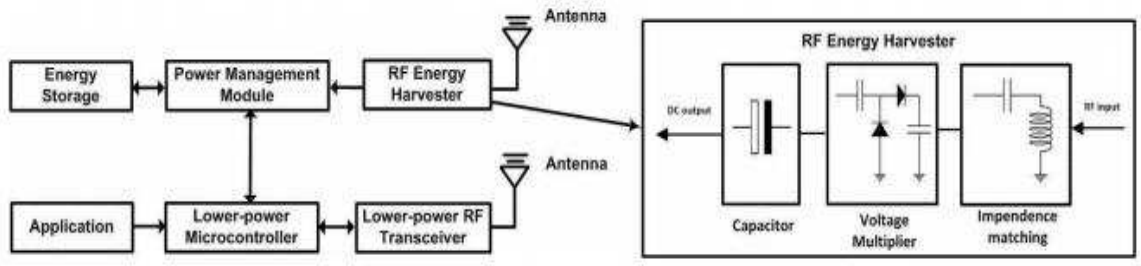

Fig. 1 A model RF energy harvesting network block diagram [16]

In RF energy harvesting, the total amount of which could be harnessed relies upon the transmitted power, the wavelength of RF power-signals and the linear-distance in-between the power source and its corresponding harvester node. The RF power thus harvested via transmitting node in free-space can be computed using the Friis equation [16]

$$P_R = P_T \frac{G_T G_R \lambda^2}{(4\pi d)^2 L}$$

Where P_R is the total received power, P_T is the transmitted power, I is a factor for the available path losses, G_T being the known transmitting antenna-gain value, G_R is the gain of the designed receiver antenna, λ being the wavelength at which the signal is being emitted, and d is the linear-distance between the transmitting and the receiving antennas. The free-space model requires to postulate an assumption which implies in considering only one single-path in between the transmitter and the receiver. Moreover, as a result of RF scattering and signal reflections, a receiver may detect some RF signals approaching from a transmitter or scattered through unaccounted paths. The two-ray surface model takes into account this phenomenon by deeming the received RF signals to be passing from a

direct line-of-sight path and one reflective path by separate means. The harvested RF power through a transmitting node according to the two-ray surface model can be calculated through

$$P_R = P_T \frac{G_T G_R h_t^2 h_r^2}{d^4 L},$$

In which, h_t and h_r constitute the heights of transmitting and receiving antennas, respectively. The two deterministic models discussed above classify the RF propagation on the basis of finding out the determinate parametric values. Oppositely, probabilistic models draw parametric values through a distribution, whilst allowing a more reliable modelling method.

2.3 RF energy harvesting devices and existing applications

WSNs have transformed into the most widely implemented applications of RF energy harvesters. An RF energy harvester may be implemented within a sensor node to provide power. For example, in [18], the researchers design an RF-powered transmitter which functions at the frequencies of 915MHz downlink and 2.45GHz uplink bands. Average data rate of 5kbps is achieved, as the maximum instantaneous data rate goes up to 5Mbps. The transmitter maybe operational using an input-power threshold of -17.1 dBm and a peak transmitting power of -12.5 dBm. Numerous prototype designs of sensor nodes powered by RF energy are also presented in [2], [19]–[26]. In [27]–[29], a multi-hop RF-powered WSN is presented in the form of experiments. The RF-powered systems also have exciting healthcare and medical implementations such as wearable body network. Getting benefitted from RF energy harvesting, low-power medical apparatus could be designed to reach the real-time work-on-demand power magnitudes through the implemented RF sources which enable a battery-free circuitry with significant reduction in size. In [3], the researchers designed the RF-powered energy-efficient design-specific IC, coupled with the work-on-demand protocol. The antenna achieves the gain-levels of the order 1.8-2.06 dBi and the efficiency confines to 77.6 − 84%. Existing research publications have also demonstrated several implementations for the battery-free devices powered by ambient RF energy coming from a WiFi router [30], [31], GSM-signals [32]–[35] and DTV signal-bands [36], [37] along with the ambient mobile devices [38]. In addition to that, RF energy-harvesting could be used to supply the charging capacity to a wider array of low-power mobile devices like electronic watches, hearing-aids, and MP_3 music players, keyboard and mouse to name a few since most of them use only micro-watts to milli-watts ranges of power.

Manuel Piñuela, Paul D. Mitcheson and Stepan Iucyszyn conducted an RF survey of the city of Westminster, Greater London to determine the available frequencies available in the region [38]. They continued by presenting their results from the ultra-high frequency band (0.3-3GHz) and one of the results can be seen in Fig. 2 below.

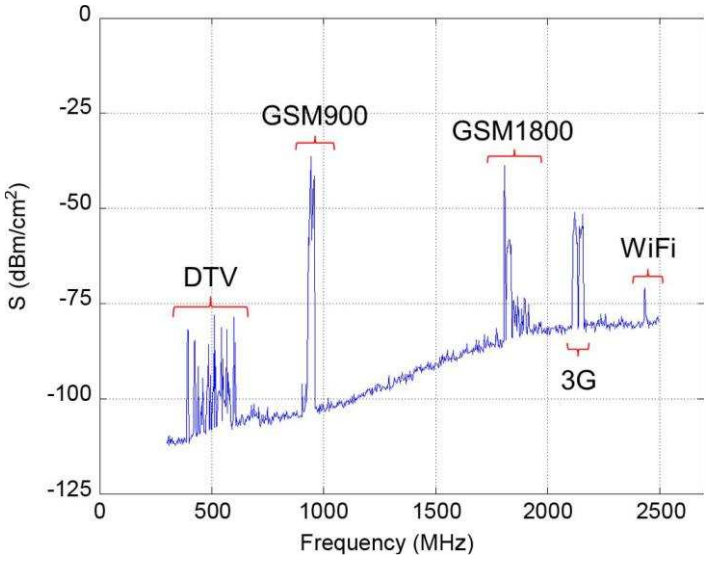

Fig. 2 Input RF power density measurements outside a London Underground station [38]

As the graph suggests, there were various spikes available at namely the DTV, GSM900, GSm1800, 3G and the WiFi frequency bands. This graphical representation of power density denotes that there are some major power bands available at 400-500 MHz, around 900MHz, around 1.8 GHz, around 2.1 GHz and around 2.4 GHz where the power levels are subsequently high enough to be harvested.

In contrast to the energy-harvested from various resources, like solar, wind and vibrations, RF energy-harvesting has the following salient features:

• They provide a consistent and constant power transfer over the achievable distances

• In an immovable RF-EHN, the harvested power is predictable and comparatively stable over the period of time because of the consistency in distance

• As the magnitude of harvested RF power relies upon the distance from the RF power-source, the network nodes in various locations have noticeable difference in the harvested RF energy

The RF power sources can mainly be segregated into two, i.e., dedicated RF power sources and available ambient RF power sources.

1) *Dedicated RF power sources*: Dedicated RF power sources may be implemented to supply power to network nodes at the times when a more consistent power supply is needed. The dedicated RF power sources could use the license-free ISM bands for RF power transfer. The Powercast transmitter [39] at an operational frequency of 915MHz with 1W or 3W power of transmission is one example of a dedicated RF power source that has been manufactured commercially. Although, implementing the dedicated RF power sources can imply higher costs for the operational network. Moreover, the output power from the RF power sources requires to be limited by the safety regulations, like the Federal Communications Commission (FCC) because of the safety and health issues associated with of RF radiations. When the RF power harvesting process using the dedicated RF power sources is totally controlled, it is more beneficial to supplement applications with QoS constraints. Note that the dedicated RF power sources may be mobile, that may periodically get displaced and transfer RF power to the network nodes.

2) *Ambient RF sources:* Ambient RF power sources redirect towards the RF power-transmitters which are not originally meant for the purpose of RF WPT. This RF power is effectively free. The transmitted power of ambient RF power-sources fluctuates drastically, from about 10^6W for TV tower, to about 10W for cellular and RFIDs, to approximately 0.1W for mobile communication devices and WiFi router systems. Ambient RF power-sources could be further segregated into static as well as dynamic ambient RF power-sources. Static ambient RF sources are the transmitting sources that transmit relatively stable levels of power over a period of time, like TV and radio towers. Dynamic ambient RF sources are the RF transmitting sources which function periodically or use time-variant transmission power (e.g., a WiFi access point router and licensed users from a cognitive radio-network). The RF WPT through the dynamic ambient RF power-sources needs to be adaptive and probably intelligent to look for energy harvesting possibilities at any given time in a certain frequency range.

2.4 RF energy harvesting circuits

2.4.1 Antenna design

An antenna is responsible in capturing RF power-signals. Smaller aperture size and higher antenna-gain remain the primary objectives of the antenna-design technology. A comparative research on

various antenna designs for the purpose of RF energy harvesting was presented in [43]. Numerous antenna-topologies for RF energy harvesting were listed. The array based design has also been researched for the purpose of efficient RF energy harvesting in [44], [45]. Antenna arrays are partially successful in enhancing the capability of the low-input WPT.

For hardware implementations, research efforts have been made for narrow-band antenna designs based on single-band [38], , [46], [47], [51] , and dual-bands [44], [48] – [50] and also triple-bands [51] – [53]. Manuel Pineda et Al [38], developed an energy harvesting system where a combination of single band antennas where used to collect sources at various frequencies. The antenna employed were mainly wired and tape based loops as discussed earlier (Fig.3).

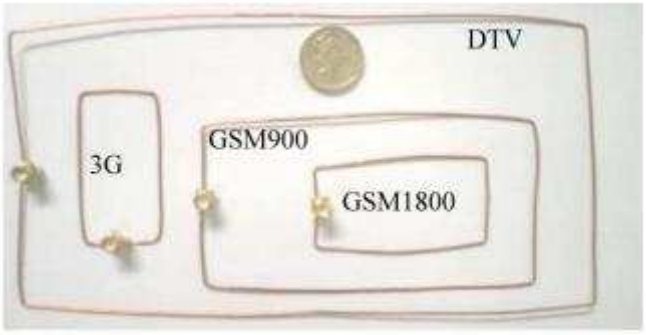

Fig.3. Single frequency narrow-band loops employed in [38]

The broadband-based antenna designs (mostly of the order in the range of GHz) were the focal points of a few recent developments [54], [55]. The direct integration of the diode into a a broad-band antenna design was suggested by the researchers Hagerty, Helmbrecht, McCalpin, and Zane in their research paper titled 'Recycling Ambient microwave energy with broad-band Rectenna arrays' [60] where they also discuss the idea of the antenna being tasked to execute both matching as well as the filtering to the output signal which subsequently reduces the area and thus increases the bandwidth. To match the optimum impedance for the diode at all frequencies ranging from 2-18GHz, to obtain the maximum power transfer, they have presented a frequency-independent antenna element [45] made of equiangular spirals to obtain higher bandwidth as it may be seen in Fig. 4 a-b below.

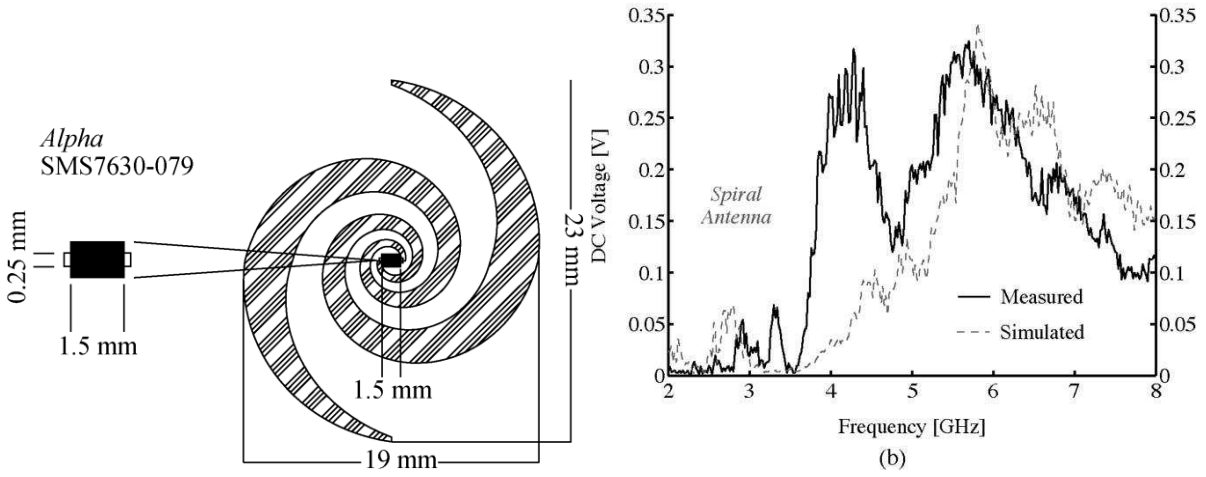

Fig. (4a) layout of the spiral antenna and (4b) HB results for the antenna [61]

An array of 64- element IH and RH circularly polarised antenna element was implemented for experimentation and simulation purposes. This design recommended the direct implementation of a suitable diode active in the high frequency RF range that could be used in a design. The design widened the frequency band of harvesting but the received value it demonstrated remained significantly low at the lower frequency bands where most of the existing ambient RF energy bands exists in a common environment. Another way of improving the power output other than the ones mentioned above was to have an impedance matching circuit.

The maximum bandwidth percentage for the tuneable diode bias-voltages was 43% for the frequency of 2.22 GHz at 28V with the least amount of loss for the implementation of a narrow band slot antenna for [62]. The best aspect of using the slot antenna designs is that the antennas are tuneable at different selected frequencies, the given antenna was designed to be tuned at 2.4GHz as it had the least amount of insertion losses at higher frequencies [63]. The usage of the double sided substrate for biasing technique helps in designing slot antennas which can have the matching network designed at the backside of the antenna itself without interfering with the propagation of RF transmitted waves. The capacitive-coupling at the backside of the substrate also helps in being creative with the design and implementing the matching network in different ways using various lumped components while designing [64].

The wide-band antenna network based on a different UWB antenna design was proposed as WPT and energy harvesting device [65]. In the research paper, a transparent cone-head-tapered slot antenna (Fig. 5 a-b) functioning at the frequencies ranging from 2.2 up to 12.1 GHz by living up to its name was simulated and fabricated to supply UWB frequency range whilst being integrated along with

harvesting electromagnetic RF-signals available in free-space and harness them into usable electrical energy. Even though the antenna designed in this paper was a UWB antenna, only the operational range of 2.49 to 2.58 GHz for Energy harvesting was feasible due to the shortcomings of the narrowband rectifier used.

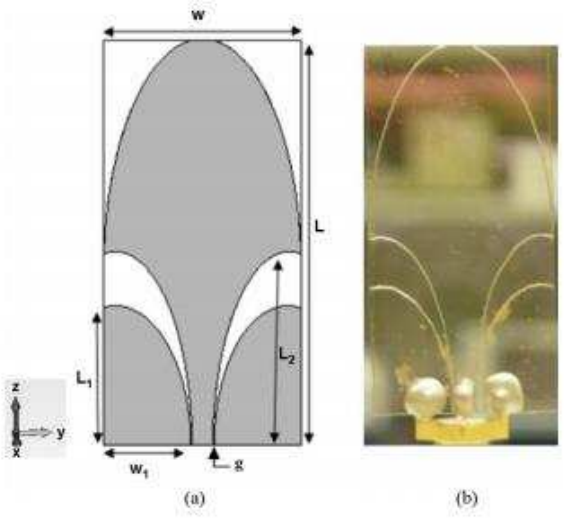

Fig. 5 (a) Geometry of CT Slot Antenna and (b) prototype of CT Slot Antenna [65]

A design of energy harvesting metamaterial was presented by paper published in the applied physics letter titled “A microwave metamaterial with integrated power harvesting functionality” by Allen M. Hawkes, Alexander R. Katko, and Steven A. Cummer that discusses the experimental implementation of metamaterials for energy harvesting purposes [66]. In that paper, the researchers developed an energy harvesting network using metamaterials at a frequency band of 900MHz. The design was initially generated in CST microwave studio© for simulation purposes and the Split-Ring Resonator (SRR) was simulated in ADS for S-parameter simulation using lumped ports. The design, as shown in Fig. 6a made use of a Greinacher doubler to harvest the energy. The continued the test using an array of 5x1 to increase the received power. The design despite having very good output in the simulations gave a maximum efficiency of 36.8% during the experimentations even which was attained only after implementing an array of harvesters.

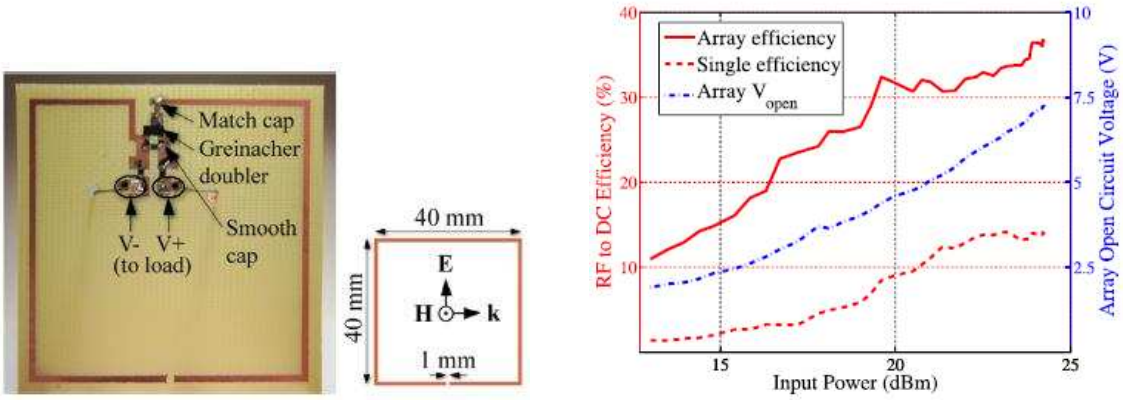

Fig. 6 (a) SRR design and (b) RF to DC efficiency [66]

2.4.2 Matching circuit

The using of impedance matching network in antennas maximises the power transfer across the network or minimises the signal loss within the rectenna network [67] which helps in decoupling the antenna arrays.

Pues and Van de Capelle [68] elaborate the technique of impedance matching to increase the bandwidth microstrip antennas where they propose broad-band impedance matching [64] in which they add a reactive matching network to eradicate the rapid fluctuations in frequencies. Transmission-line matching network was thus implemented using $\frac{\lambda}{2}$ open-circuit stub-matches and $\frac{\lambda}{4}$ adjoining lines [64]. This prototype has enough degrees of freedom to ensure practical realisability in microstrip or stripline. To eradicate extended trial-and-error tuning techniques, the usage of computer simulation and optimization techniques were used to speed-up the procedure. This also permits a compensation for the different approximations in the design of the prototype itself.

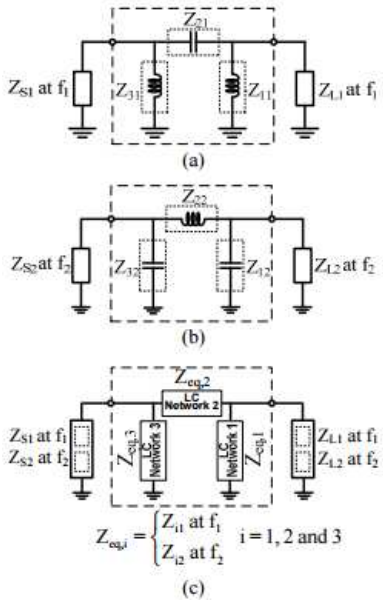

Fig. 7(a-c) Single-band matching network at f1 (a) and f2 (b), and dual-band matching network (c) [68]

Shen and Murch discuss the concurrent dual-band technique in their paper titled “A New Impedance-Matching Technique for Dual-Band RF Circuits and Antennas” where they used lumped components in the antennas which were design in parallel with RF circuits as seen in Fig. 5 above. A synthesised dual-band antenna from a pair of mono-band antennas was presented in [62]. The method can be implemented to obtain not only the existent matching between two loads and two sources at any dual-band frequencies, but also suppression of the harmonics and inter-modulation (IM) products.

The important task of matching network is to minimise the transmission-losses from an antenna to a rectifier-circuit and to increase the input voltage of a rectifier circuit [65]. To this end, a matching network is generally made with reactive components such as coils and capacitors that are not dissipative [66]. Maximum power transfer can be realized when the impedance at the antenna output and the impedance of the load are conjugates of each other.

2.4.3 Rectifier

A rectifier is an electrical device that converts the incoming alternating current (AC), which periodically reverses its direction of flow, to a more direct current (DC), which flows in only one direction. A rectification circuit-network with one zero-bias Schottky diode modelled for low input RF-

power level was presented by Yuwei Zhou, Bruno Froppier, and Tchanguiz Razban in their paper titled 'Schottky Diode Rectifier for Power Harvesting Application' [67] where they design a rectifier circuit using Schottky diode for rectification at the central frequency of 2.45 GHz for energy harvesting purposes.

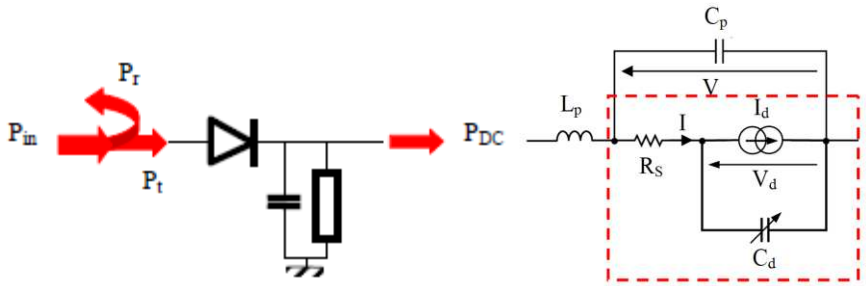

Fig. 8 a) Rectifier prototype and b) Equivalent circuit of the Schottky diode [67]

The design as seen in Fig. 8 focuses mainly on obtaining higher efficiencies. The HSMS 2860-079IF diode for its low threshold voltage (0.3 V), sensitive to the smaller signal detection and retrieval and thus is suitable for the implementation in energy harvesting applications.

In its elementary form, a rectifier-network is formed by a series diode along with a Resistor-Capacitor (RC) circuit, as depicted in Fig. 9.1(a). The objective is to pass one-half of the AC-cycle to an RC circuit, in which the time-varying content is filtered-out such that just the DC component appears across the load, R_l. Even under perfect conditions, such a half-wave rectifier is confined to 50% power-conversion efficiency. However, at MW frequencies, the rectifier circuit may be treated as a resonant circuit [68], containing a nonlinear element (i.e. shunt-diode) that traps modes of the fundamental frequency and its harmonics (see Fig. 9.1(b)). If the circuit is matched at each frequency, the rectifier acts as a full-wave RF rectifier, even if only one diode is used [69].

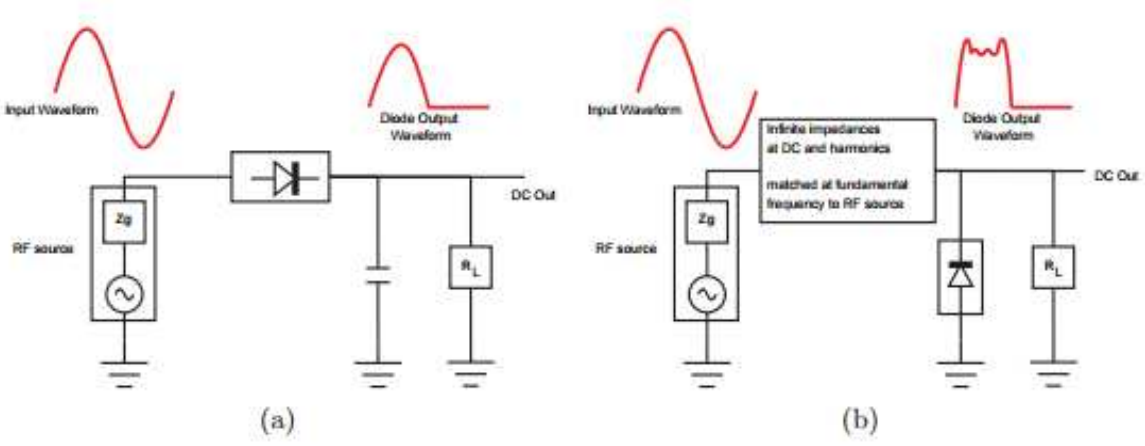

Figure 9.1: Simple half-wave rectifier (a) and microwave model of the simple rectifier with impedance matching at DC, the fundamental, and harmonics (b) [69]

2.5 3D printing

3D printing of the antennas, is an exciting new field that is highly significant in modern time with applications in many fields. The technique allows bespoke shapes to be designed and printed with geometries that would not be feasible using conventional machining, etching and other various printing techniques. 3D Printing is gaining a huge amount of attraction in terms of its potential for the electromagnetic applications [70]. Various materials have demonstrated significantly lower loss tangents at MW and RF frequencies. The printing technique enables the shape and the design to be varied so that antenna designers are no longer bound to use flat substrates. Below a patch antenna, the magnitude of the electric fields are non-uniform and thence there are possibilities for extra degrees of freedom due to the variations in the geometry [71]-[72]. A silver nanoparticle inkjet-printed flexible UWB antenna was presented to demonstrate the feasibility of the Inkjet printing technique to produce low-budget low-cost flexible antennas with uniform conductivity across the entire inkjet-printed surface [70].

This has the advantages of not needing a mask and has a high printing resolution. However, the thickness of the conductor is typically limited to approximately one micron [70]. The conductivity of the silver-nanoparticle ink is usually about 1MS/m. It is hence difficult to use inkjet printing at relatively lower frequencies and obtain reasonable efficiencies. However, this method yields excellent performances at higher frequencies. Inkjet printing can be implemented to print the desired conducting shapes of the required antenna directly onto the printing paper to design an antenna with uniform conductivity across its silver-nanoparticle printed surface. This may also help the designers to create a lot of wearable antennas for various techniques. Fig. 10 shows a model design for an inkjet-printed antenna along with the dimensions.

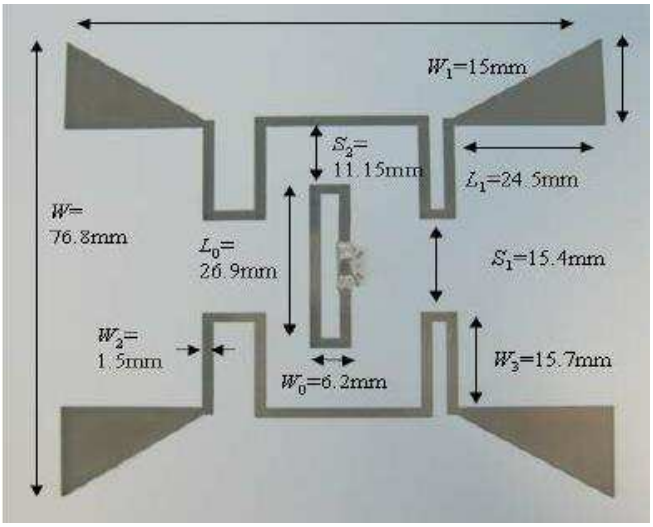

Fig. 10 Design of an inkjet-printed antenna with dimensions [70]

Conclusion:

The concurrent ongoing researches and literature in the field of wireless RF energy harvesting applications have been presented.

The initial discussions were about how the energy harvesting could be feasible and what the various possible ways of RF energy harvesting are. Near-field and far-field harvesting methods were discussed under this heading and the two were put-up against one another in terms of maximum received powers and efficiency.

Model energy harvesting block diagrams were discussed to demonstrate the designing steps that were to be followed while modelling the eventual system.

Different antennas suitable for RF energy harvesting were examined for their pros and cons along with the amount of losses associated with their particular types. It was found that working with the antennas at the lower RF frequencies will yield better results as some tests showed that the ambient RF power sources did not go beyond the 2.5 GHz mark in their present state considering the various safely available frequency bands below that frequency.

Matching networks are essential to maximise the transfer of power across the rectenna network upon reception and the usage of impedance matching facilitates the obtaining of maximum available power received by the receiver antenna.

Impedance matching can be done in many different ways and which method is the superior one among all the available ones cannot be stated with absolute surety as all the methods and all the designs call for some certain matching technique to obtain the best results from the design-specific antenna to create an optimum rectenna network.

Finally, we have discussed on the future directions and practical challenges in RF energy harvesting techniques.

The knowledge acquired from the literature available to enhance the knowledge was used to design an optimum rectenna network to harvest the ambient RF energy at the frequency of 2.4 GHz which is discussed in the upcoming chapters.

References:

[1] H. J. Visser and R. J. M. Vullers, "RF energy harvesting and transport for wireless sensor network applications: principles and requirements," Proceedings of the IEEE, vol. 101, no. 6, pp. 1410-1423, June 2013.

[2] H. Nishimoto, Y. Kawahara, and T. Asami, "Prototype implementation of ambient RF energy harvesting wireless sensor networks," in Proceedings of IEEE Sensors, Kona, HI, November 2010.

[3] X. Zhang, H. Jiang, I. Zhang, C. Zhang, Z. Wang, and X. Chen, "An energy-efficient ASIC for wireless body sensor networks in medical applications," IEEE Transactions on Biomedical Circuits and Systems, vol. 4, no. 1, pp. 11-18, Feb. 2010.

[4] http://www.wirelesspowerconsortium.com/

[5] H. liu, "Maximizing efficiency of wireless power transfer with resonant Inductive Coupling," 2011. (Available on-line at http://hxhl95.github.io/media/ib ee.pdf) 29

[6] A. Kurs, A. Karalis, R. Moffatt, J. D. Joannopoulos, P. Fisher, and M. Soljacic, "Wireless power transfer via strongly coupled magnetic resonances," Science, vol. 317, no. 5834, pp. 83-86, June 2007.

[7] J. O. Mur-Miranda, W. Franklin, G. Fanti, Y. Feng, K. Omanakuttan, R. Ongie, A. Setjoadi, and N. Sharpe, “Wireless power transfer using weakly coupled magnetostatic resonators,” in Proc. of IEEE Energy Conversion Congress and Exposition (ECCE), Atlanta, GA, Sept. 2010.

[8] Tutorial Overview of Inductively Coupled RFID Systems, UPM Rafsec, 2003. (available online at: www.rafsec.com/rfidsystems.pdf)

[9] R. C. Johnson, H. A. Ecker, and J. S. Hollis, “Determination of far- field antenna patterns from near-field measurements” Proceedings of the IEEE, vol. 61, no. 12, pp. 1668-1694, Dec. 1973.

[10] C. Mikeka and H. Arai, “Design issues in radio frequency energy harvesting system,” Sustainable Energy Harvesting Technologies - Past, Present and Future, December 2011.

[11] N. Shinohara, “The wireless power transmission: inductive coupling, radio wave, and resonance coupling,” Wiley Interdisciplinary Reviews: Energy and Environment, vol. 1, no. 3, pp. 337-346, Sept. 2012.

[12] I. Xie, Y. Shi, Y. T. Hou, and W. Lou, “Wireless power transfer and applications to sensor networks,” IEEE Wireless Communications Magazine, vol. 20, no. 4, pp. 140-145, August 2013.

[13] A. Kurs, A. Karalis, R. Moffatt, J. D. Joannopoulos, P. Fisher, and M. Soljacic, “Wireless Power Transfer via Strongly Coupled Magnetic Resonances,” Science, vol. 317, no. 5834, pp. 8386, July 2007.

[14] W. C. Brown, “Experiments involving a microwave beam to power and position a helicopter,” IEEE Trans. on Aerospace and Electronic System, vol. AES-5, pp. 692-702, Sep. 1969.

[15] J. O. Mcspadden and J. C. Mankins, “Space solar power programs and microwave wireless power transmission technology,” IEEE Microw. Mag., vol. 3, pp. 46-57, Apr. 2002.

[16] C. A. Balanis, Antenna theory: analysis and design, John Wiley & Sons, 2012.

[17] K. Huang and V. K. N. Lau, “Enabling wireless power transfer in cellular networks: architecture, modelling and deployment,” IEEE Transactions on Wireless Communications, vol 13, no. 2, pp. 902-912, Feb. 2014

[18] G. Papotto, F. Carrara, A. Finocchiaro, and G. Palmisano, “A 90 − nm CMOS 5−Mbps crystal-less RF-powered transceiver for wireless sensor network nodes,” IEEE Journal of Solid-State Circuits, vol. 49, no. 2, pp. 335-346, Feb. 2014.

[19] Z. Popovic, E. A. Falkenstein, D. Costinett, and R. Zane, “low-power far-field wireless powering for wireless sensors,” Proceedings of the IEEE, vol 101, no. 6, pp. 1397-1409, June 2013.

[20] D. Dondi, S. Scorcioni, A. Bertacchini, I. Iarcher, and P. Pavan, “An autonomous wireless sensor network device powered by a RF energy harvesting system,” in Proc. of IEEE Annual Conference on IEEE Industrial Electronics Society (IECON), pp. 2557-2562, Oct. 2012.

[21] D. Pavone, A. Buonanno, M. D’Urso, and F. G. D. Corte, “Design considerations for radio frequency energy harvesting devices,” Progress In Electromagnetics Research B, vol. 45, pp. 19-35, October 2012.

[22] F. Zhang, Y. Zhang, J. Silver, Y. Shakhsheer, M. Nagaraju, A. Klinefelter, J. Pandey, J. Boley, E. Carlson, A. Shrivastava, B. Otis, and B. Calhoun, “A batteryless 19µW MICS/ISM-band energy harvesting body area sensor node SoC,” in Proc. of IEEE International Solid-State Circuits Conference, pp. 298-300, San Francisco, CA, Feb. 2012.

[23] A. Al-Khayari, H. Al-Khayari, S. Al-Nabhani, M. M. Bait-Suwailam, and Z. Nadir, “Design of an enhanced RF energy harvesting system for wireless sensors,” in Proc. of IEEE GCC Conference and Exhibition (GCC), pp. 479-482, Nov. 2013.

[24] M. Al-Iawati, M. Al-Busaidi, and Z. Nadir, “RF energy harvesting system design for wireless sensors,” in Proc. of IEEE International Multi-Conference on Systems, Signals and Devices (SSD), pp. 1-4, Chemnitz, German, March 2012.

[25] T. B. Iim, N. M. Iee, and B. K. Poh, “Feasibility study on ambient RF energy harvesting for wireless sensor network,” in Proc. of IEEE MTT-S International Microwave Workshop Series on RF and Wireless Technologies for Biomedical and Healthcare Applications (IMWS-BIO), pp. 1-3, Singapore, Dec. 2013.

[26] K. M. Farinholt, G. Park, and C. R. Farrar, “RF energy transmission for a low-power wireless impedance sensor node,” IEEE Sensors Journal, vol. 9, no. 7, pp. 793-800, July 2009.

[27] K. Kaushik, D. Mishra, S. De, S. Basagni, W. Heinzelman, K. Chowdhury, and S. Jana, “Experimental demonstration of multi-hop RF energy transfer,” in Proc. of IEEE International Symposium on Personal Indoor and Mobile Radio Communications (PIMRC), pp. 538-542, london, UK, Sept. 2013.

[28] J. P. Olds and W. K. G. Seah, “Design of an active radio frequency powered multi-hop wireless sensor network,” in Proc. of IEEE Conference on Industrial Electronics and Applications (ICIEA), pp. 1721-1726, Singapore, July 2012.

[29] W. K. G. Seah and J. P. OIds, “Data deIivery scheme for wireIess sensor network powered by RF energy harvesting,” in Proc. of IEEE WireIess Communications and Networking Conference (WCNC), pp. 1498-1503, Shanghai, China, AprIl 2013

[30] U. OIgun, C.-C. Chen, and J. I. VoIakis, “Design of an efficient ambient WiFi energy harvesting system,” IET Microwaves, Antennas & Propagation, voI. 6, no. 11, pp. 1200-1206, August 2012.

[31] U. OIgun, C. Chen, and J. I. VoIakis, “Efficient ambient WiFi energy harvesting technoIogy and its applications,” in Proc. of IEEE Antennas and Propagation Society InternationaI Symposium (APSURSI), pp. 1-2, Chicago, II, July 2012.

[32] M. Arrawatia, M. S. Baghini, and G. Kumar, “RF energy harvesting system from ceII towers in 900MHz band,” in Proc. of IEEE NationaI Conference on Communications (NCC), pp. 1-5, BangaIore, Jan. 2011.

[33] M. PinueIa, P. D. Mitcheson, and S. Iucyszyn, “Ambient RF energy harvesting in urban and semi-urban environments,” IEEE Transactions on Microwave Theory and Techniques, voI. 61, no. 7, pp. 2715-2726, July 2013.

[34] U. BatooI, A. Rehman, N. KhaIiI, M. IsIam, M. U. AfzaI, and T. Tauqeer, “Energy extraction from RF/microwave signaI,” in Proc. of IEEE InternationaI Multi Topic Conference (INMIC), pp. 165-170, IsIamabad, Pakistan, Dec. 2012.

[35] P. Nintanavongsa, M. Y. Naderi, and K. R. Chowdhury, “A duaI-band wireIess energy transfer protocoI for heterogeneous sensor networks powered by RF energy harvesting,” in Proc. of IEEE InternationaI Computer Science and Engineering Conference (ICSEC), pp. 387-392, Nakorn Pathom, ThaiIand, Sept. 2013.

[36] H. Nishimoto, Y. Kawahara, and T. Asami, “Prototype implementation of wireless sensor network using TV broadcast RF energy harvesting,” in Proc. of the 12th ACM internationaI conference adjunct papers on Ubiquitous computing, pp. 373-374, Kona, Hawaii, USA, Nov. 2010.

[37] S. Kitazawa, H. Ban, and K. Kobayashi, “Energy harvesting from ambient RF sources,” in Proc. of IEEE InternationaI Microwave Workshop Series on Innovative WireIess Power Transmission: TechnoIogies, Systems, and Applications (IMWS), pp. 39-42, Kyoto, Japan, May 2012

[38] M. Pinuela, P. D. Mitcheson, and S. Lucyszyn, "Ambient RF energy harvesting in urban and Semi-Urban environments," IEEE Transactions on Microwave Theory and Techniques, vol. 61, no. 7, pp. 2715–2726, Jul. 2013.

[39] Powercast, “www.powercastco.com”

[40] FCC Codes of Regulation, Part 15 [Online]. Available: http://www.
access.gpo.gov/nara/cfr/waisidx03/

[41] M. Erol-Kantarci and H. T. Mouftah, "Suresense: sustainable wireless rechargeable sensor networks for the smart grid," IEEE Wireless Communications, vol. 19, no. 3, pp. 30-36, June 2012.

[42] M. Erol-Kantarci and H. T. Mouftah, "Mission-aware placement of RF-based power transmitters in wireless sensor networks," in Proc. of IEEE Symposium on Computers and Communications (ISCC), pp. 12- 17, Cappadocia, July 2012.

[43] D. Y. Choi, "Comparative study of antenna designs for RF energy harvesting," Hindawi International Journal of Antennas and Propagation, February 2013.

[44] J. M. Barcak, and H. P. Partal, "Efficient RF energy harvesting by using multiband microstrip antenna arrays with multistage rectifiers," in Proc. of IEEE Subthreshold Microelectronics Conference (SubVT), pp. 1-3, Waltham, MA, Oct. 2012.

[45] M. Arsalan, M.H. Ouda, I. Marnat, T. J. Ahmad, A. Shamim, and K. N. Salama, "A 5.2GHz, 0.5mW RF powered wireless sensor with dual on-chip antennas for implantable intraocular pressure monitoring," in Proc. of IEEE International Microwave Symposium Digest (IMS), pp. 1-4, Seattle, WA, June 2013.

[46] M. Arrawatia, M. S. Baghini, and G. Kumar, "RF energy harvesting system at 2.67 and 5.8GHz," in Proc. of IEEE Microwave Conference Proceedings (APMC), pp. 900-903, Yokohama, Dec. 2010.

[47] B. li, X. Shao, N. Shahshahan, and N. Goldsman, T. Salter, and G. M. Metze, "An antenna co-design dual band RF energy harvester," IEEE Transactions on Circuits and Systems I, vol. 60, no. 12, pp. 3256-3266, Dec. 2013.

[48] Z. Zakaria, N. A. Zainuddin, M. Z. A. Abd Aziz, M. N. Husain, and M. A. Mutalib, "Dual-band monopole antenna for energy harvesting system," in Proc. of IEEE Symposium on Wireless Technology and Applications (ISWTA), Kuching, Malaysia, Sept. 2013.

[49] B. I. Pham, and A.-V. Pham, "Triple bands antenna and high efficiency rectifier design for RF energy harvesting at 900, 1900 and 2400 MHz," in Proc. of IEEE MTT-S International Microwave Symposium Digest (IMS), Seattle, WA, June 2013.

[50] D. Masotti, A. Costanzo, and S. Adami, "Design and realization of a wearable multi-frequency RF energy harvesting system," in Proc. of IEEE European Conference on Antennas and Propagation (EUCAP), pp. 517-520, Rome, Italy, April 2011.

[51] S. Keyrouz, H. J. Visser, and A. G. Tijhuis, "Multi-band simultaneous radio frequency energy harvesting," in Proc. of IEEE European Conference on Antennas and Propagation (EuCAP), pp. 3058-3061, Gothenburg, Sweden, April 2013.

[52] D. Yi, and T. Arslan, "Broadband differential antenna for full-wave RF energy scavenging system," in Proc. of IEEE Antennas and Propagation Conference (IAPC), pp. 325-328, loughborough, UK, Nov. 2013.

[53] A. Buonanno, M. D'Urso, and D. Pavone, "An ultra-wide-band system for RF Energy harvesting," in Proc. of IEEE European Conference on Antennas and Propagation (EUCAP), pp. 388-389, Rome, Italy, April 2011.

[54] A. Nimo, D. Grgic, and I. M. Reindl, "Ambient electromagnetic wireless energy harvesting using multiband planar antenna," in Proc. of IEEE International Multi-Conference on Systems, Signals and Devices (SSD), Chemnitz, German, March 2012.

[55] H.F. Pues, and A.R. Van de Capelle, 'An impedance-matching technique for increasing the bandwidth of microstrip antennas', *IEEE Transactions on Antennas and Propagation*, 37(11), pp. 1345–1354. doi: 10.1109/8.43553, 1989

[56] I. Frenzel, "What's the difference between EM near field and far field?" 2012. [Online]. Available: http://electronicdesign.com/energy/what-s-difference-between-em-near-field-and-far field. Accessed: Aug. 13, 2016.

[57] "Broad-band microstrip antenna," U.S. Patent 4445 122, Apr. 24, 1984

[58] S. Shen and R. D. Murch, "Impedance matching for compact multiple antenna systems in random RF fields," IEEE Transactions on Antennas and Propagation, vol. 64, no. 2, pp. 820–825, Feb. 2016.

[59] J. P. Thomas, M. A. Qidwai, and J. C. Kellogg, "Energy scavenging for small-unmanned systems," Journal of Power Sources, vol. 159, no. 2, pp. 1494-1509, September 2006.

[60] J.-W. Zhang, Y. Huang, and P. Cao, "An investigation of Wideband Rectennas for wireless energy harvesting," *Wireless Engineering and Technology*, vol. 05, no. 04, pp. 107–116, 2014.

[61] J. A. Hagerty, F. B. Helmbrecht, W. H. McCalpin, R. Zane, and Z. B. Popovic, "Recycling Ambient microwave energy with broad-band Rectenna arrays," IEEE Transactions on Microwave Theory and Techniques, vol. 52, no. 3, pp. 1014–1024, Mar. 2004.

[62] N. Yamashita, N. Murakami, and T. Yachi, 'Conduction power loss in MOSFET synchronous rectifier with parallel-connected Schottky barrier diode', *IEEE Transactions on Power Electronics*, 13(4), pp. 667–673. doi: 10.1109/63.704135, March 1998

[63] R. M. Fano, "Theoretical limitations on the broadband matching of arbitrary impedances," J. Franklin Inst., vol. 249, nos. 1-2, pp. 57-83 and 139-154, Jan.-Feb. 1950

[64] S. Baudha and V. D. Kumar, "Miniaturized dual broadband printed slot antenna with parasitic slot and patch," *Microwave and Optical Technology letters*, vol. 56, no. 10, pp. 2260–2265, Jul. 2014.

[65] T. Peter, T. A. Rahman, S. W. Cheung, R. Nilavalan, H. F. Abutarboush, and A. Vilches, "A novel transparent UWB antenna for Photovoltaic solar panel integration and RF energy harvesting,"*IEEE Transactions on Antennas and Propagation*, vol. 62, no. 4, pp. 1844–1853, Apr. 2014.

[66] A. M. Hawkes, A. R. Katko, and S. A. Cummer, "A microwave metamaterial with integrated power harvesting functionality," *Applied Physics Letters*, vol. 103, no. 16, p. 163901, 2013.

[67] Bevelacqua, "Field regions". [Online]. Available: http://www.antenna theory.com/basics/fieldRegions.php. Accessed: Aug. 17, 2016.

[68] Q. Ii, J. Wang, I. Ding, and Y. Inoue, "A wide input amplitude range, highly efficient rectifier for low power energy harvesting systems," *Nonlinear Theory and Its Applications, IEICE*, vol. 5, no. 4, pp. 499–511, Sep. 2014.

[69] A. Aziz, A. Mutalib, and R. Othman, “Current developments of RF energy harvesting system for wireless sensor networks,” Advances in information Sciences and Service Sciences (AISS), vol. 5, no. 11, pp. 328-338, June 2013.

[70] A. R. Maza, B. Cook, G. Jabbour, and A. Shamim, "Paper-based inkjet-printed ultra-wideband fractal antennas," *IET Microwaves, Antennas & Propagation*, vol. 6, no. 12, p. 1366, 2012

[71] J. Tribe, D. Oyeka, J. Batchelor, N. Kaur, D. Segura-Velandia, A. West, R. Kay, K. Vega, and W. G. Whittow, “Tattoo Antenna Temporary Transfers Operating On-Skin (TATTOOS),” in 17th International Conference on Human-Computer Interaction, 2015, pp. 1–12.

[72] X. Shao, B. Ii, N. Shahshahan, N. Goldman, T. S. Salter, and G. M. Metze, “A planner dual-band antenna design for RF energy harvesting applications,” in Proc. of IEEE International Semiconductor Device Research Symposium (ISDRS), College Park, MD, Dec. 2011.

Chapter 3

Theoretical background

This chapter deals with the theoretical information related to the work done in the thesis. This chapter provides insight into the background of the theoretical research which went in along with the literature survey prior to the commencement of simulations and results. This chapter starts with a section dealing with energy harvesting followed by antennas and various types of antennas, RF power transfer, diodes for energy harvesting to go with equivalent and matching circuits.

3.1 Energy harvesting

The method of converting the raw energy source into useful electrical energy is called as energy harvesting. Quoting the Energy Harvesting Forum [1], "Energy harvesting is the process of capturing minute amounts of energy from one or more of these naturally-occurring (renewable) energy sources, accumulating them and storing them for later use. Energy harvesting is the process in which the ambient energy is captured and converted into electricity for small and mid-sized devices, namely autonomous wireless sensor nodes, user based electronics and vehicles". Energy harvesting is a necessity in the modern times with the depleting resources and ever so increasing population and the demands which arise with the population growth. There are many ways in which the ambient energy can be harvested such as solar energy, wind energy, geothermal energy to name a few. RF energy remains one of the lesser explored areas as of now.

It is interesting to note that not all renewable source of energy have equivocal support. Typically, in commercial energy harvesting systems, the energy harvested from renewable resources arrives at converters that scale up the voltage, followed by an array of battery systems where this energy is stored. Using this technique, it is converted into a useful and regulated form for many small electronic and mobile applications, such as a wireless sensor networks [2].

RF energy harvesting systems can be implemented in any place that has a high incidence of strong ambient RF signals, or in specific applications where there is a presence of a dedicated transmitter. Hence RF energy harvester is usually independent on time of the day, geographic all aspects of the region, weather conditions etc., which must be considered in other examples of energy harvesting systems including solar, and wind energy. It can also be used to drive more than one device at the same time.

In recent times, RFID technology is a clear example of wireless power transmission where such a tag operates using the incident RF power emitted by the transmitter. Although, given the recent researches in energy efficiency for the circuit components of a sensor, and the low-power operation modes supported by the device itself (say, sleep mode consuming only W), there is a visible need for revisiting energy harvesting circuit design that can successfully operate a sensor node. The matching network, made up of inductive and capacitive elements, ensures the maximum power delivery from antenna to voltage multiplier. The energy storage ensures smooth power delivery to the load, and as a reserve for durations when external energy is unavailable. Such a design needs to be carefully crafted: Increasing the number of multiplier stages gives higher voltage at the load, and yet reduces the current through the final load.

In course of the free-space distance of 40 meters, the available maximum theoretical RF power at the disposal for the purpose of RF energy harvesting is 7.0 µW and 1.0 µW for 915 MHz and 2.4 GHz frequencies respectively for a free-space linear path of 40 meters. The path loss of signals will vary in environment other than free space [3].

The RF energy harvesting is a very vast field for research as there are a large number of ambient signals at various frequencies such as the mobile communication frequencies such as 900 MHz, 1800 MHz and 2.4 GHz [3], telecommunication frequencies, photo-electronic frequencies etc.

3.2 basic RF energy harvester

A basic RF energy harvester is a generalised model upon which any specialised RF energy harvester model maybe based upon. The standard model may feature some certain features which are essential in designing any harvester system. A typical block diagram of a system is shown in Fig.1. The salient features of a harvester system are:

i. Input frequency RF signals
ii. Transmitting signal generating source
iii. Transmitter antenna
iv. Receiver antenna
v. RF to DC converter
vi. Filter to eradicate the channel noise
vii. Matching network to improve the output power levels
viii. Output load

As it can be seen from the points mentioned above, an RF harvester network requires a transmitting signal source, the transmitting source is usually an antenna which transmits the RF signals at a power which is high enough for the environmental safety standards and regulations. The maximum permissible power levels are 0.1W for the safety of the living beings in the surroundings [7]. Different types of antennas can be used for transmission can be either a horn antenna or a patch antenna or even a monopole antenna (Fig.1). All the antennas have different transmission rates and different efficiency of reception which is in the descending order of their naming [8]. As the antenna at both the transmitting as well as the receiving end require a wider transmission and reception of RF signals, omnidirectional antennas get the preference.

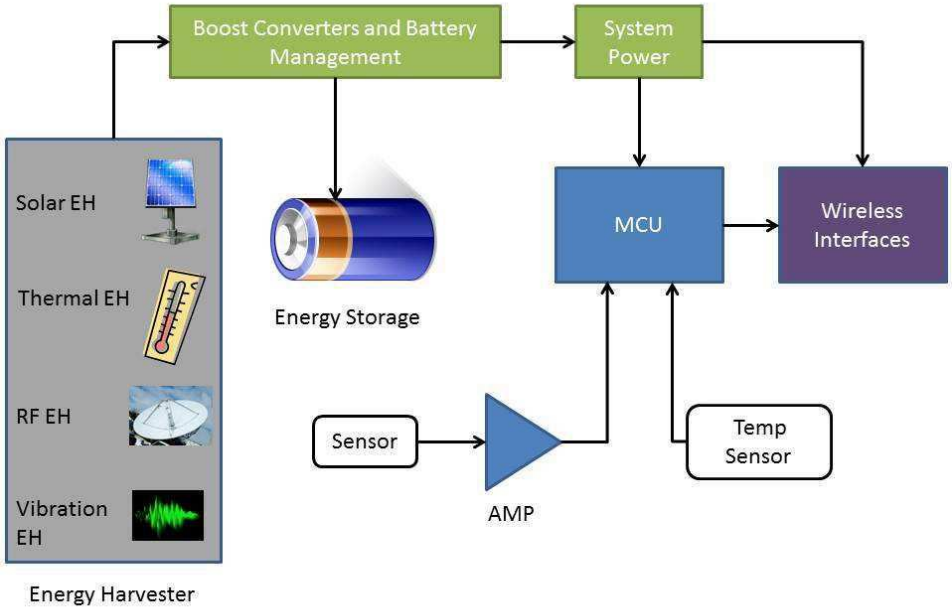

Fig. 1 Model energy harvesting system diagram [2]

Fig.2 shows a block diagram of a model RF harvesting network. The figure shows the block diagram from the receiver end. When the RF has been received at the receiver end, it carries a variety of noises and distortions along with the non-uniform RF signal. The signals are thus required to be convereted into DC to make better use of the power and to use it to power devices. There can be two ways in which this maybe done which are either excuting a full wave rectification or a half wave rectification. Full wave rectification is preferred as it transmits more DC power than the half wave rectification does. There can be a number of ways in which the full wave rectification can be achieved. Usage of diodes, microstripes, microcontroller chips to name a few provides a method of rectification.

Fig.3 shows the block diagram of the RF-DC converter. Since there are numerous ways to obtain the conversion as quoted above, the designs at times use the design specific converters to obtain the necessary DC power levels.

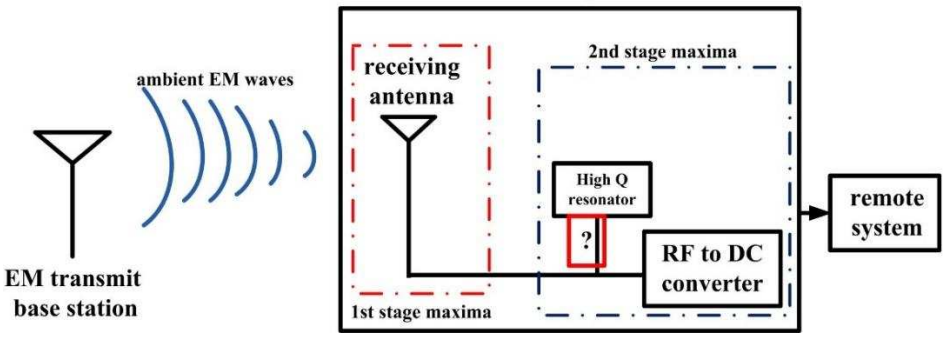

Fig.2 Block diagram of receiver antenna and RF-DC converter [8]

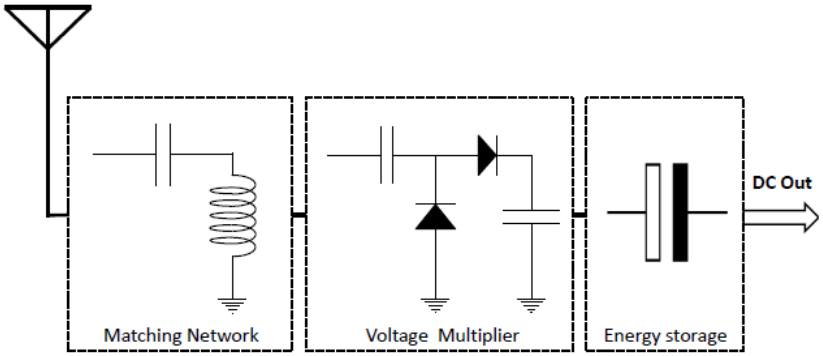

Fig. 3 a block diagram of a model RF energy harvester system [8]

3.3 Antennas

The process of energy harvesting requires receiver antennas which can retrieve the ambient RF energy and which can thus be used in the form of energy. Thence, the antennas which were suitable for this kind of purpose required the prerequisites of being able to function at the Radio Frequency range, being manageable in size and being able to harvest the maximum amount of power. After preliminary examinations based on the antenna properties, the antennas which were best suited for the desired task of energy harvesting were the slot antennas, the monopole antennas, the dipole antennas and the Ultra-wide-Band antennas.

Dipole antennas are the most elementary and the most frequently used antenna of its kind. As the name suggests, this antenna has a characteristic property of functioning with two poles instead of the single pole in the monopole antennas. The dipole antennas are made up of two terminals or "poles" in which the RF current flows. This current and the associated voltage it induces causes electromagnetic or radio signal to be radiated.

The half wave dipole is formed from a conducting element which is wire or metal tube which is an electrical half wavelength long. It is typically fed in the centre where the impedance falls to its lowest. In this way, the antenna consists of the feeder connected to two quarter wavelength elements in line with each other. The voltage and current levels vary along the length of the radiating section of the antenna. This occurs because standing waves are set up along the length of the radiating element.

One wavelength at 2.4 GHz is $\lambda = c / f$ = 0.125 meters. Hence, the half-wavelength dipole antenna's length is 0.0625 meters.

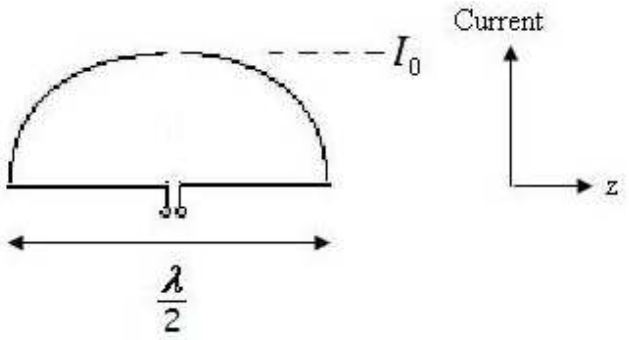

Fig. 4 Distribution of Electric current in a dipole antenna [9]

The formula for the electric field is given by:

$$E_\theta = \frac{j\eta I_0 e^{-jkr}\cos\left(\frac{\pi\cos\theta}{2}\right)}{2\pi r\sin\theta}$$

$$H_\phi = \frac{E_\theta}{\eta}$$

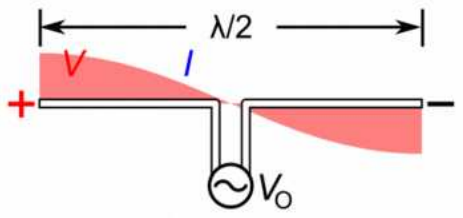

Fig. 5 Figure showing the difference in polarity across a dipole antenna [9]

Slot antennas are used usually at the frequency range of 300 MHz and 24 GHz [10]. The slot antennas are in demand because they can be etched or fabricated out of whatever surface they are to be mounted on, and have radiation patterns which are roughly omnidirectional for most of its designs. It needs to be noted that a voltage source is applied across the short end of the slot antenna. This induces an E-field within the slot, and currents that move around the length and the breath of the slot, both contributed to radiation. The dual antenna has a lot of similarity to a dipole antenna. The voltage source is applied at the centre of the dipole, so that the voltage source is rotated.

Rather than a λ/2 wavelength of centre-fed wire in free space making up a dipole antenna, a dipole slot antenna is usually a λ/2 wavelength long slot in a large ground plane. It can be fed in a number of ways (Fig.3). One frequently used method is to place slots in a waveguide. With the correct placement and gaps in between slots, an array of slots can act as a directional and effective antenna. Or it may be a slot in the ground plane on a PCB with the signal fed to the centre edges, often a bit off centre to match impedances. Fig. 3 shows the two types of slot antennas.

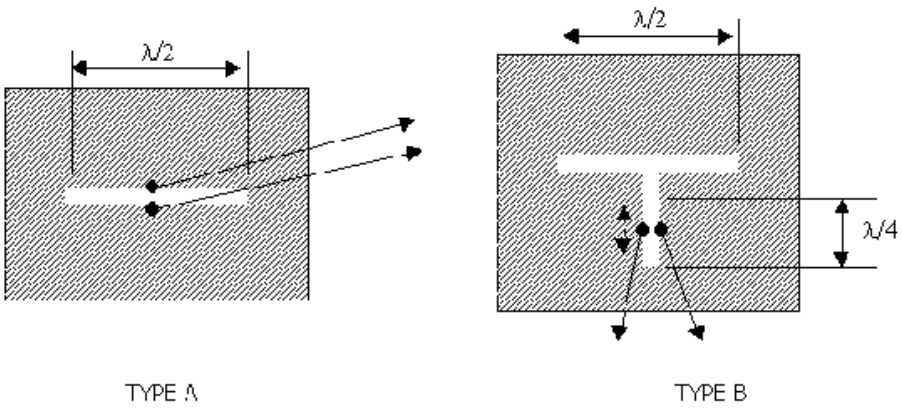

Fig.3 types of slot antennas [5]

These antennas can be suitable because they can all be designed in significantly smaller sizes using substrate having thickness in microns and can still obtain very good output matching at the desired frequency [10]. The various antenna types, their designs and their specifications are discussed in the subsequent chapters.

Slot radiators are a very economical for the designing of frequency scanning arrays. Slot antennas are *λ/2*-wavelength extended slots, carved on a conductive plate, and charged in the centre. This slot demonstrates the patterns based on the *Babinet's principle* as resonant radiator [11]. *Jacques Babinet* (1794 - 1872) was a physicist and mathematician, he devised the theorem which stated that similar diffraction patterns are generated by two complementary screens [11]. This principle links the radiated fields and impedance from an aperture or slot antenna to that of the E-field of a dipole antenna. The principle, by definition can be stated as "*The field at a given point behind a plane having a screen, if added to the field at the same point when the complimentary screen is substituted, is equal to the field at the point when no screen is present"*[11]. The principle takes account of the critical vector nature of the electronics and assumes flat, plane aperture of the screen which also possesses perfect conductivity and absolute thinness. Also, the complementary screen is assumed to be having infinite permeability thereby making one of the screen a perfect conductor of electricity and making the other one a perfect conductor of magnetism. Since neither the infinite conductivity nor infinite permeability can be realised, the material is chosen in such a way that the original as well as the complimentary screens are made of perfectly conducting materials while the magnetic and the electric quantities are interchanged everywhere [10].

The relationship between the impedance of the slot antenna in terms of the complimentary dipole antenna knowing the impedance of the dipole can be defined as [10]:

Assuming,

Z_s = Impedance of the slot

Z_d = known Impedance of the complimentary dipole

Z_0 = Intrinsic impedance of the surrounding medium

$$Z_s = Z_0^2 / 4.Z_d$$

Using this formula, the impedance of the slot can be calculated if the impedance of the complimentary dipole antenna as well as the impedance of the surround medium is known. The impedance of the surround media is usually a constant available for usage. Hence, the impedance of the slot could be easily obtained [11].

3.4 Diodes and rectifiers

Rectification in the RF energy harvesting networks is implemented to convert the received RF signals as well as the AC distortions and to eradicate the noises and distortions from unwanted frequencies picked up by the network. The signal, once rectified ideally works as a DC signal which can then be used to measure or to use the received DC power. Full-wave and half-wave rectifications are possible but in most of the designs for energy harvesting, full-wave rectification is preferred to maximise the received power. There are several ways using which the rectification can be achieved. The half-wave rectification are the simplest of all the rectification methods and can simply be achieved by adding a single Schottky or any other diode in forward biasing. A positive half-wave is obtained if the diode is added to the positive end and a negative half-wave is obtained otherwise. In full-wave rectification however, there are a lot of methods using which the rectification can be achieved such as a bridge rectifier, dual-polarity centre-tap full-wave rectifier, microstrips phase-shift for rectification to name a few [11].

In the dual-polarity centre-tap full wave rectifier, two diodes are used in forward biasing in parallel to each other to obtain the positive full wave rectification [9]. This method is achieved by simply adding two forward biased antenna right at the antenna output port. The model design can be seen in Fig. 4b below.

The bridge rectifier for full-wave rectification makes use of 4 diodes to obtain a full wave rectification, 4 diodes are added together in a combination as seen in Fig. 4a below. The advantage of using a bridge rectifier is that a rectification can be obtain with only one single input using the bridge, as it was not the case with the centre-tap rectifiers.

The microstrip phase shifting rectifiers on the other hand, use a method of rectification that is way too different from that of the other half-wave and full-wave rectifiers. Their way of function, as the name suggests is that they first split the input signals into two and then the microstrips, which are designed on a design specific basis shift the phase of the signal in order to move half of the split signal into the position where no rectification will be observed in the other half of the signal [11]. The signal is thus rectified using the half-wave rectification so that the part of the signal rectified through the microstrip superimposes right where the other signal doesn't get a peak. The figure can be seen below (Fig. 4c).

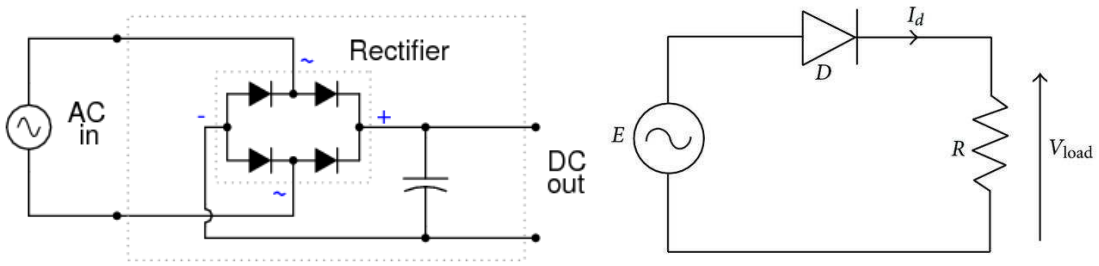

a) Bridge rectifier [11] b) half-wave rectifier [11]

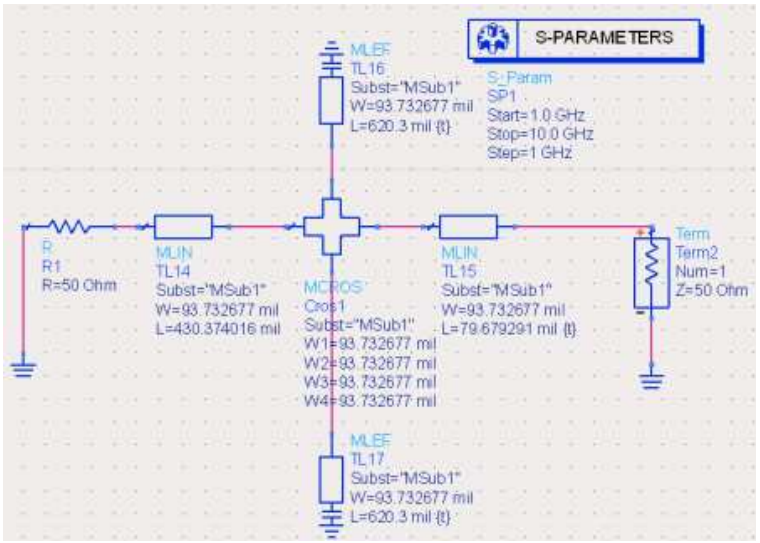

c) full-wave microstrip phase shifting rectifier [9]

Fig. 4 a, b and c showing the different types of rectifiers

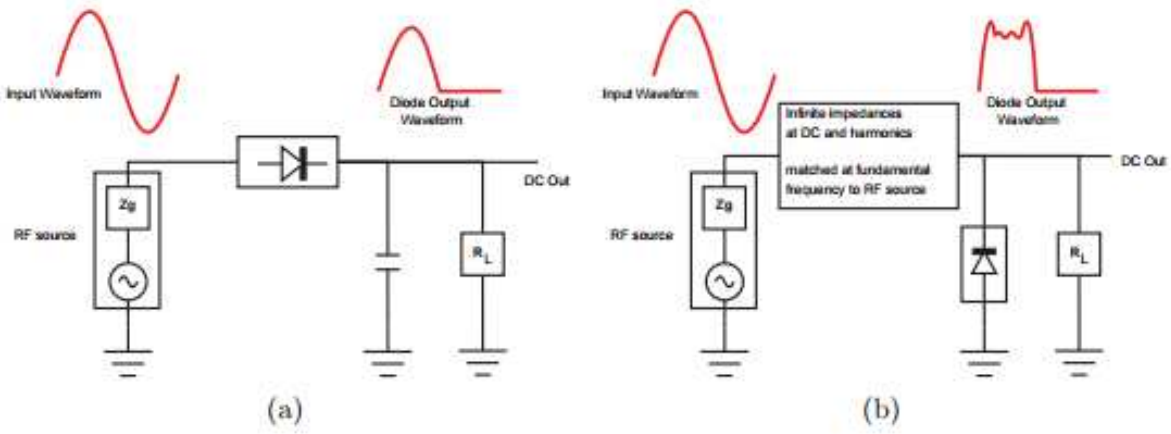

Fig. 5 (a) Simple half-wave rectifier (b) microwave model of the simple rectifier with impedance matching at DC, the fundamental, and harmonics [11]

The diodes used at the RF range are generally the Schottky diodes. Schottky diodes are usually used in high frequency applications, and specifically for the gain control stages in the RF component of devices and circuits. They may also be placed in power rectifiers and Solar cell applications. low capacitance (<1 pF) Schottky diodes are suitable to all high frequency applications.

Certain devices have a capacitance 93% below the industry standard BAT54, or less than a-third of the present low capacitance diodes such as the BAS40, achieved with no trade off in breakdown voltage specification [9]. The diodes which functioned best at the frequency of 2.4 GHz and were available in the market were HSHS 2862 by Avago and SMS7630-079IF by skyworks [12]. The critical data of the diodes can be seen in the figures below.

Part Number	Minimum V_B @ 100 µA (V)	Typical C_T @ 0.15 V (pF)	V_F @ 0.1 mA (mV)	V_F @ 1 mA (mV)	Maximum Pair Configuration ΔV_F @ 1 mA (mV)	Typical R_V (Ω)
SMS7630 series	1	0.3	60 to 120	135 to 240	10	5000

Table 1 Technical specifications of the SMS7630 diodes

Equivalent Linear Circuit Model, Diode chip

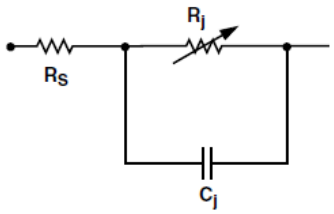

R_S = series resistance (see Table of SPICE parameters)

C_j = junction capacitance (see Table of SPICE parameters)

$$R_j = \frac{8.33 \times 10^{-5}\ nT}{I_b + I_s}$$

where

I_b = externally applied bias current in amps

I_s = saturation current (see table of SPICE parameters)

T = temperature, °K

n = ideality factor (see table of SPICE parameters)

SPICE Parameters

Parameter	Units	Value
B_V	V	7.0
C_{J0}	pF	0.18
E_G	eV	0.69
I_{BV}	A	1 E - 5
I_S	A	5 E - 8
N		1.08
R_S	Ω	6.0
P_B (VJ)	V	0.65
P_T (XTI)		2
M		0.5

Table 2 Critical data for the HSMS 2862 SOT-23 packaging

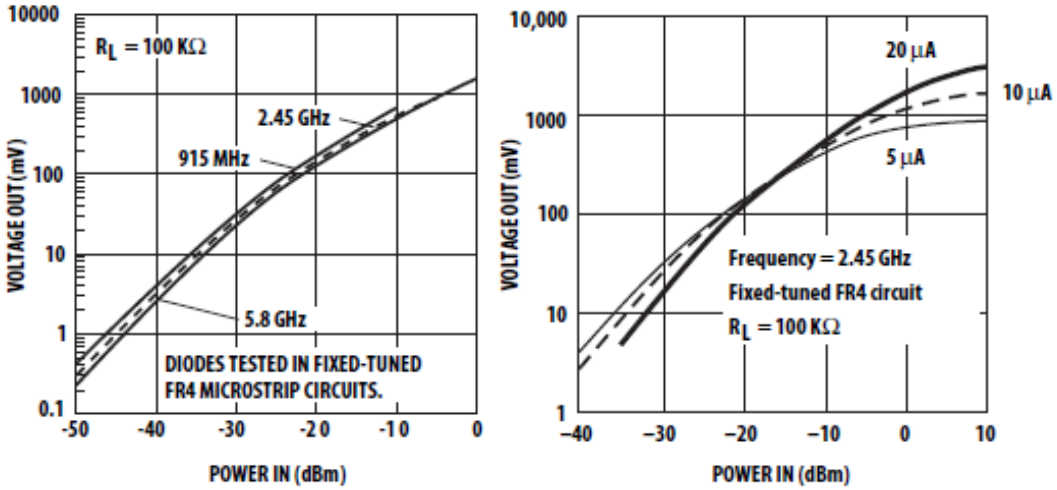

Fig. 6a & 6b input voltage vs the output voltage graphs

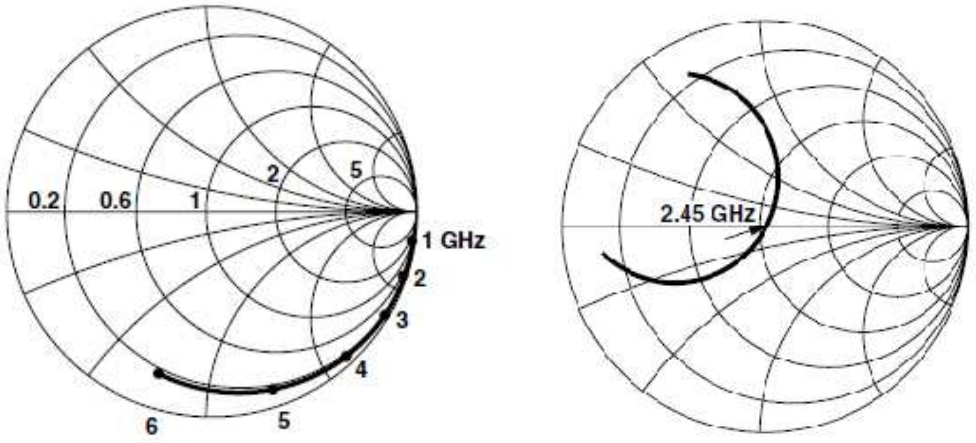

Fig 7a & 7b. Smith charts showing the function of diode in detector circuit (7a) at 2.45 GHz (7b) [10]

The figures and the datasheets above describe the diodes suitable for the RF high frequency range.

3.5 S-parameter or network parameters

At RF frequencies, most devices can be characterised using equivalent network parameters. This is particularly important for rectenna application. Scattering or S-parameters (the salient constituents of a scattering matrix) denote and demonstrate the electrical behaviour of linear electrical systems when a signal is applied [13].Scattering parameters, or S-parameters as they are generally called, do not make use of the open-circuitry conditions to compute the linear electric systems. The parameter entities are measured in the various units of power [13]. Properties such as gain, VSWR, reflection coefficient, loss in return can be found using the S-parameters.

The scattering matrix [14] relates the voltage wave's incident on the ports to those reflected from the ports. The scattering matrix (S matrix) is defined as:

$$\begin{bmatrix} V_1^- \\ V_1^- \\ . \\ . \\ V_N^- \end{bmatrix} = \begin{bmatrix} S_{11} & S_{12} & \dots & S_{1N} \\ S_{21} & & & . \\ . & & & . \\ . & & & . \\ S_{N1} & & & S_{NN} \end{bmatrix} = \begin{bmatrix} V_1^+ \\ V_2^+ \\ . \\ . \\ V_N^+ \end{bmatrix}$$

Where V_n'' is the amplitude of the voltage wave that is reflected off the port n and V_n+ is the amplitude of the voltage wave incident on the port n. An arbitrary element of the [S] matrix may be determined as:

$$S_{ij} = \left. \frac{V_i^-}{V_j^+} \right|_{V_k^+ = 0 \; for \quad k \neq j}$$

Assuming that we have 2 different ports namely port 1 and port 2 like in the matrix above, the parameter S_{12} denotes the trend of the transferred power from port-2 towards port-1. S_{21} denotes the trends of the transferred power from port-1 towards port-2.

Thus, in general, S_{ij} is calculated by driving port j with an incident wave of voltage V_j+, measuring the reflective wave amplitude, Vi-, coming out of port i.

In practical and experimental usage, the S_{11} parameter is the most frequently used parameter of them all. It denotes the amount of power reflected off the antenna aperture or antenna apparatus depending on the design [13].It is also referred to as reflection coefficient of the antenna. If S_{11}=0 dB then the entire power is reflected of the antenna and none of it gets radiated. S_{11} value of -10 dB implies a reflection of -7dB if the received power was 3dB [14]. To test an antenna for its S_{11} values, the pattern of its reflected power is plotted for various frequencies using a Vector Network Analyser (VNA) and while observing the plot, the frequency at which the antenna radiates the best can be observed [15]. Fig. 8 denotes a model S_{11} graph with the matching and the matching frequency value.

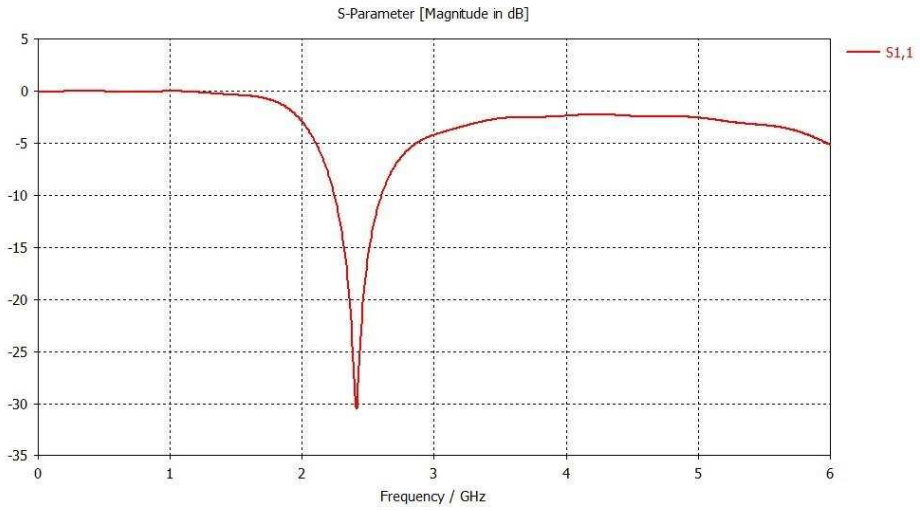

Fig. 8 Typical reflection coefficient graph or S_{11} parameter for a matched antenna [16]

In the graph shown in Fig. 8, it can be observed that the Magnitude in dB attained a maxima of -30dB at the frequency of 2.4 GHz. This demonstrates that the antenna is well matched at the frequency of 2.4 GHz and using simulation tools such as CST [16] and changing the dimensions of the antenna aperture, various results such as the frequency of matching and the magnitude of matching can be altered.

3.6 Matching circuits

A matching circuit is in principle a filter, but there are apparent differences between filter design and antenna matching circuit design. Filters are usually designed to function in a 50 Ohm system,

where closed form solutions for optimal filter design are available. In contrast, antenna matching circuits need to take into account the complex antenna impedance that changes rapidly with frequency and thus the closed form solutions are not available any longer. In addition, in matching circuit design it is easy to take into account a complex frequency-dependent. In matching circuit design it is easy to add stop band definitions so that the combination of antenna and the matching circuit is filtering out unwanted interfering signal.

In matching circuit design it is natural to use the power wave definitions of the reflection coefficient and the scattering matrix, because they correctly describe the propagation of power in microwave networks [12- 15]. Standard textbooks typically only express the reflection coefficient and scattering matrix in terms of the traveling waves, which are the physical waves traveling in transmission lines. However, due to multiple reflections, the traveling waves do not describe the propagation of power. For example in the case of conjugate matching (which is known to be optimal for power transfer) the traveling wave reflection coefficient is nonzero. In contrast, the power wave definition gives zero reflection for the conjugately matched case.

It is well known that, to get the maximum power transfer from a source to a load, the source impedance must equal the complex conjugate of the load impedance, or:

$R_S + jX_S = R_l - jX_l$

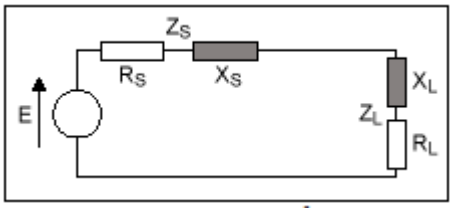

For this condition, the energy transferred from the source to the load is maximized. In addition, for efficient power transfer, this condition is required to avoid the reflection of energy from the load back to the source. This is particularly true for high-frequency environments like video lines and RF and microwave networks.

The procedure of how a matching circuit works can be described using a Smith chart. The Smith chart is a polar plot of the complex reflection coefficient (also called gamma and symbolized by Γ). Or, it is defined mathematically as the 1-port scattering parameter s or s_{11}.

A Smith chart can be developed by examining the load where the impedance must be matched. Instead of considering its impedance directly, you express its reflection coefficient Γ_l, which is used to characterize a load (such as admittance, gain, and transconductance). The Γ_l is more useful when

dealing with RF frequencies.

We know the reflection coefficient is defined as the ratio between the reflected voltage wave and the incident voltage wave:

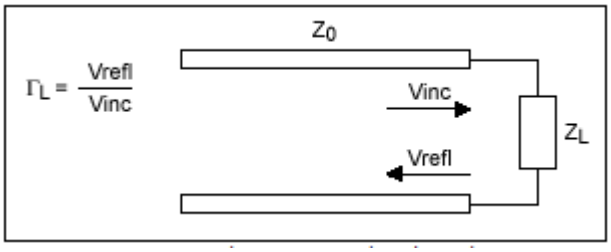

The amount of reflected signal from the load is dependent on the degree of mismatch between the source impedance and the load impedance. Its expression has been defined as:

$$\Gamma_L = \frac{Vrefl}{Vinc} = \frac{Z_L - Z_0}{Z_L + Z_0} = \Gamma_r + j\Gamma_i$$

Because the impedances are complex numbers, the reflection coefficient will be a complex number as well.

In order to reduce the number of unknown parameters, it is useful to freeze the ones that appear often and are common in the application. Here Z_0 (the characteristic impedance) is often a constant and a real industry normalized value, such as 50Ω, 75Ω, 100Ω, and 600Ω. We can then define a normalized load impedance by:

$$z = \frac{Z_L}{Z_0} = \frac{R + jX}{Z_0} = r + jx$$

The initial series R-I-C network was estimated to have relatively lower resistive values so that there would not be any hindrance in the flow of current. The second R-C network required to have an inductor in series with the resistor and was required to have significantly lower value (in the range of pH). The values were estimated using the following formula [3]:

$$Z = \sqrt{(R^2 + (X_L - X_C)^2)}$$

$X_l = \omega_l$ = Inductive impedance

X_C= Capacitive impedance

R= Resistive impedance or resistance

f = Frequency

To maintain a standard 50-Ω impedance to start off the estimation of values, it is practically and mathematically feasible to implement values in a manner which resulted in $X_l=X_c$. For the same to happen, with the help of the following formulas, the initial values were calculated which can be seen in the subsequent chapters.

When developing the Smith chart, there are certain precautions that should be noted. These are among the most important:

- All the circles have one same, unique intersecting point at the coordinate (1, 0).
- The zero Ω circle where there is no resistance (r = 0) is the largest one.
- The infinite resistor circle is reduced to one point at (1, 0).
- There should be no negative resistance. If one (or more) should occur, we will be faced with the possibility of oscillatory conditions.
- Another resistance value can be chosen by simply selecting another circle corresponding to the new value.

Another function of the Smith chart is the ability to determine impedance matching. This is the reverse operation of finding the equivalent impedance of a given network. Here, the impedances are fixed at the two access ends (often the source and the load), as shown in Fig. 9. The objective is to design a network to insert between them so that proper impedance matching occurs.

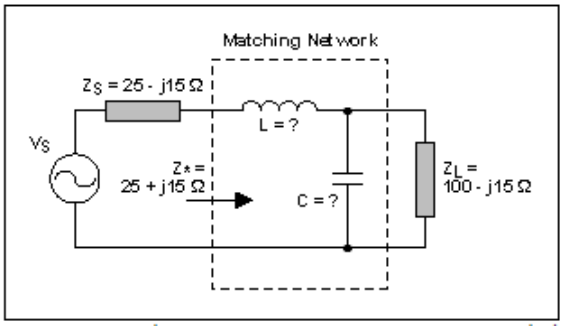

Fig. 9 The matching network circuit

At first glance, it appears that it is no more difficult than finding equivalent impedance. But the problem is that an infinite number of matching network component combinations can exist that create similar results. And other inputs may need to be considered as well (such as filter type structure, quality factor, and limited choice of components).

The matching network circuit designing was used in this thesis to find the matching for the desired frequency of 2.43 GHz and to design a chip that merges the rectifying microstrip lines with the matching circuit. The circuit which was implemented can be seen in the Fig. 10 below.

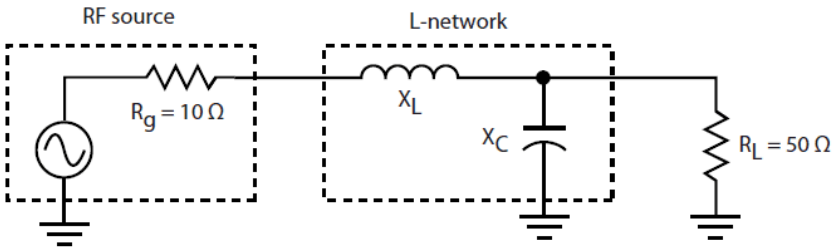

Fig. 10 Circuit diagram of a matching circuit designed [14]

The matching circuit for the specified design used in this thesis is discussed in the upcoming chapters.

3.7 Free space power equations

The power received and the power transmitted ratio is given by the Friis equation [10] which is as follows:

$$P_R = \frac{P_T G_T G_R \lambda^2}{(4\pi R)^2}$$

Where,

P_r: Power at the receiver end of antenna

P_t: output power from the transmitting end of the antenna

G_t, Gr: gain of the transmitter and the receiver antenna

λ: wavelength

R: distance between the antennas

The Friis Transmission Equation [10] is an equation used to determine the power received from antenna with a gain G_r, when transmitted from another antenna with gain G_t, a distance R apart from one another, and operating at frequency f or wavelength λ. It associates with the free space path loss, antenna gains and wavelength to the received and transmit powers. Since λ can be expressed in terms of the speed of light and frequency, the Friis equation can also be rewritten as [12]:

$$P_R = \frac{P_T G_T G_R c^2}{(4\pi R f)^2}$$

Equation above denotes that power is lost at higher frequencies. This is a fundamental result of the Friis Transmission Equation. This points that for antennas with specified gains, the energy transfer will be highest at lower frequencies. The difference between the power received and the power transmitted is known as path loss [12].

3.8 Electromagnetic simulation methods

The antennas that are developed using the CST software are generally simulated by using the Finite difference time-domain calculation (FDTD) which is embedded in the CST Microwave studio software. The FDTD method is a common grid-based differential time-domain numerical modelling method. Maxwell's equations are modified to central-differential equations, discretised, and implemented in software. The equations for the electric-field are solved at a known instant in time, then the equations for the magnetic-field are solved in the next known instant in time, and this method is conducted over and over again. CST Microwave Studio software is an electromagnetic simulator which is based upon the Finite Integration Technique (FIT) [12-15]. FIT discretizes the following integral form of Maxwell's equations, rather than the differential one [13]:

$$\oint_{\partial A} \vec{E} \cdot d\vec{s} = -\int_A \frac{\partial \vec{B}}{\partial t} \cdot d\vec{A}, \qquad \oint_{\partial A} \vec{H} \cdot d\vec{s} = \int_A \left(\frac{\partial \vec{D}}{\partial t} + \vec{J} \right) \cdot d\vec{A}$$

$$\oint_{\partial V} \vec{D} \cdot d\vec{A} = -\int_V \rho \cdot dV, \qquad \oint_{\partial V} \vec{B} \cdot d\vec{A} = 0$$

E [V/m] - electric field

H [A/m] - magnetic field

D [q/m2] - displacement vector

B [Wb/m2] - mag. Flux density

ρ[q/m2] - vol. charge density

A [m2] - element area

V [m3] – volume

The equations, for electric field and the magnetic field are arbitrarily named A and B respectively. Equation A and B are solved numerically by defining a finite calculation domain working as a boundary condition for the application problem of simulation. This domain is sub-divided into several small grid cells. As is shown in Fig.11a, for every-single grid mesh a secondary grid-mesh is declared orthogonally to the original one. A spatial discretisation of Maxwell's equations is conducted on the two orthogonal grid systems, in which the new degrees-of-freedom are added as integral values [21].

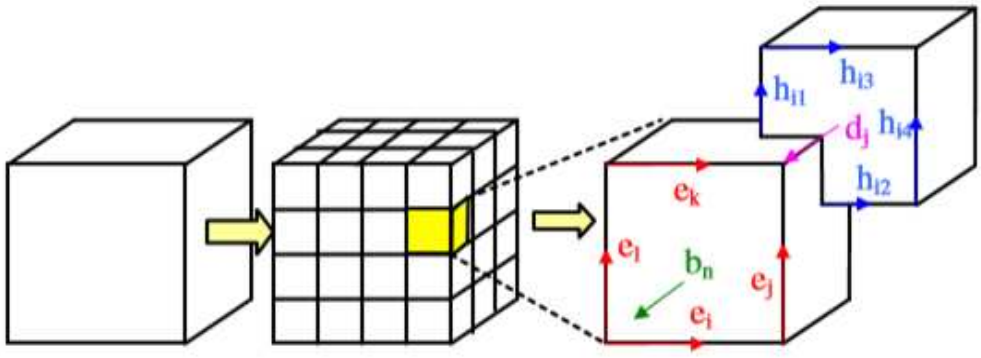

Fig. 11a Grid system implemented for spatial discretisation [21]

Maxwell's equations are formulated for each of the cell facets separately. By replicating the process for all the available cell facets, the calculation rule can be summarised in a C matrix as the discrete equivalent of the analytical curl operator.

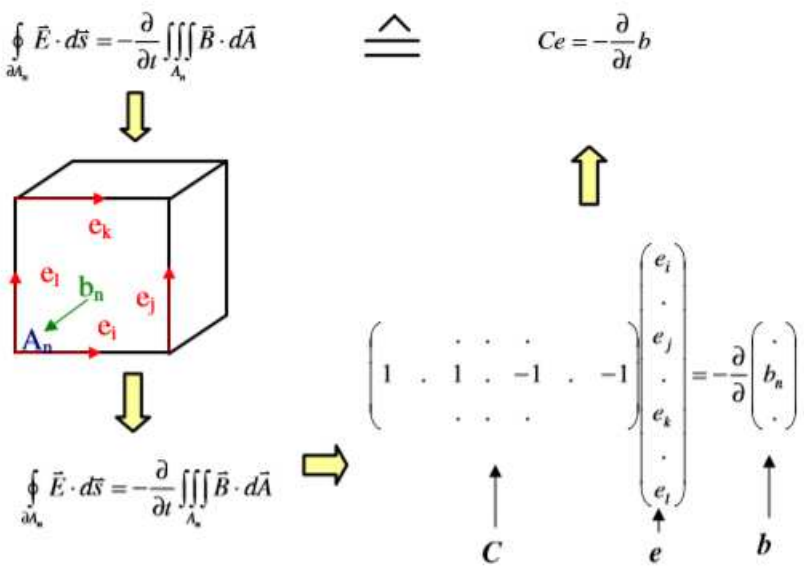

Fig. 11b. Matrix C, the discrete equivalent of analytical curl [13]

Applying Ampere's law on the two grids, a discretized Maxwell's Grid-Equations (MGE) set is obtained:

$\mathbf{C_e = -\frac{d}{dt}b, \hat{C}h = \frac{d}{dt}d + j}$ ---------- C

$\mathbf{C\hat{S}^T = \hat{C}S^T = 0, S_b = 0}$ ---------- D

These material equations generate numerical inaccuracy because of the spatial discretisation. By declaring the essential co-relation between the voltages and the fluxes mean their respective values need to be approximated across the grid edges and the entire cell areas, respectively [14].

$$\hat{D} = \varepsilon\hat{E} \qquad d = M_\varepsilon e$$
$$\hat{B} = \mu\hat{H} \quad \Rightarrow \quad b = M_\mu h$$
$$\hat{J} = \sigma\hat{E} + \hat{J}_S \qquad j = M_\omega e + j_S$$

The equations separated in differential equations have, in numerous ways affected the numerical, theoretical and algorithmic aspects [14] and outcomes which are the basis of the algorithms used in CST microwave studio[16].

Conclusion:

This chapter dealt with the prerequisite theoretical background for this thesis. It started with a discussion on energy harvesting which spoke of the inception and the possibilities related to the designing of energy harvesting system. Different types of antennas which can potentially be used for energy harvesting purpose were discussed next which are all simulated and then tested, the outcome of which are discussed in the subsequent chapters. After antenna, the diodes necessary for rectification were discussed and their attributes and characteristics were stated. The concept of matching circuit and how it is used and its implementation in the design was discussed afterwards. Matching of the design will again be discussed in detail in the subsequent chapters.

References:

[1] "Energy harvesting forum,". [Online]. Available: http://www.energyharvesting.net/. 2009 Accessed: Aug. 13, 2016.

[2]T. Ie Triet, “Efficient Power Conversion Interface Circuits for Energy Harvesting Application”, *Doctor of Philosophy Thesis*, Oregon StateUniversity, USA, 2008.

[3] Y. Kawahara, K. Tsukada, and T. Asami, 'Feasibility and Potential Application of Power Scavenging from Environmental RF Signals', Proc. IEEE Intl. Conf on Antennas and Propag., Charleston, pp 1-4, June 2009.

[4] R.A. Hill, B.A Munk, “The effect of perturbating a frequency-selective surface and its relation to the design of a dual-band surface,” IEEE Trans. Antennas and Propag., vol.44, no.3, pp. 368-374, March 1996.

[5]] H.-D. Chen, J.-S. Chen and J.-N. Ii, “Ultra-wideband square-slot antenna”, Microw. Opt. Technol. lett., vol. 48, no. 3, pp.500-502, Jan. 2006.

[6] R.M.S. Cruz, A.G. D'Assunao, P.H. da F Silva, “A new design proposal for UWB applications,” , 2010 International Workshop on Antenna Technology (iWAT), pp.1-4, 1-3 March 2010.

[7] I. Moustafa and B. Jecko, “Design and Realization of a Wide-Band EBG Antenna Based on FSS and Operating in the Ku-Band,” International Journal of Antennas and Propag., vol. 2010, Article ID 139069, 2010.

[8] A. Aziz, A. Mutalib, and R. Othman, “Current developments of RF energy harvesting system for wireless sensor networks,” Advances in information Sciences and Service Sciences (AISS), vol. 5, no. 11, pp. 328-338, June 2013

[9] J. Kraus and R. Marhefka, Antennas for all applications. New York: McGraw-Hill, 2002.

[10] C. A. Balanis, *Antenna theory: Analysis and design*, 3rd ed. Chichester, United Kingdom: Wiley-Blackwell (an imprint of John Wiley & Sons ltd), 2005.

[11] Dipl and C. Wolff, "Radar basics - slot antennas," Dipl.-Ing. (FH) Christian Wolff. [Online]. Available: http://www.radartutorial.eu/06.antennas/Slot%20Antenna.en.html. Accessed: Aug. 29, 2016

[12] P. Nintanavongsa, , U. Muncuk, D.R. lewis, and Chowdhury, K.R. ‘Design optimization and implementation for RF energy harvesting circuits’, *IEEE Journal on Emerging and Selected Topics in Circuits and Systems*, 2(1), pp. 24–33. doi: 10.1109/jetcas.2012.2187106, 2012

[13] P. Bevelacqua, "S-parameters for antennas (S11, S12),". [Online]. Available:s http://www.antenna-theory.com/definitions/sparameters.php. Accessed: Aug. 26, 2016.

[14] http://jcatsc.com/media/ee541/lectureSupplements/02-Scattering.pdf. Accessed: Aug. 30, 2016

[15] T. Weiland,: “Time Domain Electromagnetic Field Computation with Finite Difference Methods”, International Journal of Numerical Modelling, Vol. 9, pp. 295-319, 1996.

[16] CST Microwave Studio 2010 www.cst.com

[17] N. Behdad, and K. Sarabandi, ‘A wide-band slot antenna design employing a fictitious short circuit concept’, *IEEE Transactions on Antennas and Propagation*, 53(1), pp. 475–482. doi: 10.1109/tap.2004.838778 , 2005

Chapter 4

Designing of the antenna

4.1 Introduction

The RF power to be harvested is within the WLAN band. The antenna has to be designed to operate at a resonant frequency that is centered at 2.45. The antennas have been designed for an input impedance of 50-Ω, and an attenuation of less than -10 dB across the desired frequency band. The results should mean that the antenna receives and thus harvests sufficient amount of power at the desired matching frequency. Various designs were investigated and their simulations were examined to deduce the best possible models of those are described in the following sections.

4.2 The dipole antenna

A dipole antenna was designed to match at the 2.4 GHz band using CST. The dimensions of the antenna are given in the table 1. As we can observe from the width of the antenna, the total length of the dipole was 32.5mm which is in accordance with the λ/2 wavelength of the half wavelength dipole antenna. The designed can be seen in figure 1.

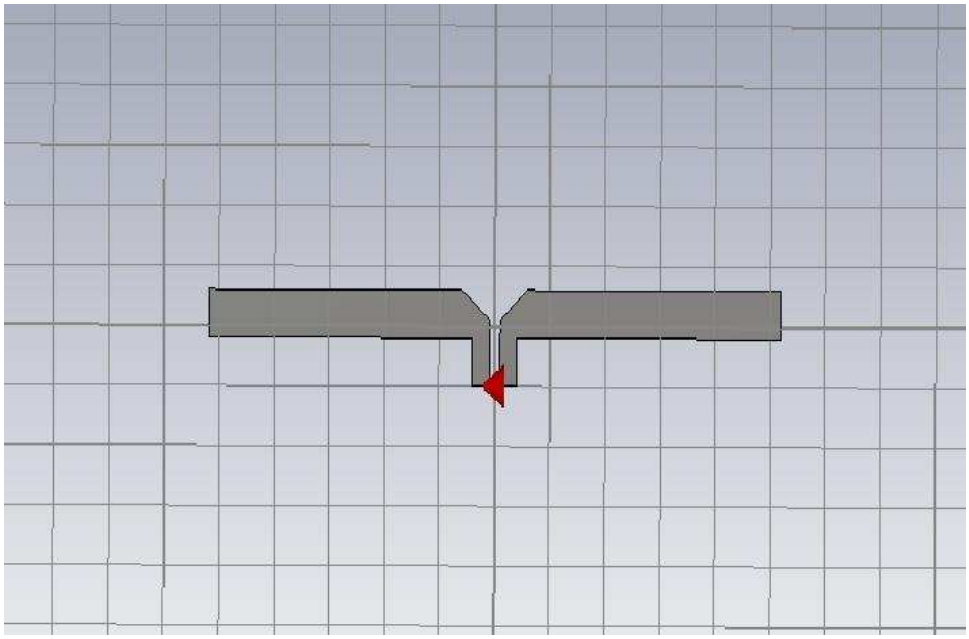

Fig. 1 layout of the dipole antenna in CST

S. NO	Component	Dimension
1	Width of one antenna pole	16 mm
2	Gap between dipoles	1 mm
3	Height of the aperture	8 mm
4	Total width of the antenna	33.5 mm
5	Width of the feeder	1.5 mm

Table 1. The design specifications of the dipole antenna [Fig. 1]

The S-parameter results of the dipole antenna thus designed are shown in the figure 2.

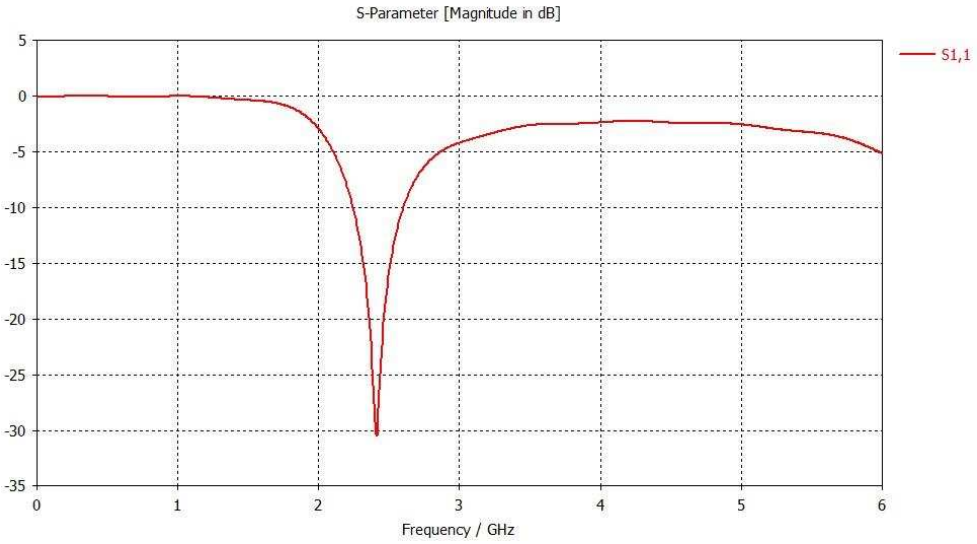

Fig. 2 S-parameters of the dipole antenna in CST

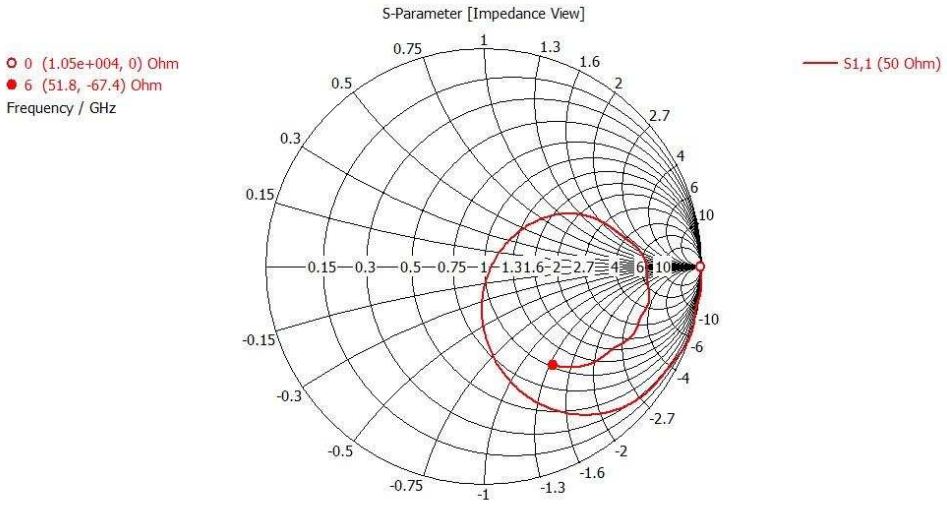

Fig. 3 Z-port Smith chart representation

Going through the S-parameters of the dipole antenna in Fig.2, a perfect matching at 2.412 GHz can be observed. The maximum depth of the trough was measured at -31.27 dB which solidified the expectations with the design and the bandwidth at the -10 dB level was measured to be 0.146 which, despite a well matched S-parameter, was significantly low from the expectations. The substrate was also implemented while designing and the results look very good with the same

substrate. The passband was quite narrow to allow some experimental deficiency and thus, some other antennas were simulated.

4.2.1 Surface currents

The surface currents can be defined as the distribution of the current intensity across an active antenna network. The analysis of the surface current on the radiators indicates that the proposed antenna has a radiation mode of standing wave current in low frequency and traveling wave current in high frequency.

At 2.4 GHz (Fig.4), there are strong currents in the feeder line that are coupled through one another which is connected to the feed. As the wavelength is larger at 2.4 GHz, currents tend to flow throughout most of the body of the antenna starting from the feed, capacity coupling to a feed and connecting through the back metal walls to the other feed which makes the antenna function.

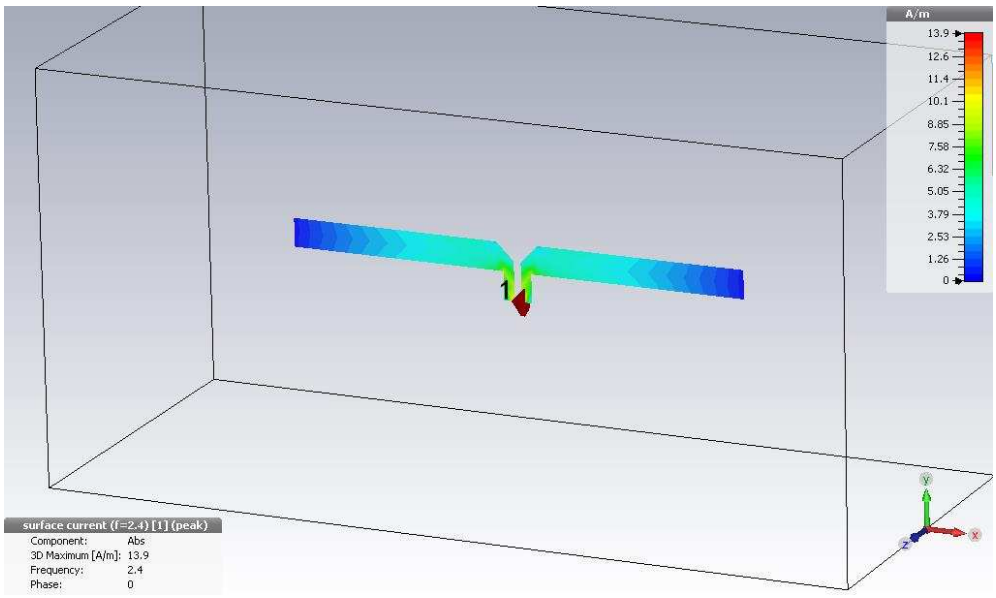

Fig. 4 Surface current plot for the dipole antenna

4.2.2 Radiation pattern

As the graphs below (Fig.5) suggests, the radiation patterns of the planar dipole antenna are of a

standard dipole antenna. The 3D radiation pattern denotes that it's an omnidirectional antenna which works the best around its central line of propagation. The gain of this specific antenna was 2.357 dB which is within the expected range.

Generally, a dipole antenna requires a balun. A Balun is used to "balance" unbalanced systems - i.e. those where power flows from an unbalanced line to a balanced line (hence, balun derives from *bal*ance to *un*balanced).

The 3D farfield pattern can be seen below in Fig.5. A directive gain of 2.357 dBi can be seen from the graph and the graph also denotes the expected omnidirectional properties of the dipole antenna.

In Fig. 8, we can see the omnidirectional properties of the antenna become visible.

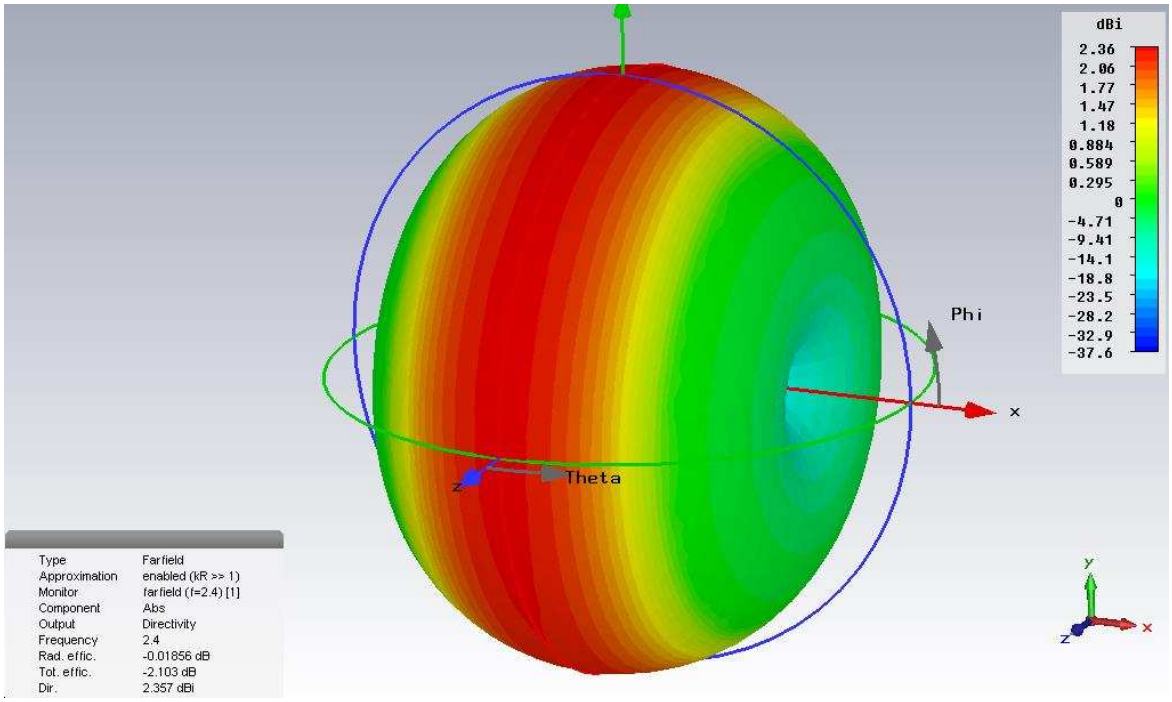

Figure 5 3D dipole antenna radiation patterns

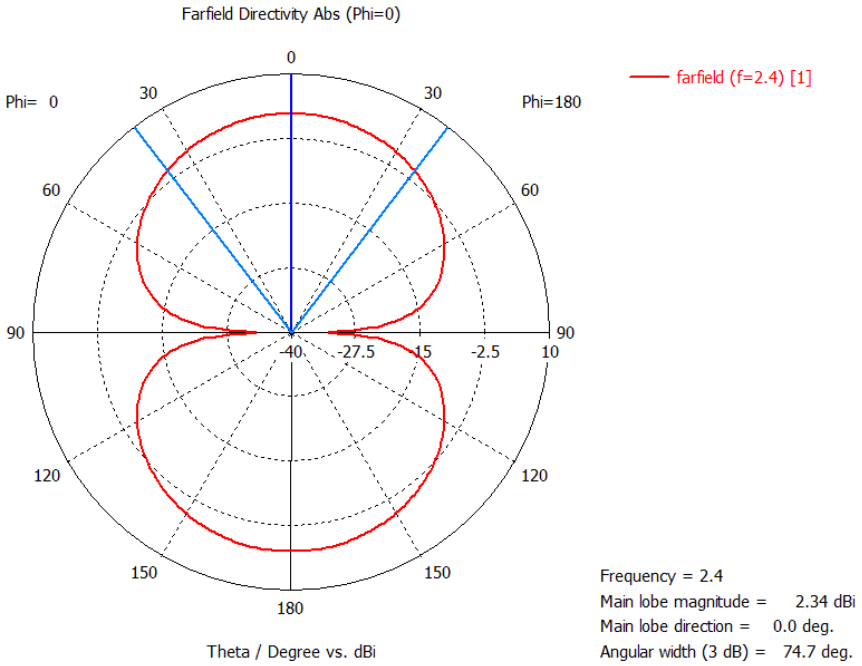

Fig. 6 XZ-PIane radiation pattern

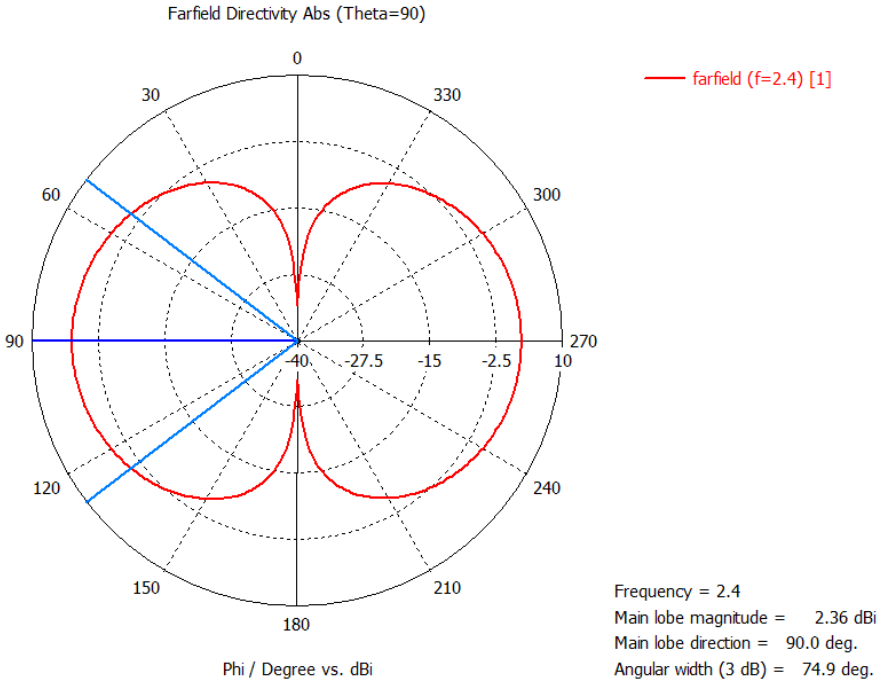

Fig. 7 XY-PIane radiation pattern

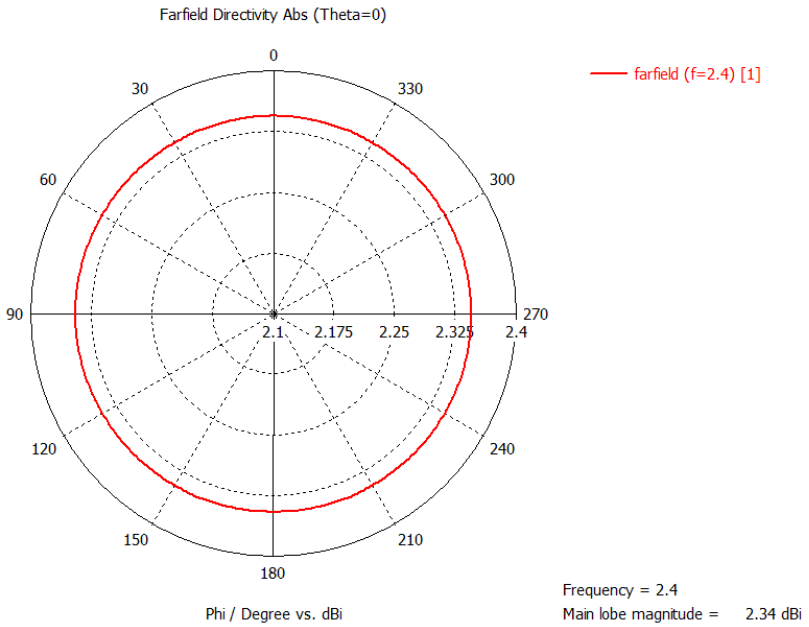

Fig. 8. YZ- plane which denotes the omnidirectional antennas

4.3 The UWB antenna

Conventional Ultra-Wide-Band (UWB) antennas include printed dipoles, monopoles (electrical-type antennas) and slot antennas (magnetic-type antennas). As is well-known, most of these antennas are omnidirectional, low-gain antennas.

A UWB planar monopole antenna was designed to resolve the issues encountered with the dipole antenna. As we observed in section 4.2, the dipole antenna although gave a good match, but the bandwidth it provided was significantly low which would have made it less efficient for wider bands of frequencies.

The idea was to be able to harvest a wider range of RF energy available in the ambient environment. As the RF available in an ultra-wide band (UWB) range, the idea of using a UWB antenna was evaluated. The antenna concept was based on a book titled Antenna by Kraus [2].

The antenna design made to match our requirements was matched at 50 Ω and was designed in CST. The design, as it can be seen in Fig.9 had an Ultra-Wideband and had the matchings from 2.4 GHz to 5.6 GHz to demonstrate its UWB nature. The dimensions of the design were 50mmX48mm with a

hemispherical feeder design and a ground plane. They are specified further in Table2. The shape and the Specifications of the design can be seen in the following:

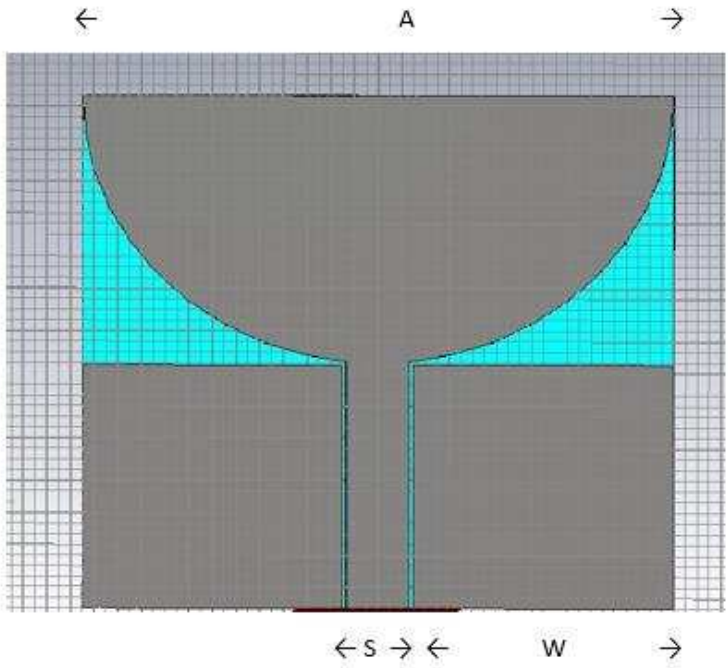

Fig. 9 CST design of the UWB antenna

S. No	Component	Dimensions
1	Radiating patch diameter	Ø25 mm
2	Radiating patch height	25 mm
3	Feed line height(H)	24 mm
4	Feed line width(S)	5.4 mm
5	Ground planes width(W)	22 mm
6	Ground plane height(l)	22.8 mm

Table 2 UWB antenna dimensions

The S-parameter results of the antenna (Fig. 13) also show the various peaks which would be obtained if the higher frequency levels were approached. At 2.4 GHz though, the antenna was well

matched with S_{11} levels below -10dB from 2GHz to well over 15GHz. Troughs as low as -27.14 dB were observed at 2.4 GHz, which were lesser than the dipole antenna. Troughs going as low as -33 dB were observed too at higher frequencies.

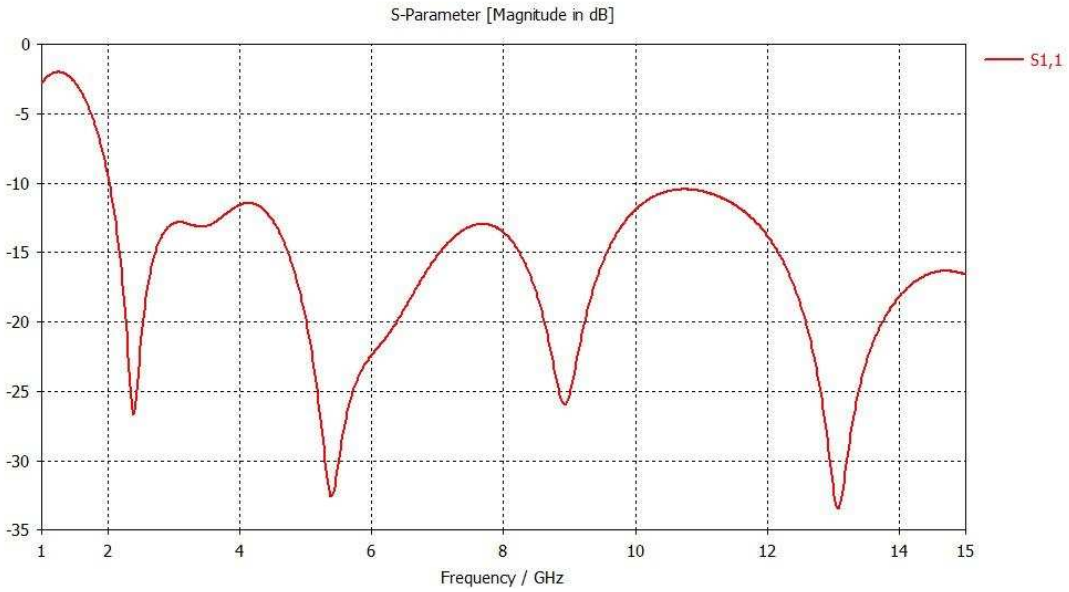

Fig. 10 S-parameter results of the Antenna

4.3.1 Surface currents

The surface currents of the antenna were simulated and they can be seen below. In Fig. 11, the surface current distribution at 2.4 GHz is denoted. A very evenly distributed currents can be seen in the semicircular radiator as well as in the ground plane. The boundaries for the surface currents are uniform and well defined. The simulation results display that the current density is at its peak on and around the edges of the radiator. One the two ground planes, the surface currents observed were significantly lower. While the surface currents on the two identical sides of the radiator are correspondingly identical, a majority of its area has far lesser values of currents which can there be ignored. The current is standing wave current in low frequency region while it is traveling wave current in high frequency region. Current in high frequency region. According to the theoretical analysis, when standing wave current has an electrical length shorter than the wavelength, the maximum radiation direction is perpendicular to the current direction.

At 5.4 GHz however (Fig. 12), the non-uniformity of the surface currents is clearly visible. The regions for peak values are also significantly scattered as compared to Fig. 11.

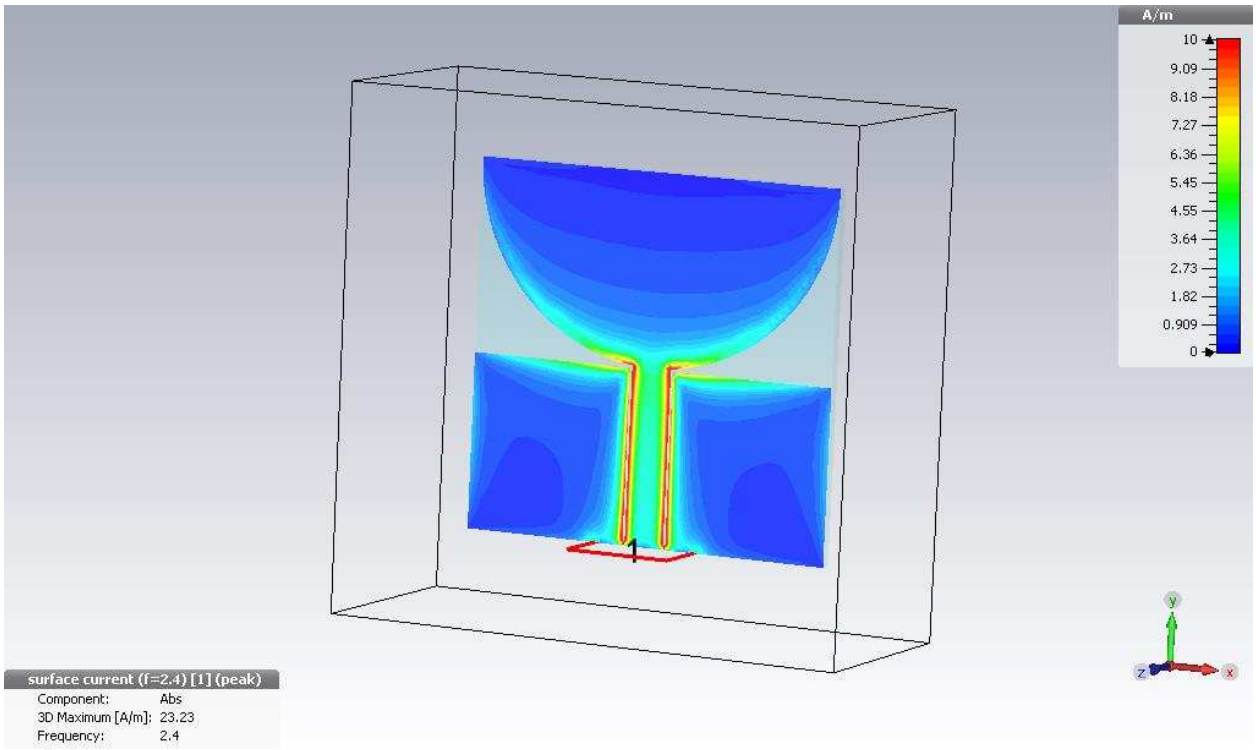

Fig. 11 UWB surface currents at 2.4 GHz

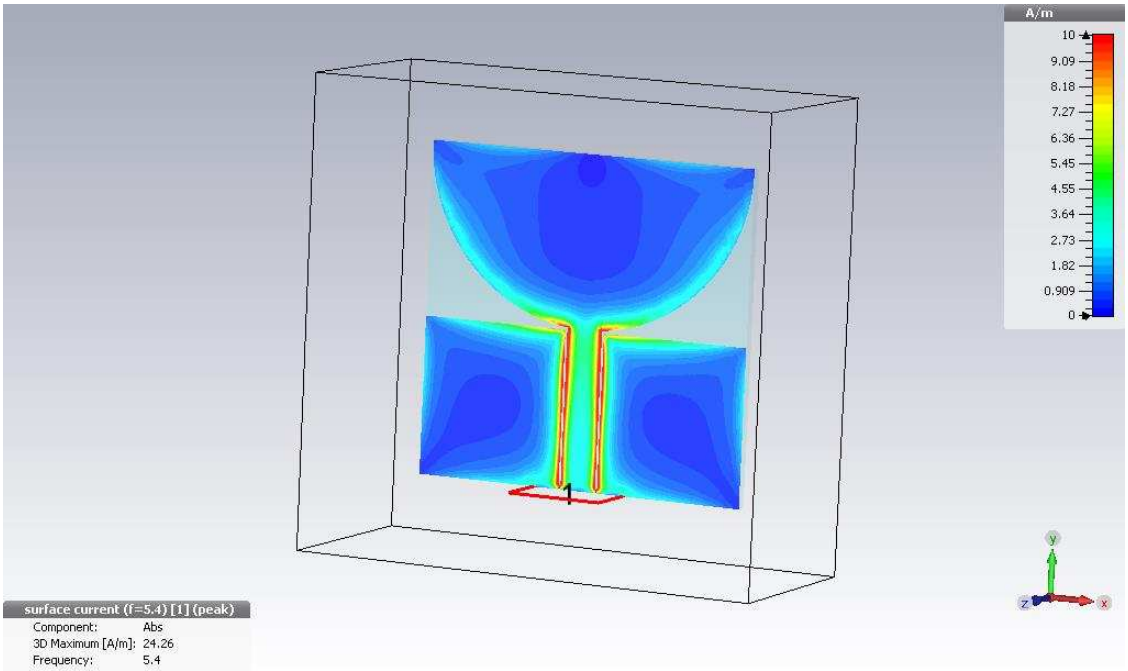

Fig. 12 UWB Surface currents at 5.4 GHz

4.3.2 Radiation patterns

The 3D farfield results at 2.4 GHz as seen in Fig. 13 denote an omnidirectional antenna which is not the case with the same antenna at 5.4 GHz(Fig. 16). The gain at 2.4 GHz was 3.314 dBi and at 5.4 GHz, the gain was 2.82 dBi but it was not as directive as it was at 2.4 GHz. The radiation patterns and the surface current graphs clearly show that the UWB antenna works better at the frequency of 2.4 GHz than at 5.4 GHz. The radiation pattern peaks at the midpoint of the Z-plane are seen in Fig. 13 and 17.

In Fig. 18-20 the radiation patterns for XY, YZ and XZ planes can be observed. Figure 18 shows XZ plane radiation pattern which then denotes the omnidirectional proterty of the antenna. The max gain of 2.723 dB is also indicated in Fig. 18. While comparing Fig.16 and Fig. 20 in the XZ plane, it can be seen that the simulated omnidirectional gain at 5.4 GHz turned out to be 2.82 dBi.

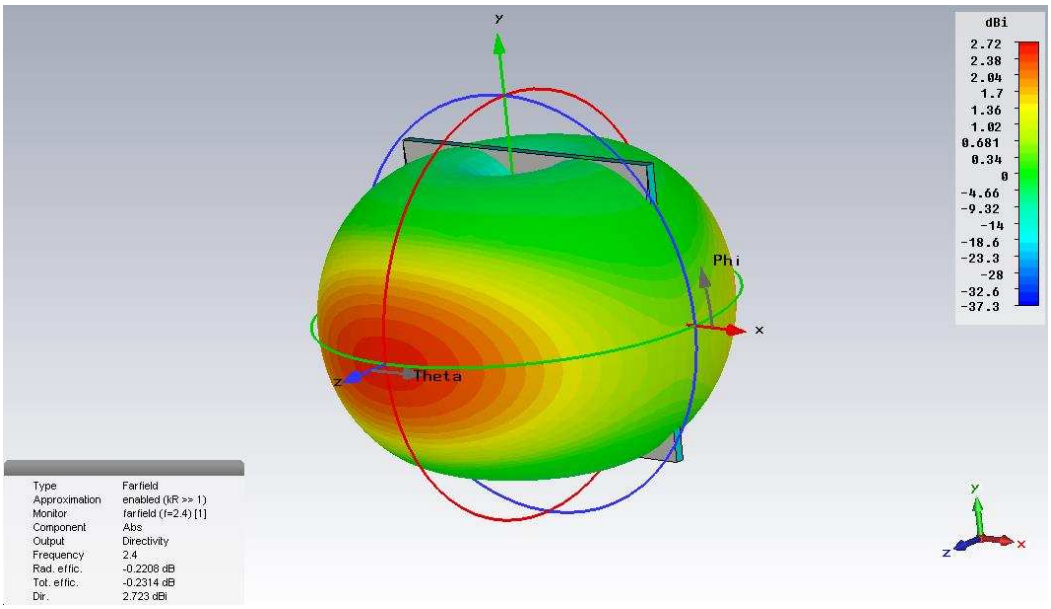

Fig. 13 3D Radiation pattern of the UWB antenna

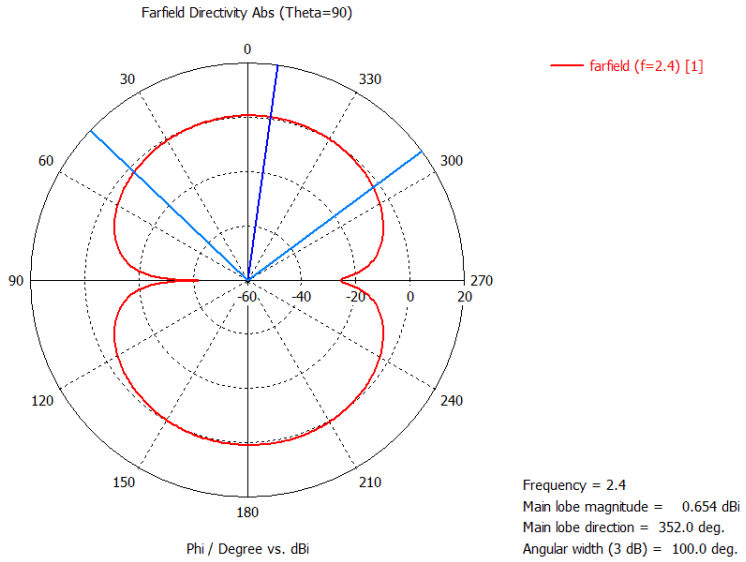

Fig. 14 XY-Plane radiation patterns

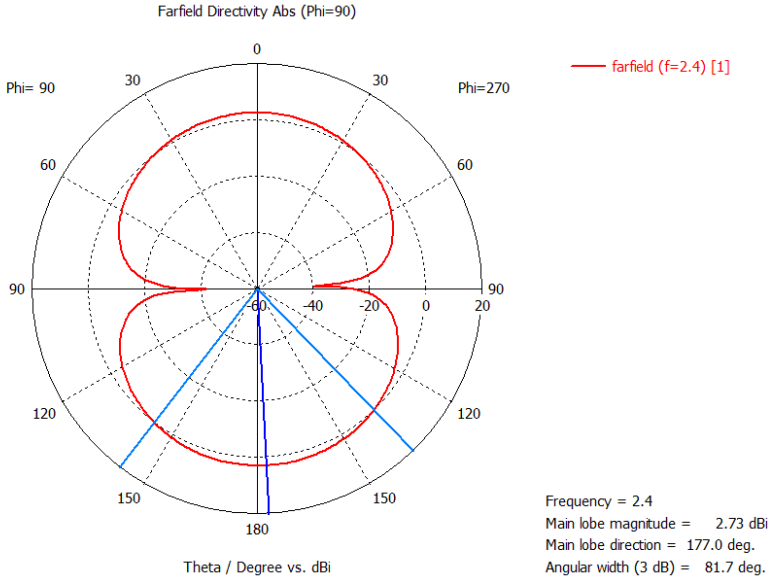

Fig. 15 YZ-Plane radiation patterns

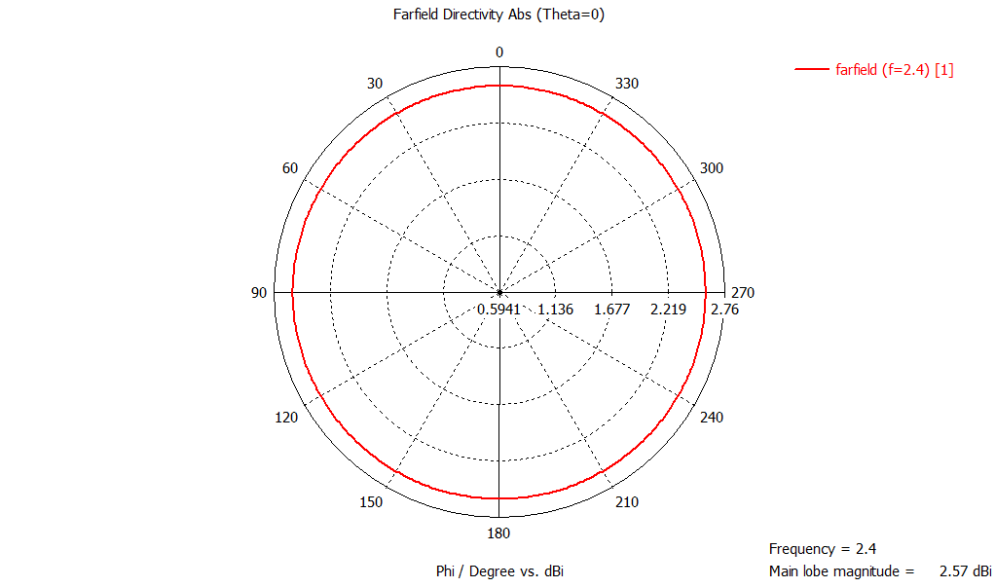

Fig. 16 XZ-PIane radiation patterns

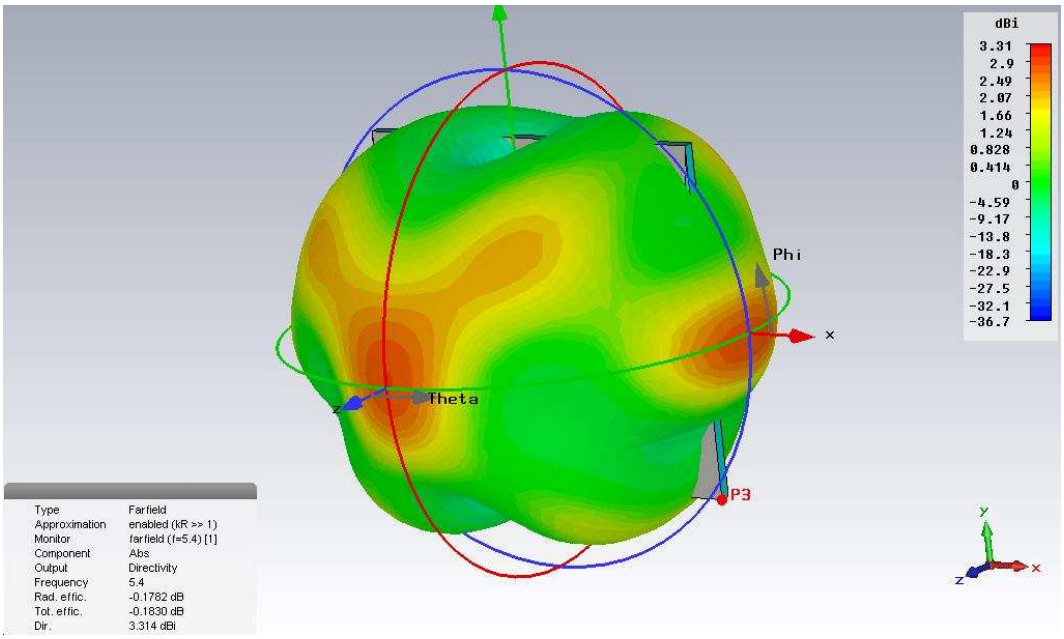

Fig. 17 3D farfieId radiation pattern at 5.4 GHz

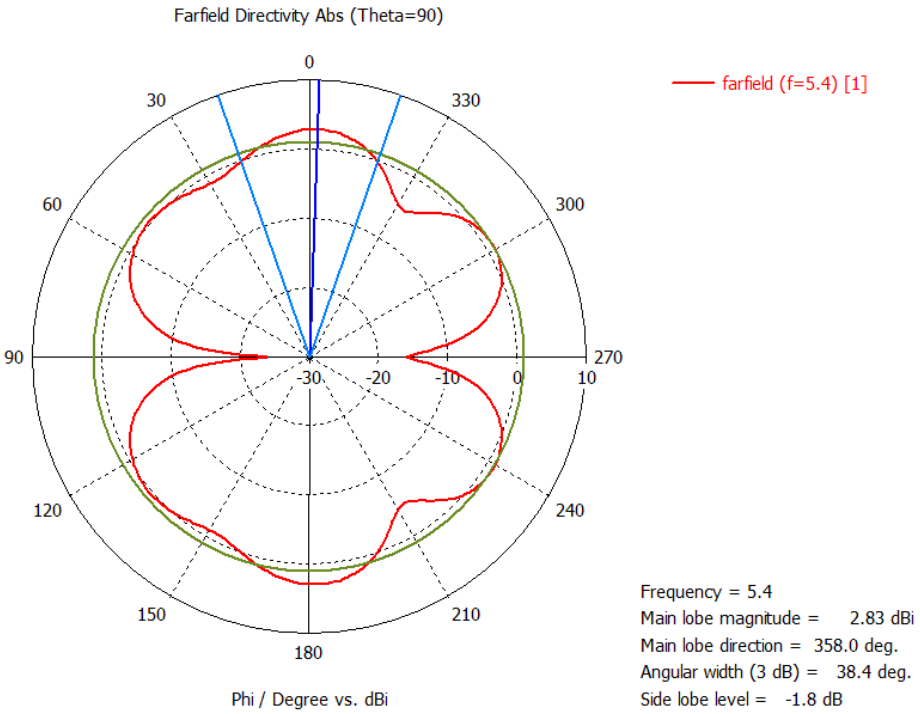

Fig. 18 Radiation pattern in XY plane

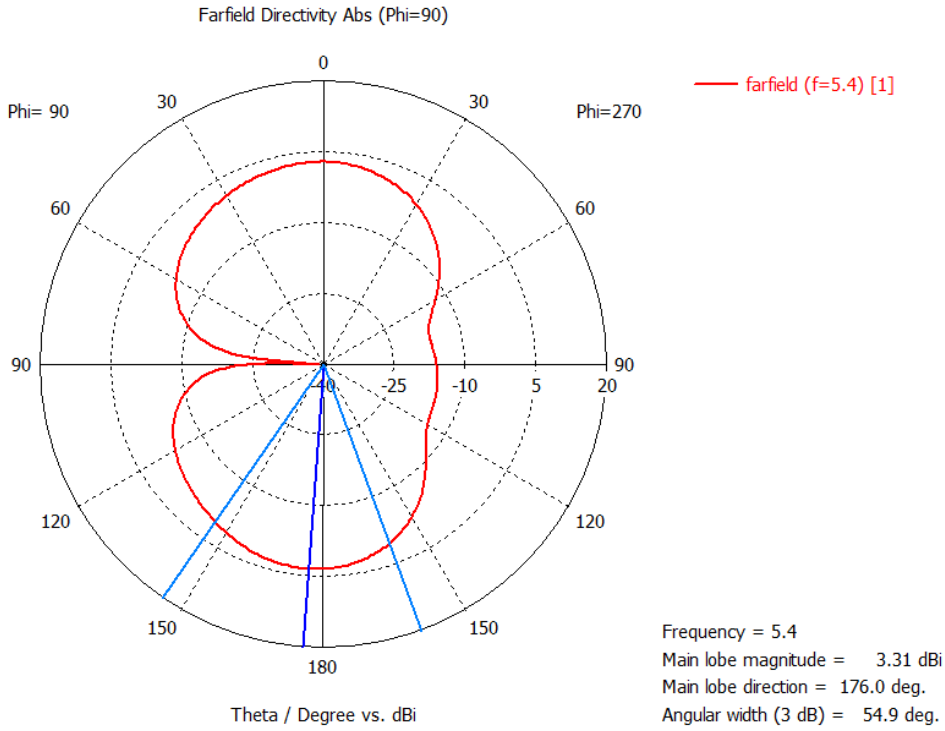

Fig. 19 Radiation pattern in YZ plane at 5.4 GHz

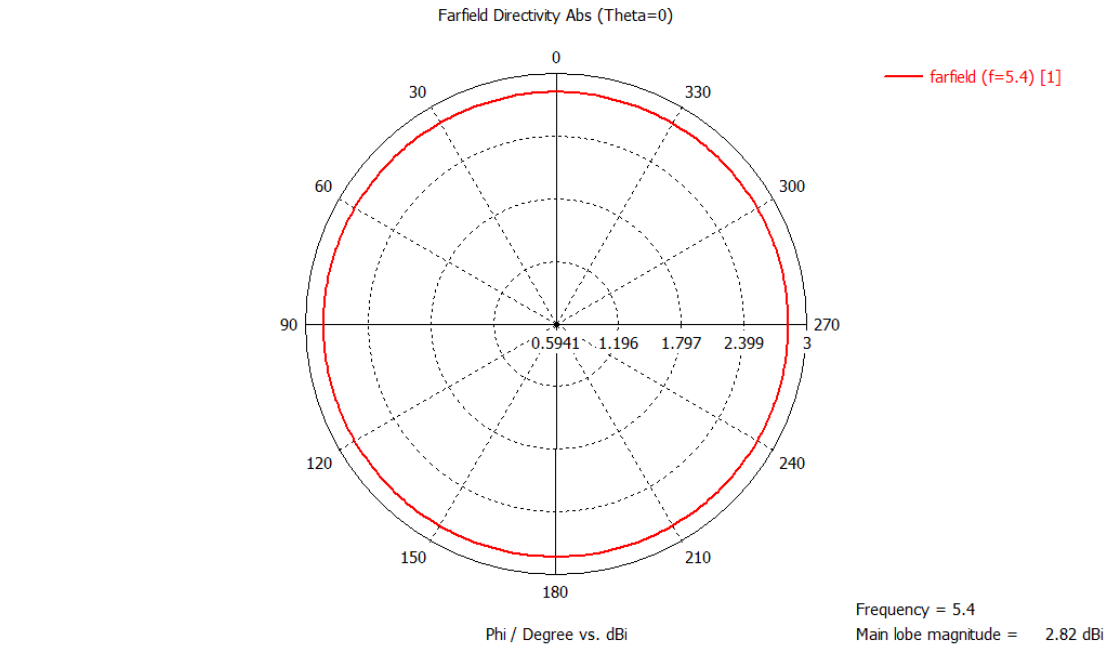

Fig. 20 Radiation pattern in XZ plane at 5.4 GHz

4.4 Slot antenna

Printed slot antennas have several advantages over the conventional microstrip antennas. They have a wider bandwidth and enable realization of bidirectional and unidirectional radiation patterns. Furthermore, slot antennas are less sensitive to manufacturing tolerances than the conventional microstrip antennas. Slot antennas have earlier been discussed in section 3.3.

With a careful choice of the dimensions of the slots and fingers, these resonances can be merged together over the operating band and consequently the antenna can be used over a very wide bandwidth.

4.4.1 Half wavelength (λ/2) slot antenna

A half wavelength λ/2 slot antenna is a slot antenna in which the total length of the slot is roughly

half of the wavelength of the frequency desirably used. The wavelength λ can be calculated using the following formula:

$$\lambda = \frac{c}{f}$$

where,

λ= Wavelength, in meters

c= speed of light, $3x10^8$ m/s

f= desired matching frequency, in Hz

Using the formula, the wavelength for the 2.4 GHz frequency was calculated and it was found to be 62.5 mm.

Positioning of the slot is crucial for the efficiency of a microstrip antenna. It can be evaluated by the output characteristics of a slot antenna. The simulations can be made with a fixed feeding point and two types of slot shapes. The slot positions can be varied from one edge of the radiating conductor (AB), while moving towards the feeding point. The gain is maximum when the vertex of the slot is almost above the feeding point, but gain value falls drastically as the vertex crosses the feeding point. A similar nature is shown by return loss and bandwidth. It may be concluded that if the slot (irrespective of shape) is moved towards a fixed feeding point along the x axis (without moving in Y axis), then the antenna gives a maximum bandwidth and gain with slot is placed near the feed point. Return loss values though may differ in the location of their maxima and minima from slot to slot and depending on their resonant frequencies.

The exact half wavelength for the antenna to be matched at 2.4 GHz when calculated using formula mentioned on the previous page turned out to be 31.25 mm thus the slot length has to correspond to this length. A simple slot antenna was designed using the given specifications. The design can be seen in figure 21a and 21b. In 21a, the slot is situated at the middle of the slot. In Fig. 21b, the slot has been shifted towards the right of slot by a distance of 27.55 mm from the middle of the slot.

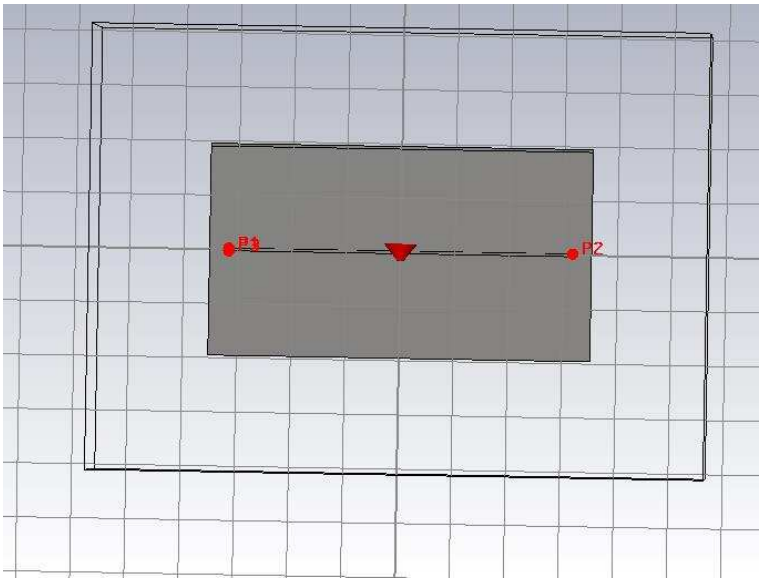

Fig. 21a. λ/2 slot antenna with the port in the middle

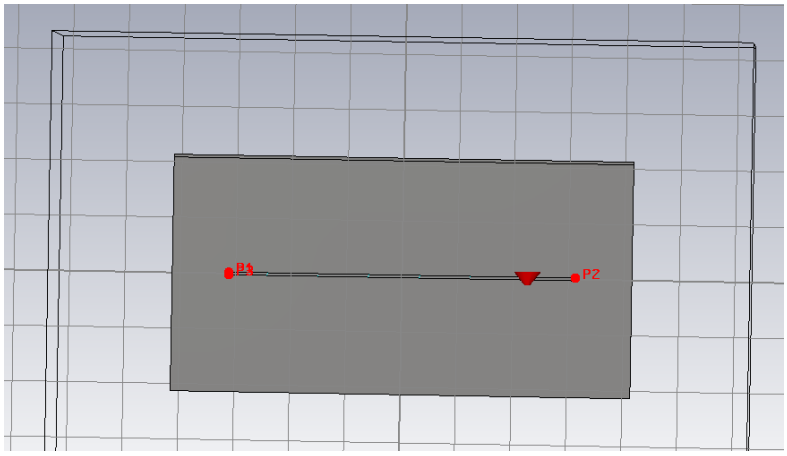

Fig. 21b. λ/2 slot antenna with the slot at a distance of 25.55 mm right of middle

S. No.	Component specification	Measurement
1	Width	40.70 mm
2	Height	36.25 mm
3	Slot length	31.77 mm
4	Slot width	0.28 mm
5	Distance of the port from center	25.55 mm

Table 3 Design specification table

4.4.2 S parameters and surface currents

The S_{11} parameter of the antenna can be seen in the figure 22. The antenna is not very well matched at the frequency of 2.4 GHz and the parametric analysis, as seen in figure 23 denotes an ill matched antenna which remains unable to harness RF at higher levels.

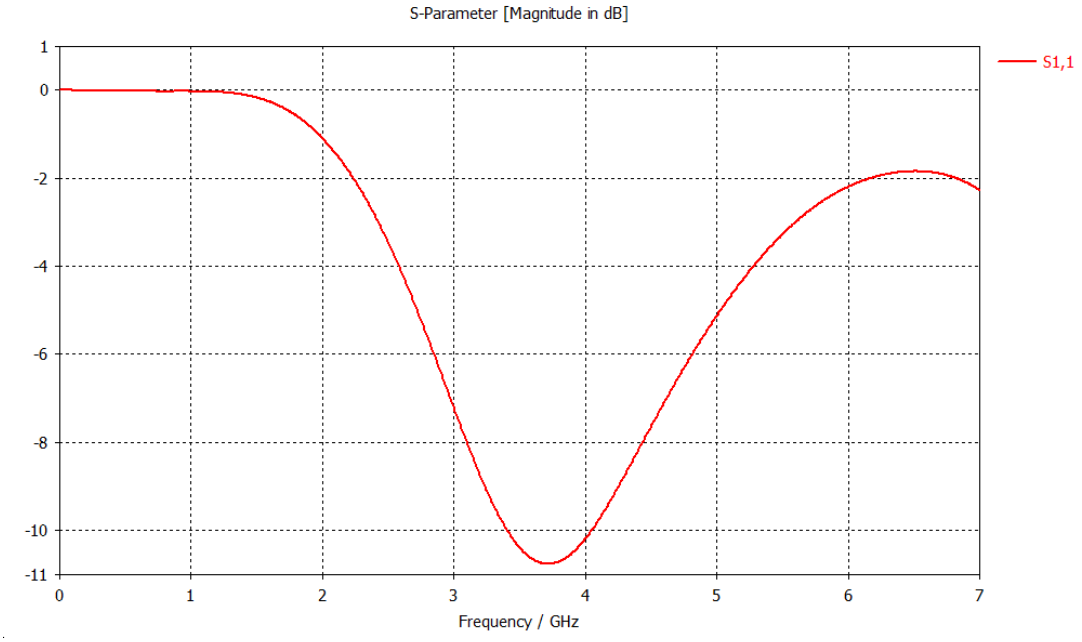

Fig. 22a Results for the half wavelength antenna with the port at the middle

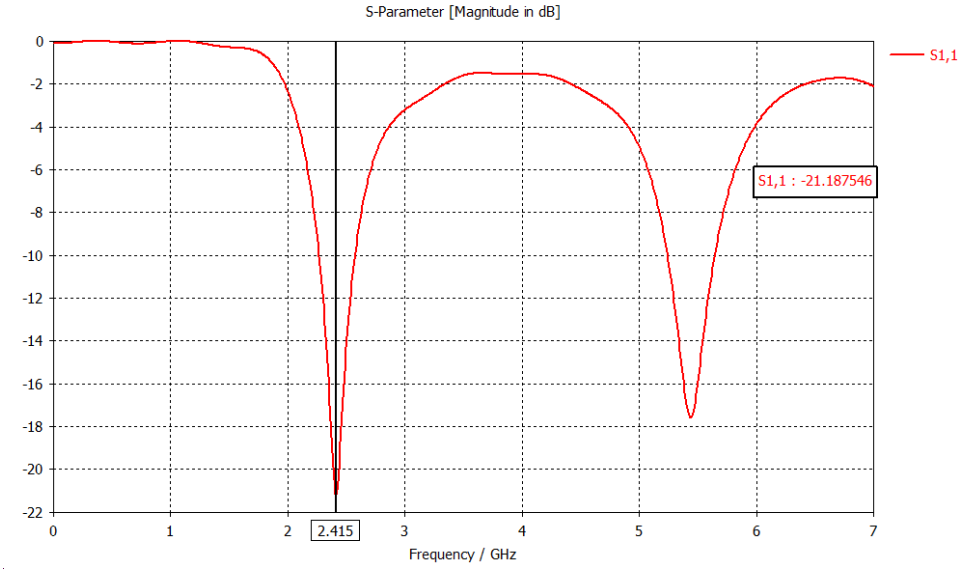

Fig. 22b S_{11} parameter results

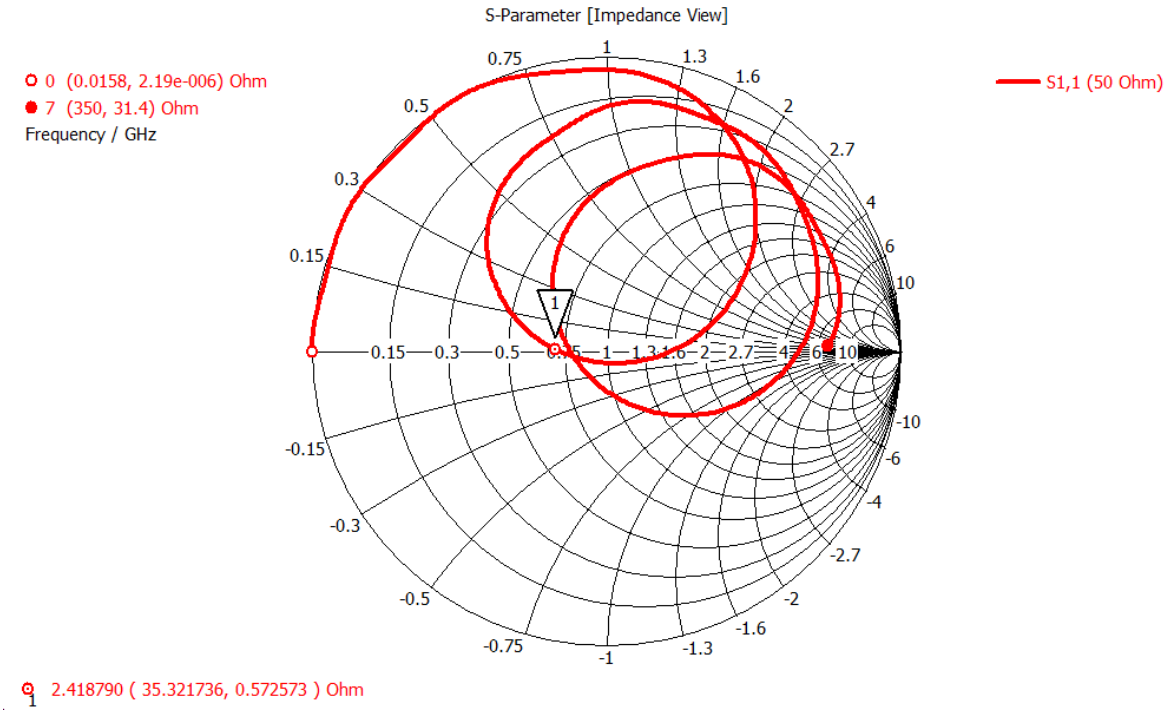

Fig. 22c Smith chart simulation

The fig. 23(a & b) gives us an idea of the level of matching we may achieve with the parametric analysis and using the stepping-up technique of the antenna designing. Figures 23a and 23b give us the parametric analysis with varied width and length. The matching at 2.415 GHz improves drastically and the match gives the best trough depth of -30.31 dB. The -10dB bandwidth of 0.088 provides a very narrow band which would hinder the harvesting of a wider band of frequencies. Fig. 24 shows the surface currents of the antenna.

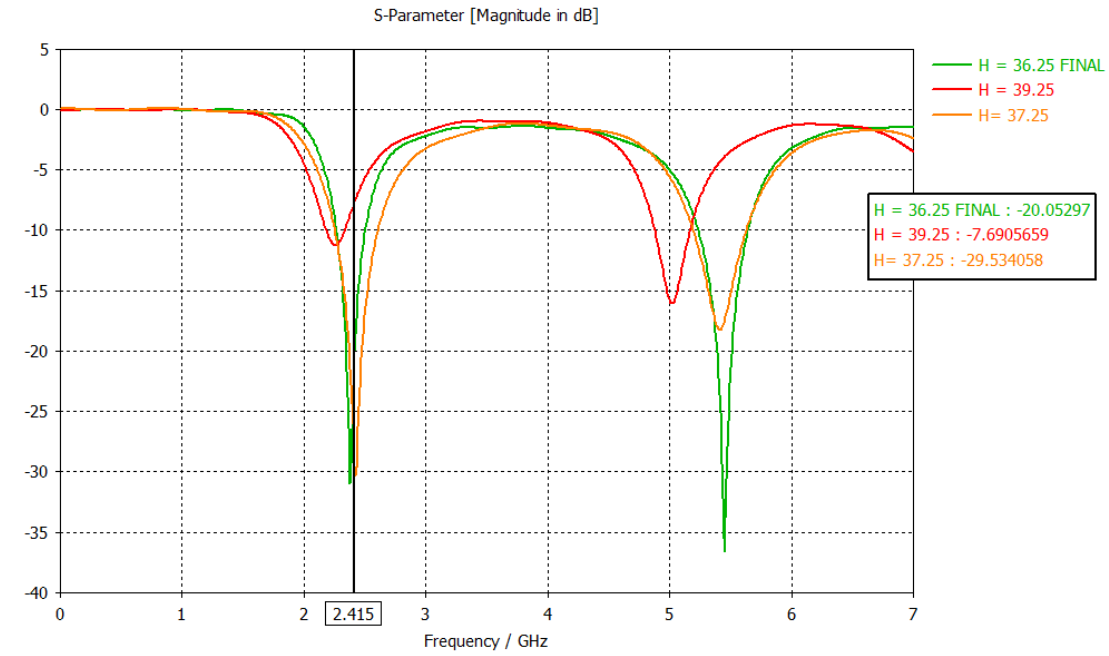

Fig 23a parametric analysis by varying the heights

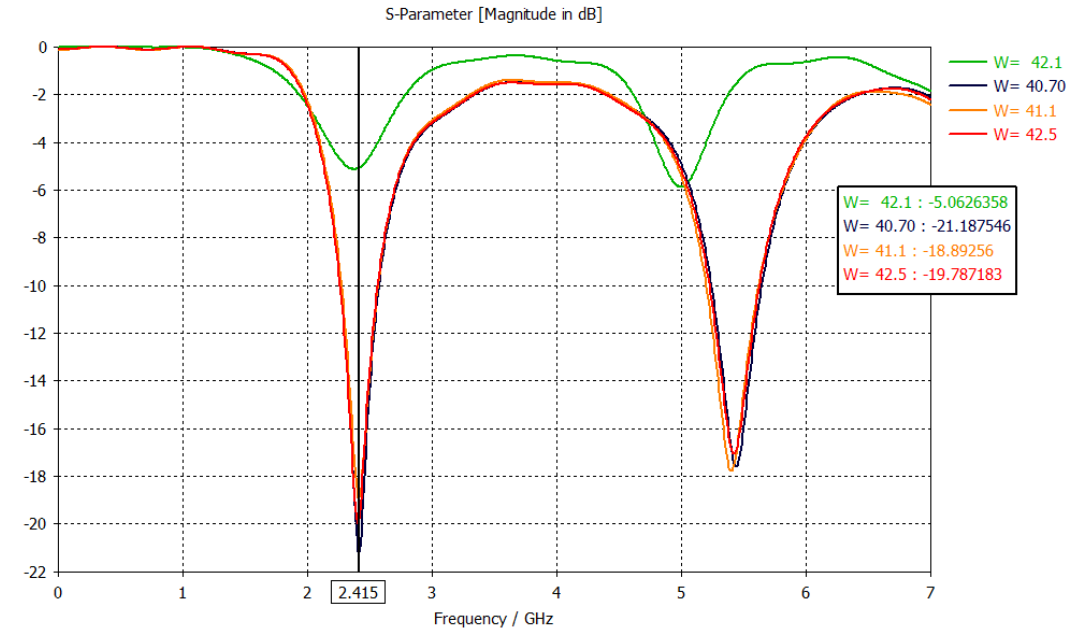

Fig. 23b parametric analysis by varying the width

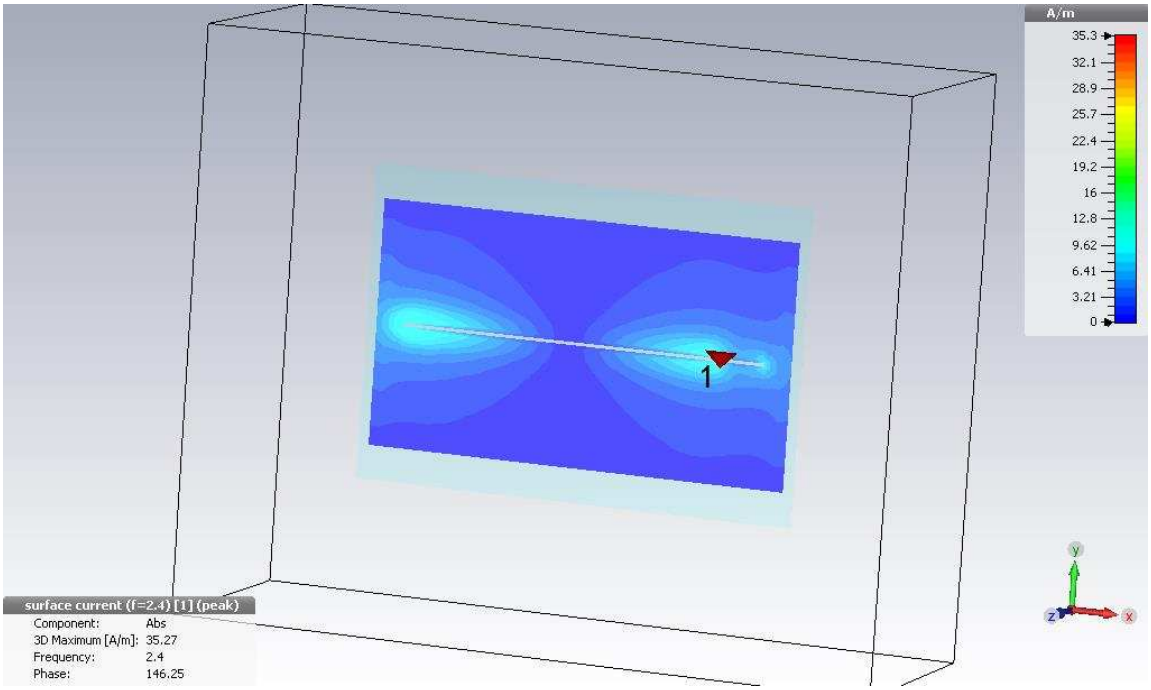

Fig. 24 Surface currents in the λ/2 antenna

4.4.3 Radiation patterns

The radiation patterns of the antenna can be seen in the figures below (25 a-d). The figure 25a depicts the 3D farfield radiation pattern of the antenna. In fig. 25a, the directional properties of the slot antenna become clearly visible. The maximum directive gain was simulated to be 5.475 dBi. The antenna obtained its highest gain at its centre along the Z-axis.

In Fig. 25 b, c & d, the radiation patterns are displayed for XY, YZ and XZ planes respectively. These patterns reconfirm the directional properties of the antenna.

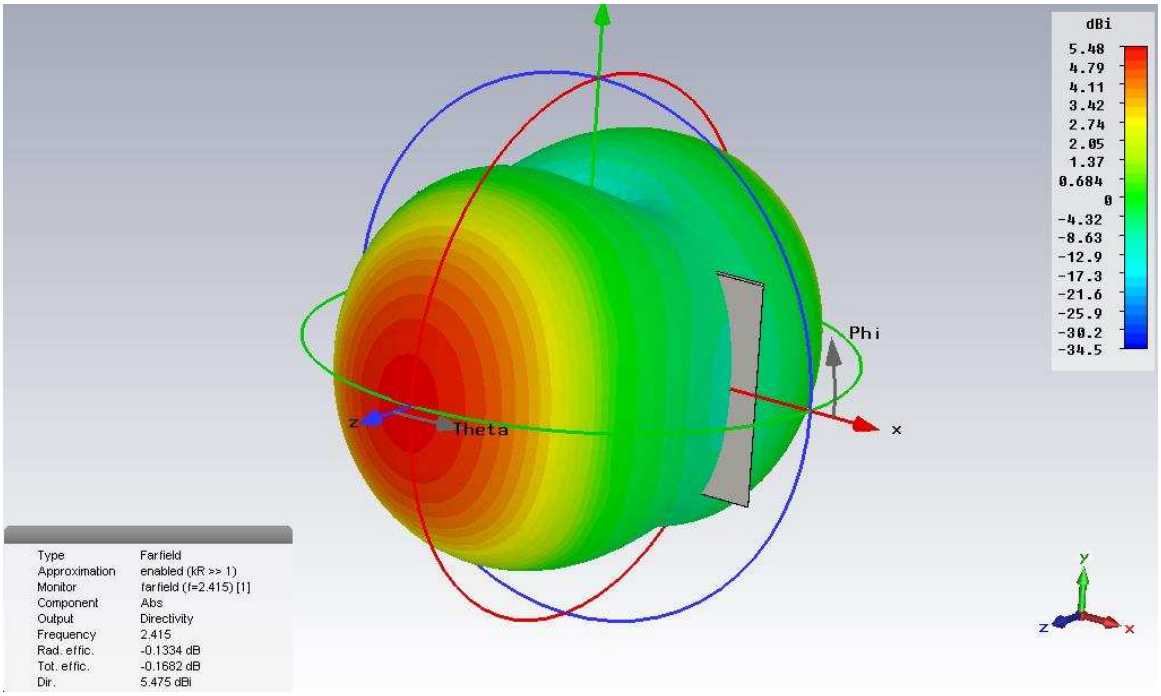

Fig. 25a 3D farfield results of the antenna

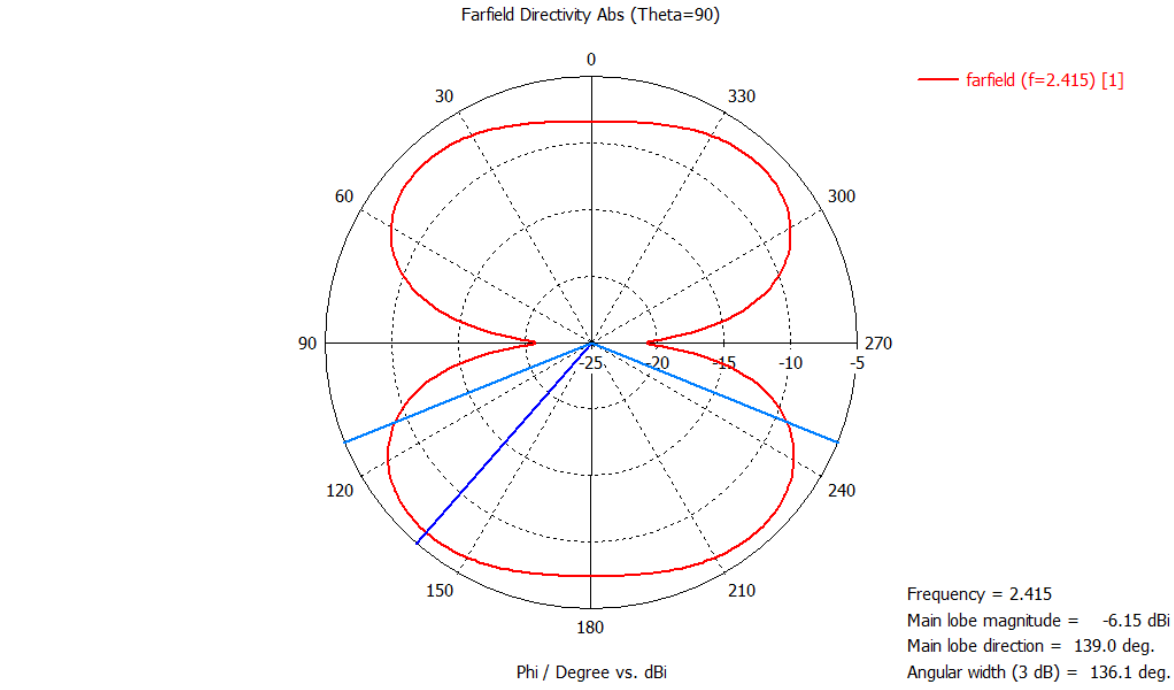

Fig. 25b Radiation pattern in the XY plane

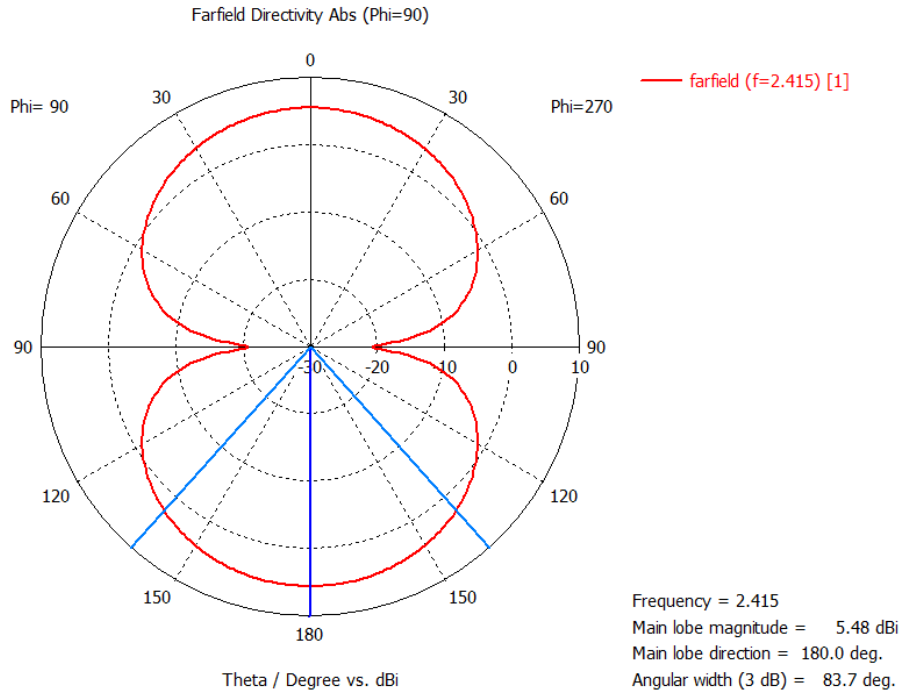

Fig. 25c Radiation pattern in YZ plane

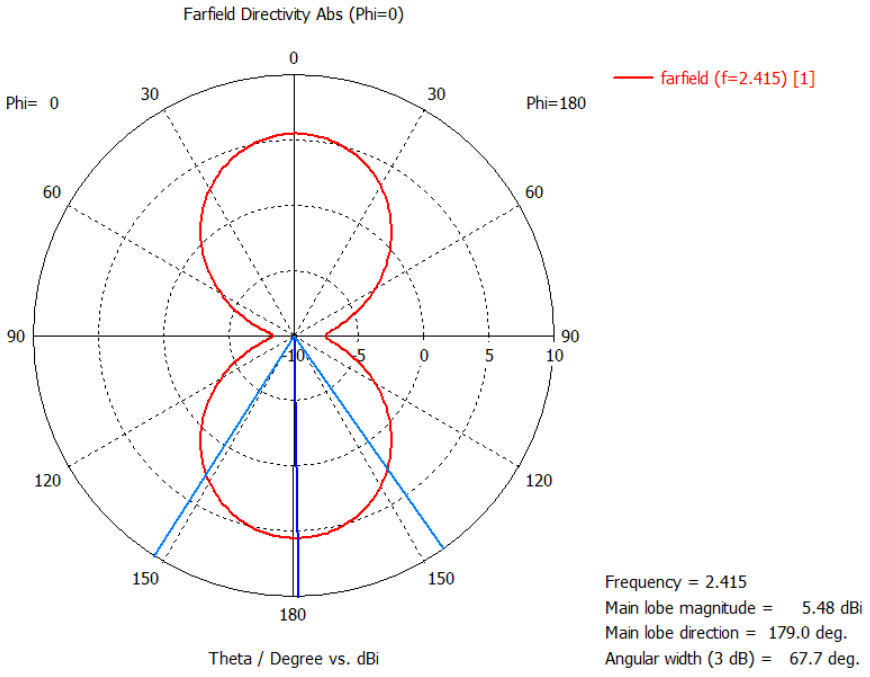

Fig. 25d Radiation pattern in XZ plane

4.4.4 full wavelength (λ) slot antenna

Theoretically, by feeding a λ/2 slot near an edge by a microstrip line, the magnetic current distribution (electric field along the slot) can be manipulated to create a null near the feed point which produces a second resonance mode with a frequency slightly larger than that of the first one. When appropriately fed, these two resonances can merge and result in an antenna with a much larger bandwidth or two separate bands of operation with similar radiation characteristics. Microstrip-fed, slot antennas were theoretically and practically studied.

Also, experimental investigations on very wide slot antennas are reported by various authors [2]–[5]. The drawback of these antennas are: 1) they require a larger surface areas for the slot and a much larger area for the conducting plane around the slot and 2) the cross polarization levels change versus frequency and is relatively higher at certain frequencies in the band [2]–[4], and [6]. This is mainly because of the fact that these antennas can support two orthogonal modes with close resonant frequencies. The advantages of these antennas is that their wide-band element can be used as a building block in design of multi-element antennas that can generate larger overall bandwidths with lesser number of radiating elements and much smaller size than the existing multi-element antennas such as log-periodic arrays etc.

To create the full λ-wavelength slot antenna, a simple slot antenna design was selected and the layout of the same can be seen in the figure 26 and 27 below. The total length of the antenna was 98 mm and the total width of the antenna was 60 mm. The length of the slot however was 96 mm and the width was 1 mm. The thickness of the mylar substrate used in designing the antenna was 0.6mm. The HSMS 2862-079 diode was used at the port. The diode has been discussed in section 3.3.

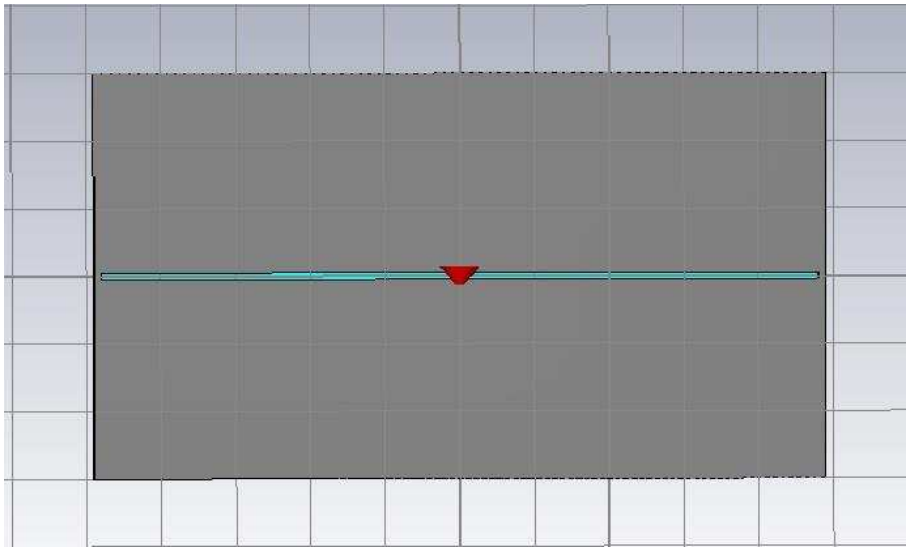

Fig. 26 Front of the 50-Ohm slot antenna

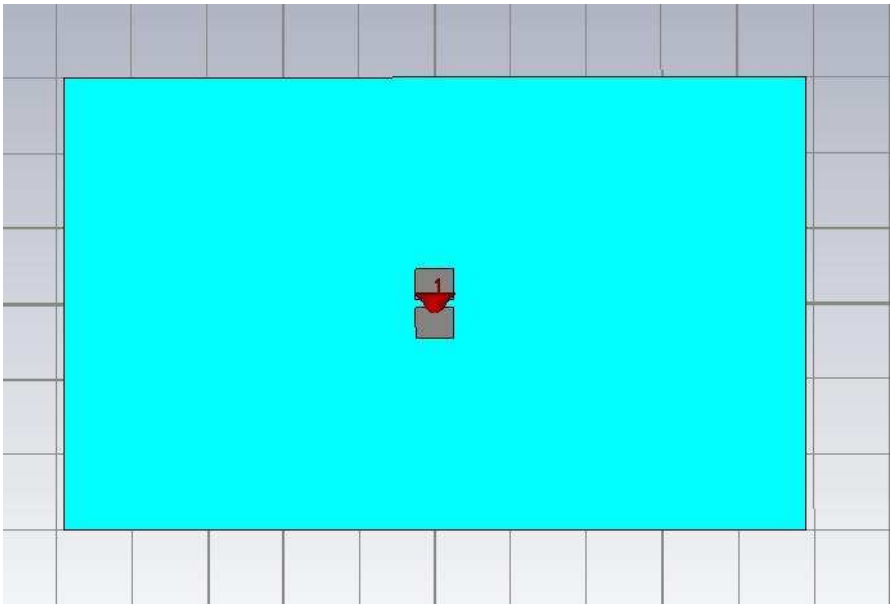

Fig. 27 Backside of a slot antenna

4.4.5 S-parameters:

The S-parameter simulations for the design can be seen below. The antenna here has been matched at value of -25.06 dB at 2.415 GHz. A bandwidth of 0.185 made this antenna very much suitable for the purpose of energy harvesting.

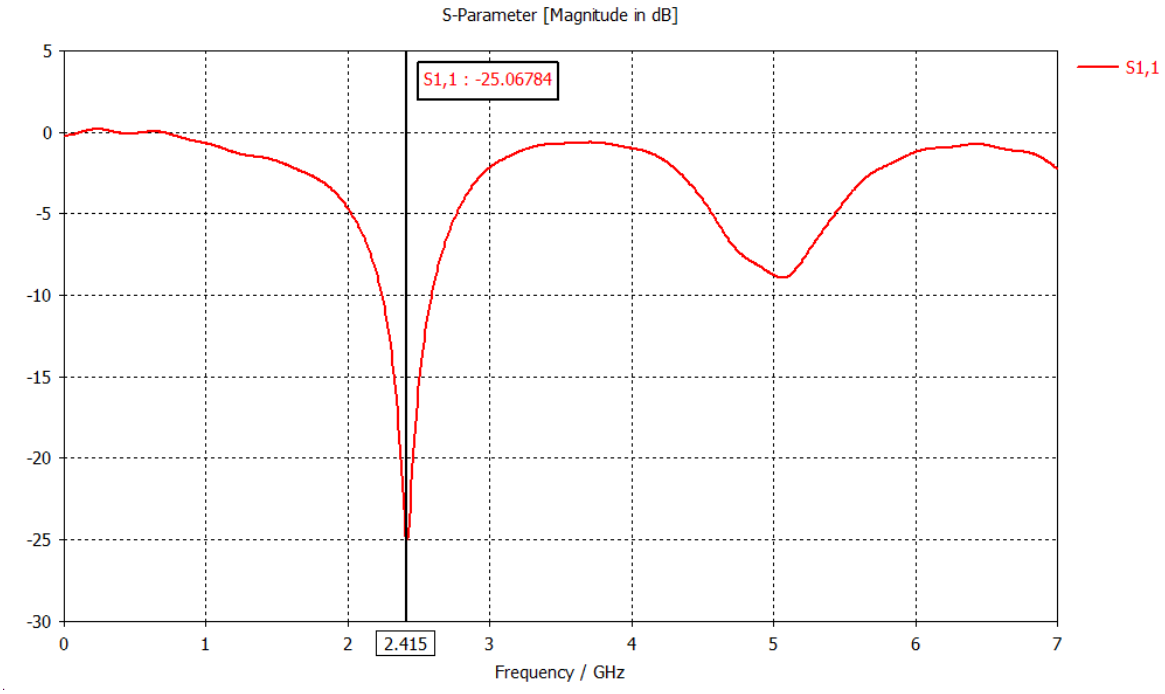

Fig. 28 S-parameters of the slot antenna

4.4.6 Parametric analysis:

The parametric analysis of the slot antenna can be seen in the figures 29a,b and c below. Figure 29a denotes the analysis while varying the height, figure 29b denotes the analysis by varying the width, figure 29c denotes the analysis with varied slot length.

In the graphs below,

A – Width of the antenna

B – Height of the antenna

S- Slot length of the antenna

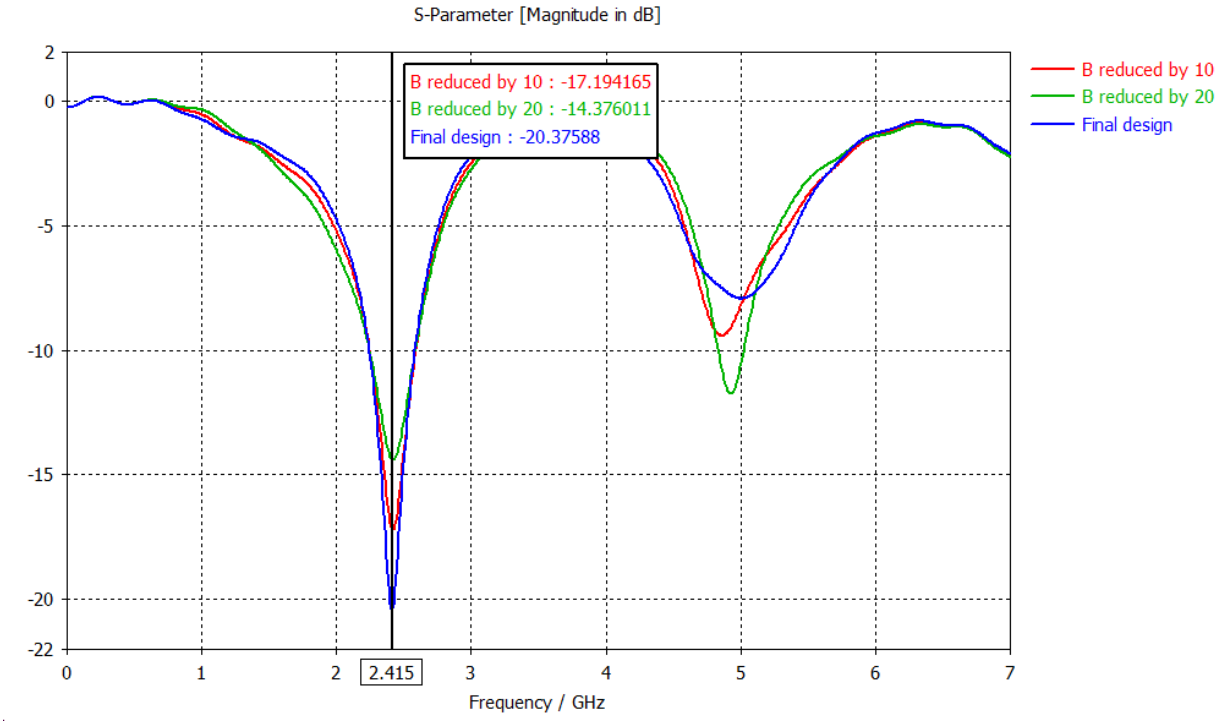

Fig. 29a parametric analysis while varying the height

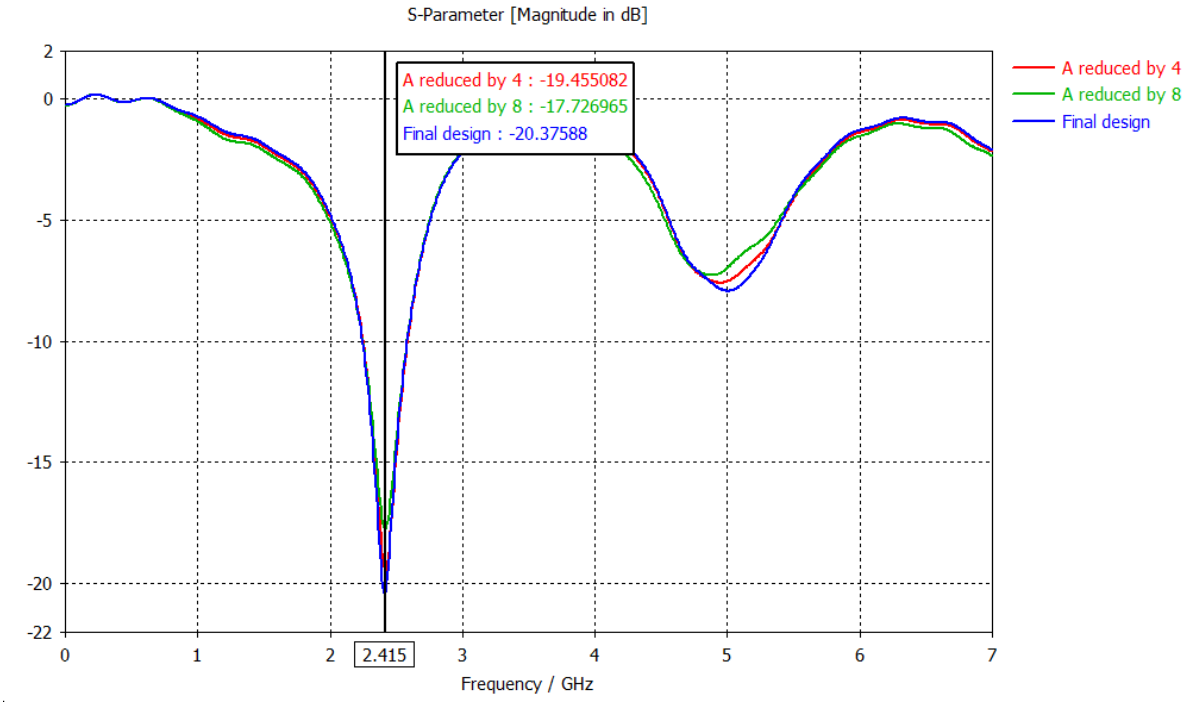

Fig. 29b parametric analysis while varying the width

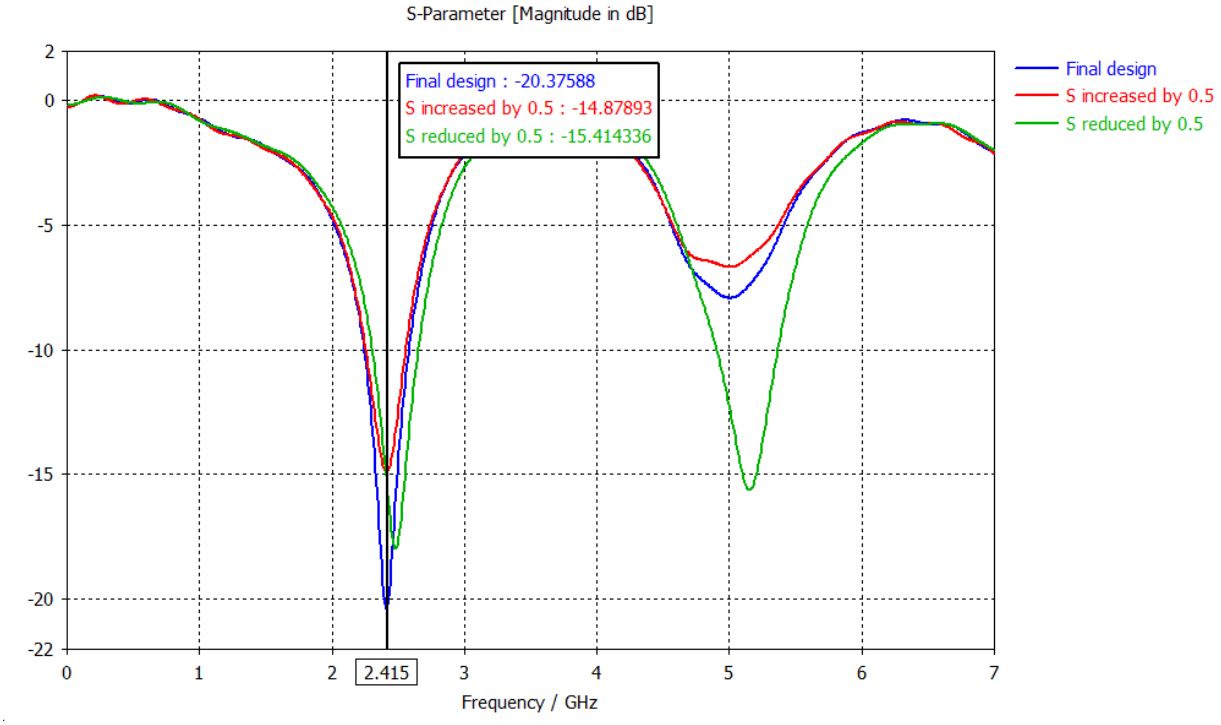

Fig. 29c. Parametric analysis while varying the slot length

4.4.7 **Surface currents**:

The surface currents for the 50-Ohm slot antenna can be observed in Fig. 30. It denotes 2 different modes as expected with the usage of a full wavelength, λ slot antenna. The peak value of current is expectedly observed at the edges and right at the middle position of the port where the diode was placed.

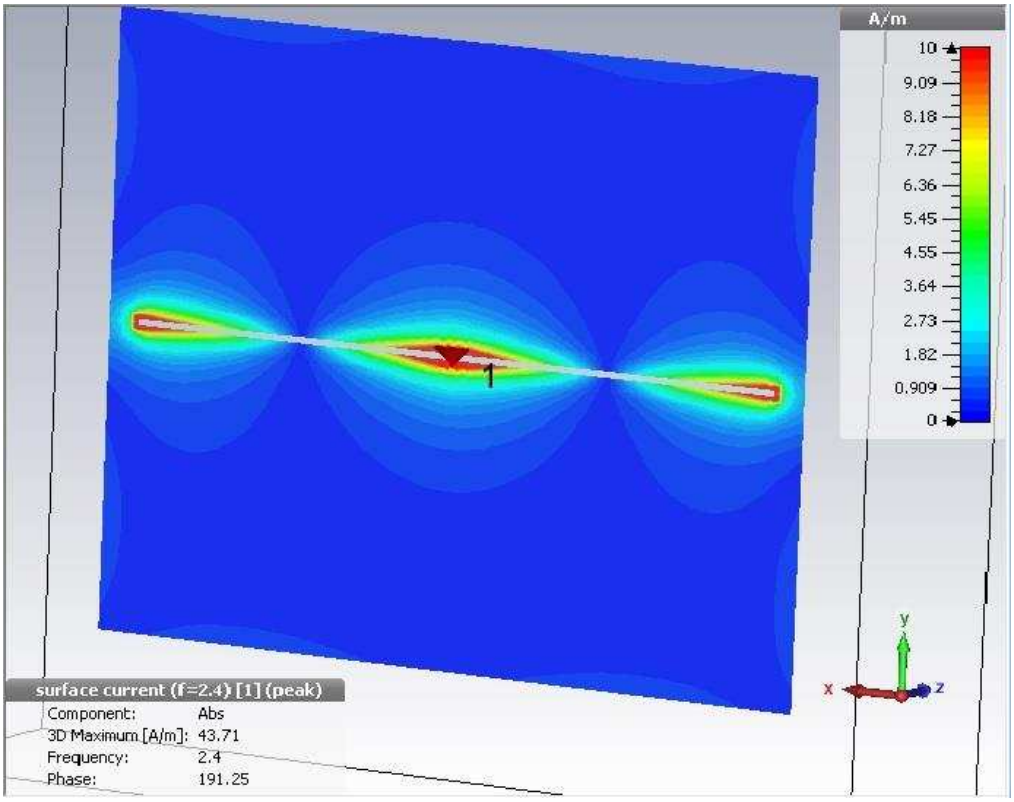

Fig. 30 Surface currents of the 50-Ohm slot antenna

4.4.8 Radiation patterns

The radiation patterns from Fig. 31 denote the directional properties of the antenna. As expected, the 3D Farfield pattern attains its maxima in line with the location of the port and the antenna has a Dir. Gain of 6.625 dBi. The Polar 2D patterns (Fig. 32-34) also point to the same with directional plots.

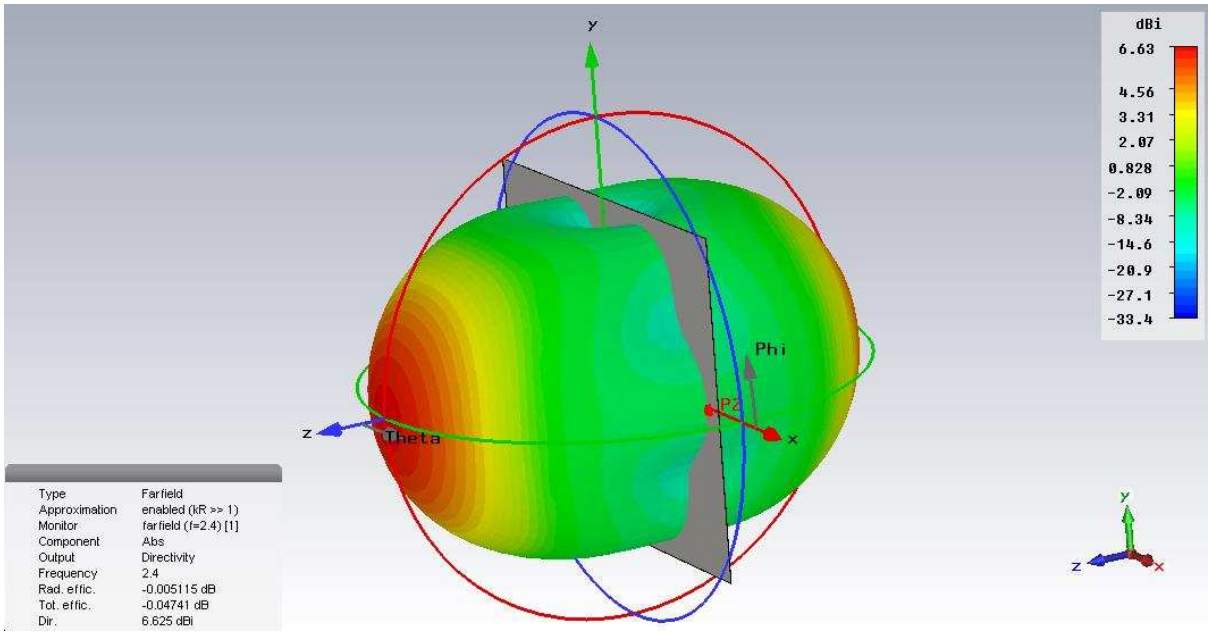

Fig.31 Farfield Radiation pattern

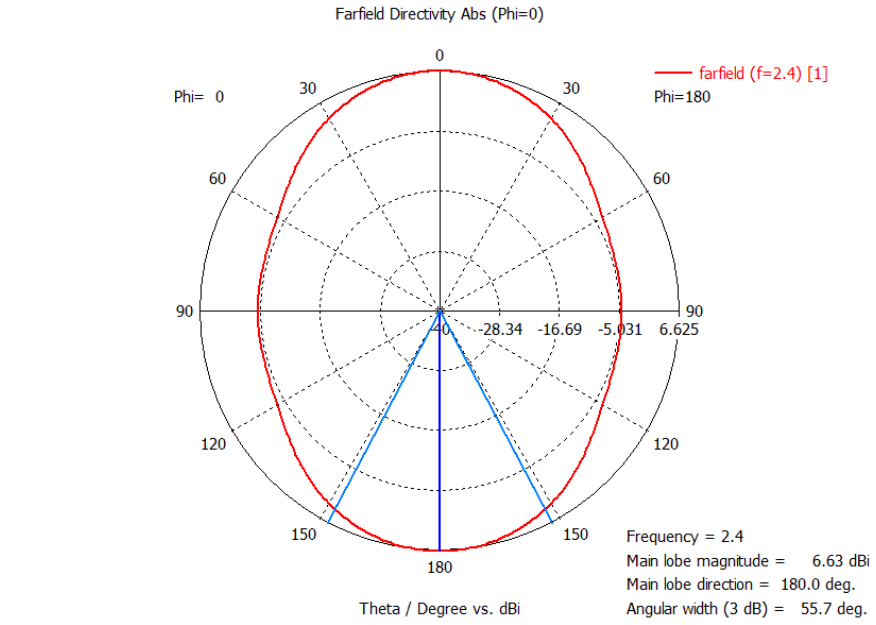

Fig. 32 Radiation pattern – xz plane

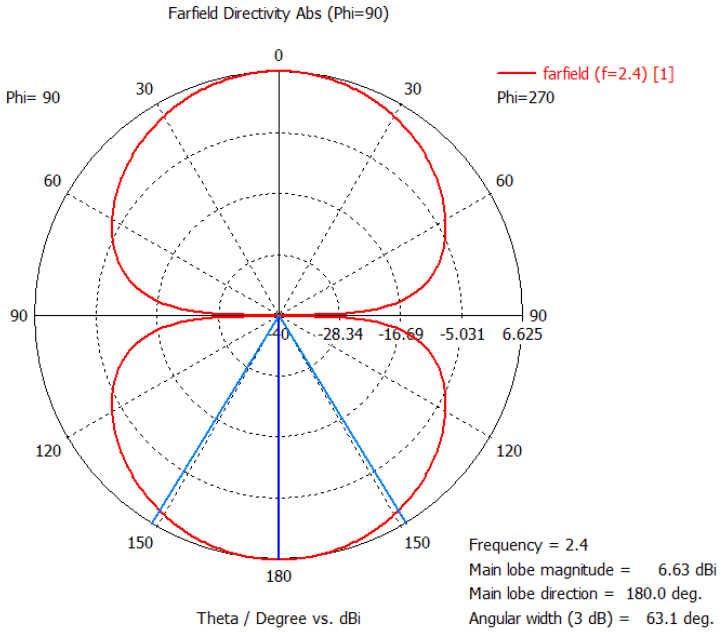

Fig. 33 Radiation pattern – yz plane

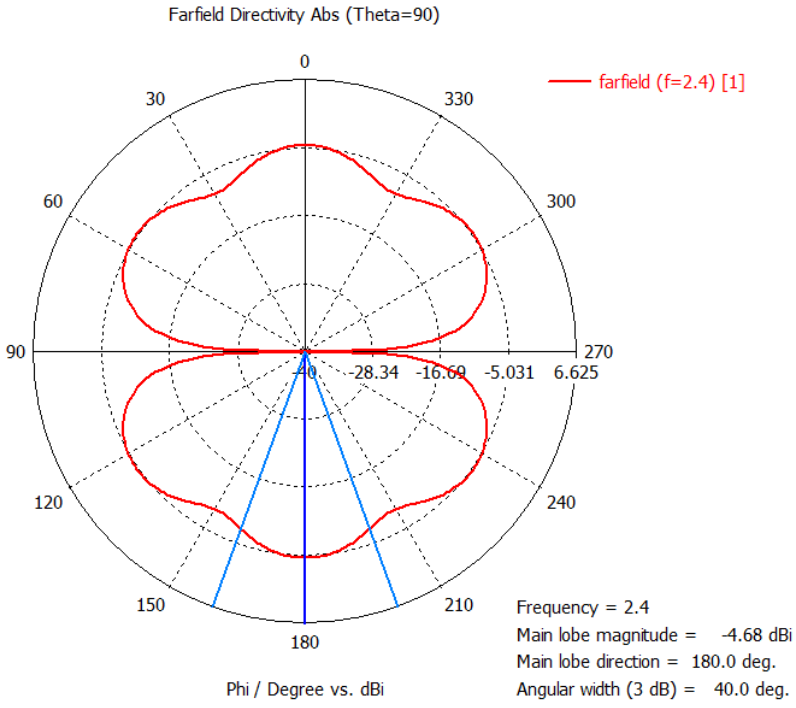

Fig. 34 Radiation pattern in XY-plane

It is possible to designs the slot antenna to match the impedance of a rectifier. Both real and imaginary part need to be matched. As an example, a design has been matched for the 20-Ω of the HSMS 7630-079 diode, the chip has been discussed in section 3.4. It should be noted that the imaginary part should also be matched. There is no information available from the manufacturer regarding the complex impedance of the chip. A process to create a matching circuit for a typical 50 ohm input impedance is described in the following chapters.

A slot antenna with wider dimensions was also simulated to compare the difference in matching with a bigger antenna. The results are shown below in Fig. 35-37. Although the antenna gave a wider bandwidth, the cost efficiency of the antenna due to its huge size and cumbersome aperture demoted the feasibility of the design as a cost efficient antenna for energy harvesting purposes.

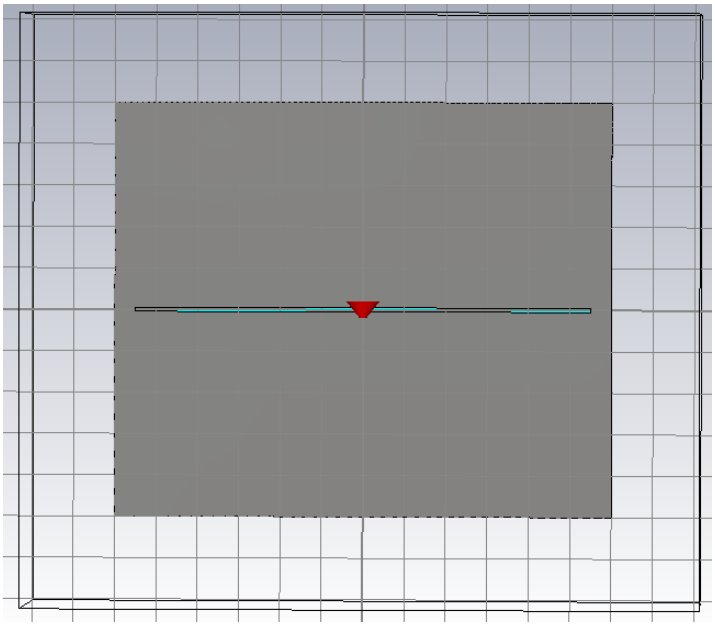

Fig. 35 front of the 20 Ohm slot antenna with wider dimensions (120mm X 100mm)

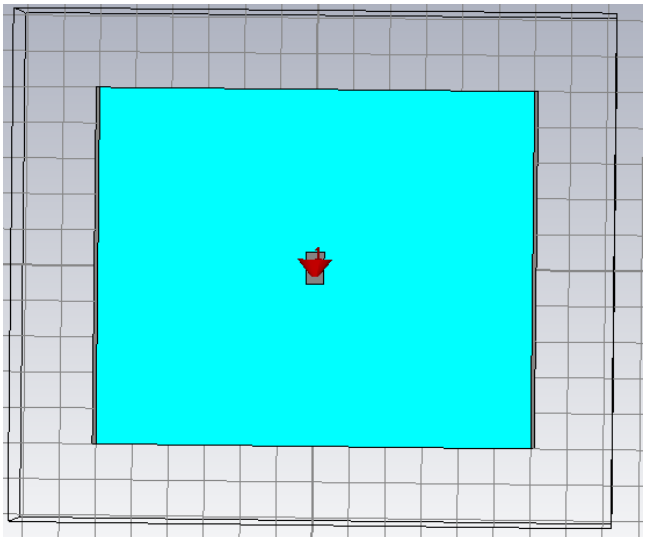

Fig. 36 Backside of the same antenna

S. No	Parameter	Dimensions
1	length of the antenna	120 mm
2	Width of the antenna	100 mm
3	length of the slot	114.75 mm
4	Width of the slot	1.25 mm

Table 4 Dimensions of the slot antenna with larger dimensions

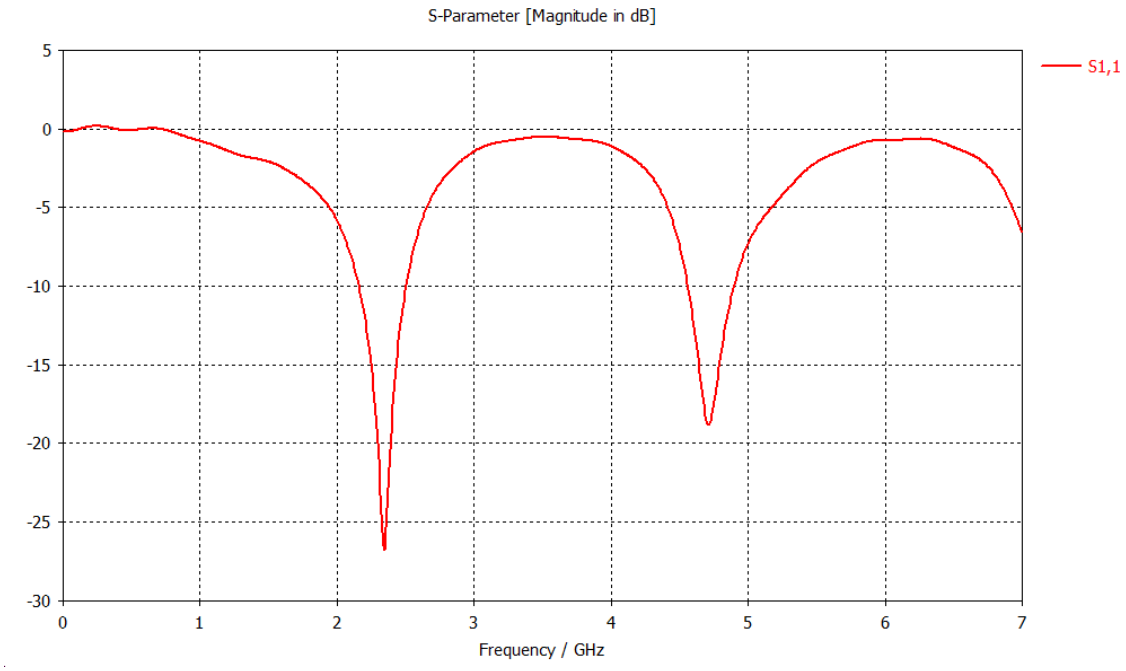

Fig. 37 S-parameter results

Conclusion:

Various antennas are discussed in this chapter. Their S_{11} patterns at 2.4 GHz are shown and along with that, their surface currents and radiation patterns were denoted and discussed in the sub-sections. The chapter started with the discussion on dipole antennas and continued into UWB antennas and slot antennas. The chapter gradually demonstrated the S-parameters along with the surface currents and the radiation patterns along with the discussion involving the antenna which were considered during the construction of this thesis.

The section 4.1 defined the goals which were set while exploring the antennas and the expectations which were present from every antenna which was evaluated. The requirements of a wideband

antenna working at the WiFi frequency and with a very good matching at 2.4 GHz or nearest to that was discussed.

In section 4.2, the dipole antennas were discussed. A half-wave dipole antenna was designed and simulated. The S_{11} simulations results of the half-wavelength dipole antenna had a significantly good matching of -31.67 dB at 2.41 GHz. The 3D farfield radiation pattern demonstrated the omnidirectional properties of the antenna and the directive gain of the antenna was simulated to be 2.357 dBi. The omnidirectional gain of the antenna was simulated to be 2.34 dBi. However, due to a very narrow bandwidth and balun properties of the antenna, it was not very suitable for the purpose of energy harvesting.

In section 4.3, the Ultra-Wide-Band (UWB) antennas were discussed. The main advantage of using a UWB antenna as the name suggests, has a very wide band of -10dB passband frequency. The matching was simulated at as -27.14 dB at 2.4 GHz and went as low as -33 dB for higher frequencies. The surface currents distributions at 2.4 GHz and 5.4 GHz were displayed. The distribution patterns at 2.4 GHz were more even and uniform across the inner edges of the feedline and the ground planes. At 5.4 GHz however, the distribution wasn't as even and uniform as it was for 2.4 GHz. The 3D farfield results denoted the directional properties of the antenna with a directive gain of 2.723 dBi achieved. The omnidirectional properties along the XZ plane radiation pattern can be observed with a lobe magnitude of 2.82 dBi. The antenna was fabricated and tested and the results would be compared and discussed in chapter 8.

Section 4.4 dealt with the slot antennas. The section was divided into two sections which dealt with λ/2 wavelength slot antenna and λ-wavelength slot antenna respectively. In the chapter where λ/2 antenna was discussed, two antennas were compared which were same in dimensions but the positioning of the port was different. In the first design, the port was placed in the middle of the slot and in the second one, the port was moved to the side of the slot. The design in which the port was displaced by 25.55 mm from the center of the slot (Fig. 27b) gave a matching of -21.18 dB at 2.415 GHz. The middle positioning of the slot gave no match whatsoever at the desired frequency. A parametric analysis was done for the antenna and the main criteria, the length of the aperture and the height of the antenna aperture were varied and the results were thus examined which were on display (Fig 36a-c). The variation in matchings and positioning of a match with changes followed a familiar pattern. Reducing the height reduced the quality of the match and moved the matching to the left and the right of the desired frequency. Increasing the height moved the match to the right of the desired frequency hence giving a match at a higher frequency and decreasing the height resulted in a match towards the left of the desired frequency at a lower value. In case of length, the analysis

followed the pattern of improved and unimproved match with the changes in frequency. The reducing the length reduced the matching. When the slot length was analysed, the simulation displayed some very intriguing results (Fig. 36c). The matching worsened at the frequency with both increase and decrease in the length of the slot

References

[1] Z. Zakaria, N. A. Zainuddin, M. Z. A. Abd Aziz, M. N. Husain, and M. A. Mutalib, "Dual-band monopole antenna for energy harvesting system," in Proc. of IEEE Symposium on Wireless Technology and Applications (ISWTA), Kuching, Malaysia, Sept. 2013.

[2] B. I. Pham, and A.-V. Pham, "Triple bands antenna and high efficiency rectifier design for RF energy harvesting at 900, 1900 and 2400 MHz," in Proc. of IEEE MTT-S International Microwave Symposium Digest (IMS), Seattle, WA, June 2013.

[3] D. Masotti, A. Costanzo, and S. Adami, "Design and realization of a wearable multi-frequency RF energy harvesting system," in Proc. of IEEE European Conference on Antennas and Propagation (EUCAP), pp. 517-520, Rome, Italy, April 2011.

[4] S. Keyrouz, H. J. Visser, and A. G. Tijhuis, "Multi-band simultaneous radio frequency energy harvesting," in Proc. of IEEE European Conference on Antennas and Propagation (EuCAP), pp. 3058-3061, Gothenburg, Sweden, April 2013.

[5] D. Yi, and T. Arslan, "Broadband differential antenna for full-wave RF energy scavenging system," in Proc. of IEEE Antennas and Propagation Conference (LAPC), pp. 325-328, loughborough, UK, Nov. 2013.

[6] A. Buonanno, M. D'Urso, and D. Pavone, "An ultra-wide-band system for RF Energy harvesting," in Proc. of IEEE European Conference on Antennas and Propagation (EUCAP), pp. 388-389, Rome, Italy, April 2011.

Chapter 5

Designing the equivalent circuit of the antenna

5.1 Finalised CST antenna design

In chapter 4, the selection of the antenna using CST as a tool was discussed. The λ-wavelength slot antenna was selected. The antenna (Fig. 1) gave a significantly good match with a wider bandwidth which is ideal for the purpose of energy harvesting. The matching results can be seen in Fig.2.

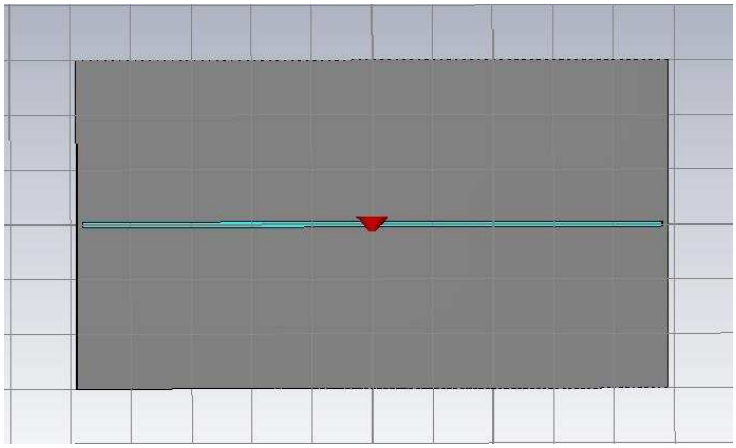

Fig. 1 Selected slot antenna design

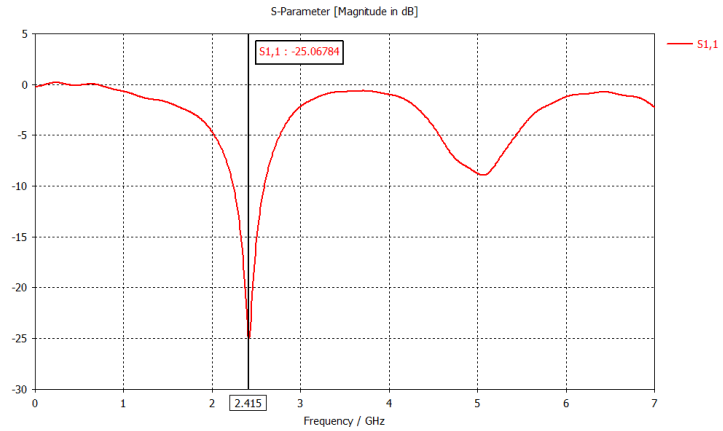

Fig. 2 the S-parameter match of the antenna with the matching at 2.415 GHz

Once the optimised antenna was finalised in CST, it was then required to export the antenna system to ADS for a real time simulation using an input signal and comparing that with the output of the antenna as well as investigating the changes in the selected input signal to evaluate the working efficiency of the antenna.

The CST antenna was thus converted into a *touchstone* *.s1p file, which is effectively a notepad text file with the numerical data and design information assembled in it. For that, the design impedance was set at 50-Ω and the file was exported to touchstone.

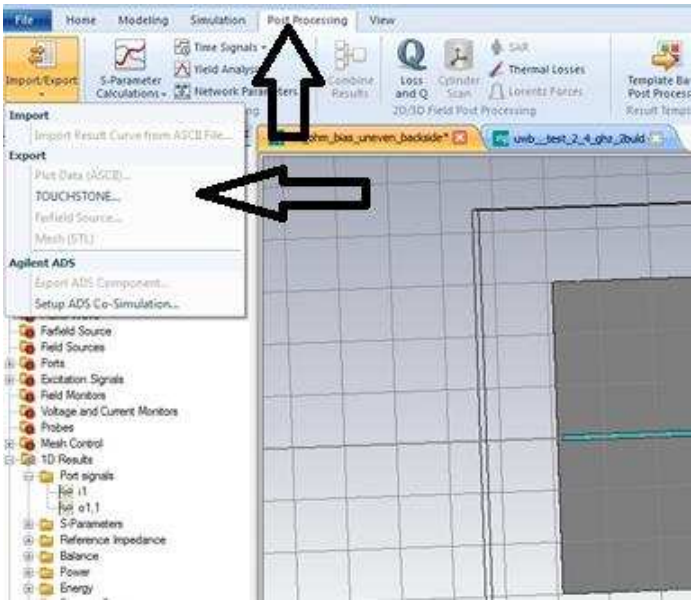

Fig. 3 Steps for the conversion of the file to an s1p file

To use this file in ADS, the s1p component in a schematic design was called and placed. To use the s1p component, the s1p file saved from CST is called from inside the component. The s1p component will then refer to the data stored in the called file and the CST antenna file will therefore be implemented. The component can be seen in Fig. 4 below.

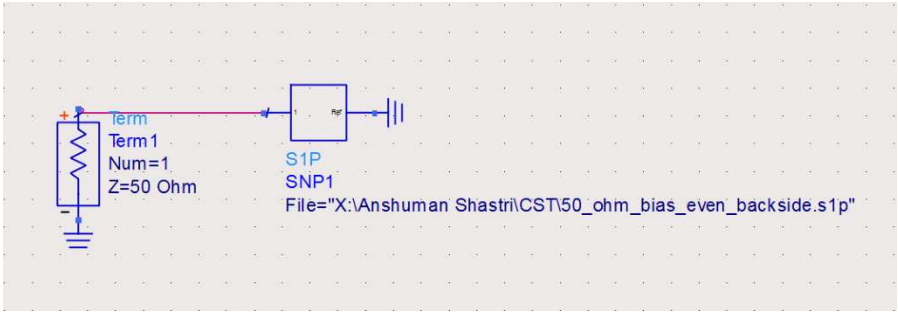

Fig. 4 The s1p component in ADS

Once the component has been placed and the desired file has been called by the component, to simulate the S-parameter properties of the antenna and to verify if the antenna followed the same simulation patterns as it did in CST. For this purpose, we placed a terminal-port of 50-Ω near the antenna and simulate its S-parameter properties via S-parameter component. The results can be seen In Fig.5 below. Fig.5 denotes that the antenna worked perfectly with ADS. The antenna was thus ready to be used in ADS.

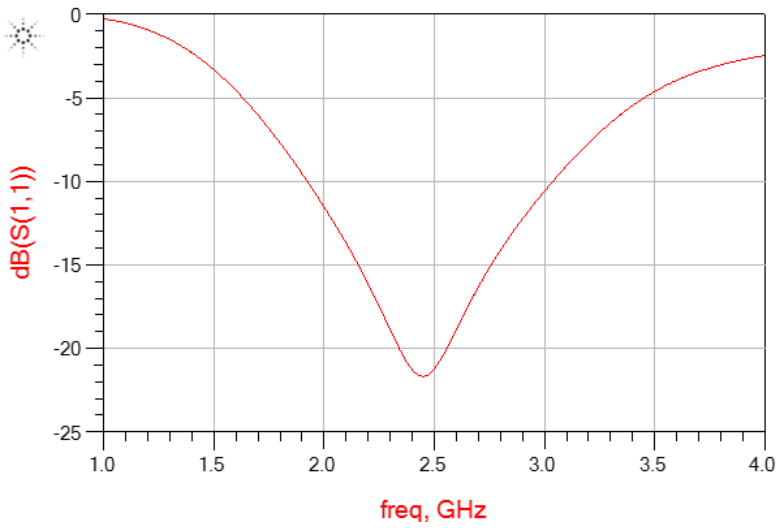

Fig. 5 The S-parameter plot of the antenna

5.2 Development of equivalent circuits

Whenever it is needed to predict how something is going to behave it is not necessary to analyse things down to the lowest possible level. For example, when current flows in a resistor, one does

not need to know what happens to every atom in the resistor. The ability to describe what happens to a large number of atoms in the resistor by using a macromodel for the resistor is convenient.

Thevenin Equivalent Circuits - or TECs - are macromodels that are used to model electrical sources. Those sources are as diverse as batteries, stereo amplifiers and microwave transmitters [3]. A Thevenin Equivalent Circuit is used to explain some of the things that happen when you use sources. The Thevenin's Theorem states that it is possible to simplify any linear circuit, no matter how complex, to an equivalent circuit with just a single voltage source and series resistance connected to a load. Thevenin's Theorem is especially useful in analysing power systems and other circuits where one particular resistor in the circuit (called the "load" resistor) is subject to change, and re-calculation of the circuit is necessary with each trial value of load resistance, to determine voltage across it and current through it. Thevenin's Theorem makes this easy by temporarily removing the load resistance from the original circuit and reducing what's left to an equivalent circuit composed of a single voltage source and series resistance. The load resistance can then be re-connected to this "Thevenin equivalent circuit" and calculations carried out as if the whole network were nothing but a simple series circuit

Equivalent circuit of a receiver antenna, is a method to create a Thevenin equivalent of the antenna to improve the understanding of the antenna functioning and to implement an equivalent of an antenna in an exchange between software which do not support each other's files. Since circuit simulation is generally executed in time-domain simulator such as SPICE and ADS, a generalised model antenna equivalent circuit is required for simulation purposes.
To design the equivalent circuit of an antenna, the first and the foremost requirement is the matching of the input impedances. In the Wide Band communication systems, Antennas work as pulse-Phase Shifters. Bandwidth limitations of the antenna result in as the frequency-domain transfer function and time-domain distortion. The equivalent circuit design should capture the distortion so that one can compensate at the transmitting end or the receiving end.

Extensive studies have revealed the determination of the input-impedance function. The model introduces a load resistor or a filter-network to reproduce the radiated waveform. By designing the filter or a combination of filters, the radiated waveform was reproduced and after some extensive optimisation, the results matched to those of the radiated waveform.

One of the signature benefits of the hybrid narrower-band model with a comparable macro-model usage in the design is the reduced complexity of the circuits describing the macro-model network thus implemented which generally improves the steadiness of the data fitting process by minimising the effect of macro-model variables.

Since circuit simulation were generally executed in time-domain simulator such as SPICE and ADS as mentioned earlier, a generalised model antenna equivalent circuit was required for simulation purposes. To generate the equivalent circuit, the antenna was to be used in time-domain to generate the transient plots of the real and imaginary parts of the transmitted signal from the antenna. To shift to the time-domain solver, the transient component is placed and the simulation and the real and the imaginary parts of the input and the output impedances, namely Z1 and Z2 were determined. A plot showing the attributes of the real and the imaginary parts was plotted for both input impedance and output impedance respectively and they can be seen in Fig. 6a and Fig. 6b respectively.

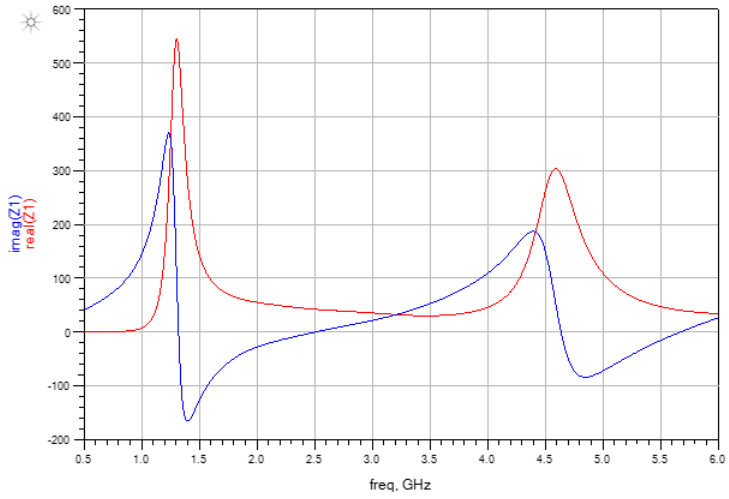

Fig. 6a Initial transient input impedance (Z1) plot without tuning

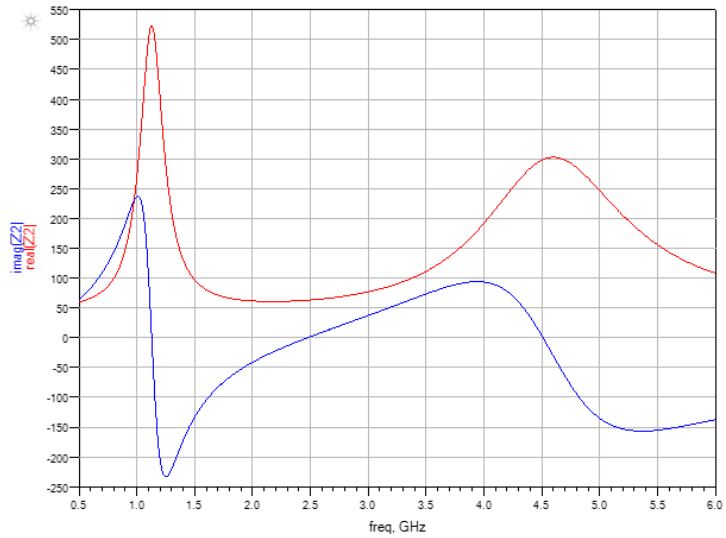

Fig. 6b Initial transient output impedance (Z2) plot without tuning

Once the transient impedance results were available, they gave an idea as to how the response of the equivalent circuit of the antenna would appear. The idea now was to estimate an initial equivalent circuit which would match the initial impedance plot of the antenna. The method of which is discussed in the section below.

5.3 Assumptions of the equivalent circuit and initial assumed values

While observing the S-parameter as well as the transient output impedances Z1 and Z2 correlations of the real and the imaginary patterns of the antenna, it was examined and estimated that to construct an equivalent antenna, it was estimated to require one Series R-I-C network along with a pair of parallel R-C networks connected in series with values selected in manner which enables obtaining the initial peak at 1.25 GHz and a second R-C parallel network with a resistors and an inductor in series to go with a capacitor in parallel and which has values which give a peak at 4.75 GHz.

Using the formula to obtain the X_l and X_C values, suitable equations for some initial values of I and C were calculated at 1.25 GHz and 4.75 Ghz respectively. The estimated equivalent circuit with its initial assumed values can be seen in Fig. 7 below.

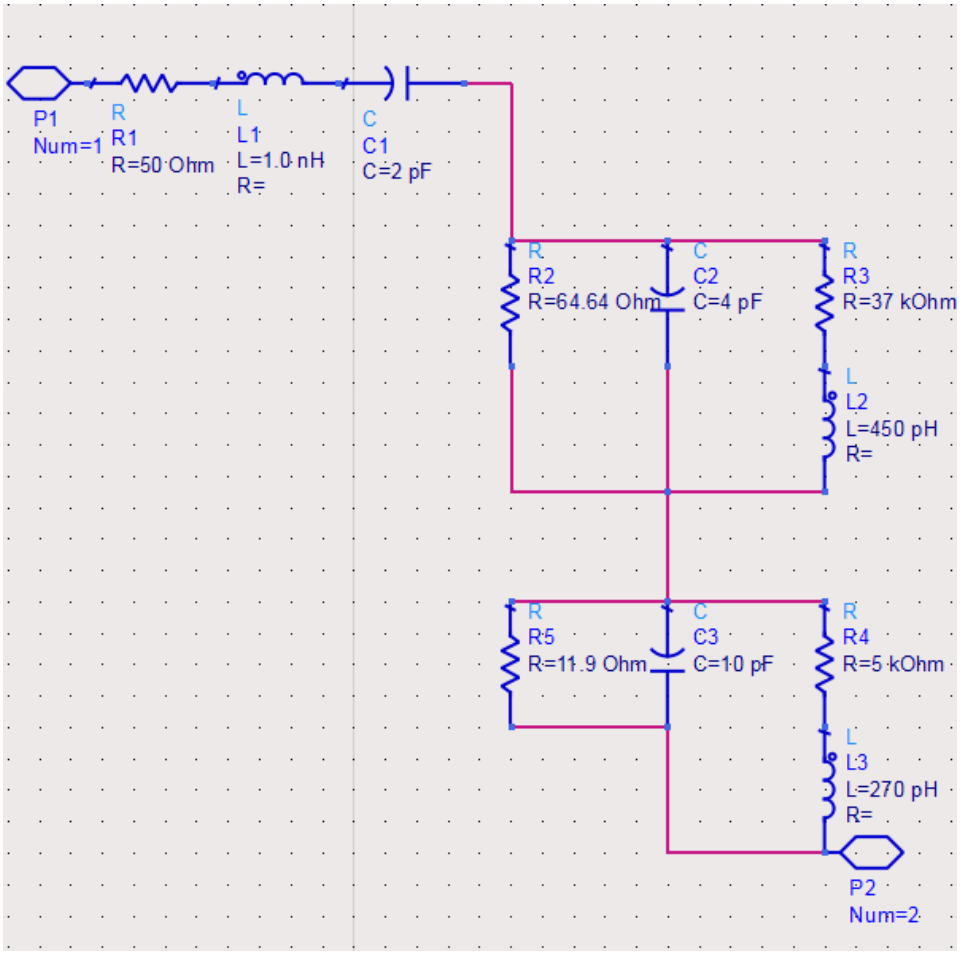

Fig. 7 Initial assumed equivalent circuit design

Once the estimated equivalent circuit was designed, it was pushed into heiarchy to create a component which was then placed in place of the antenna component in the Transient simulation circuit. Once the heiarchy component was simulated, its results were evaluated.

The results thus evaluated were significantly offset from the places where we expected and anticipated them to be. To solve this issue, the technique of Tuning was used. In tuning, the parameters are assigned a range in which they can be changed. With every parameter now acting as a variable, by changing the variables, the effect of that particular change in the simulation results can be observed. A Tuning panel can be seen in the fig. 8 below.

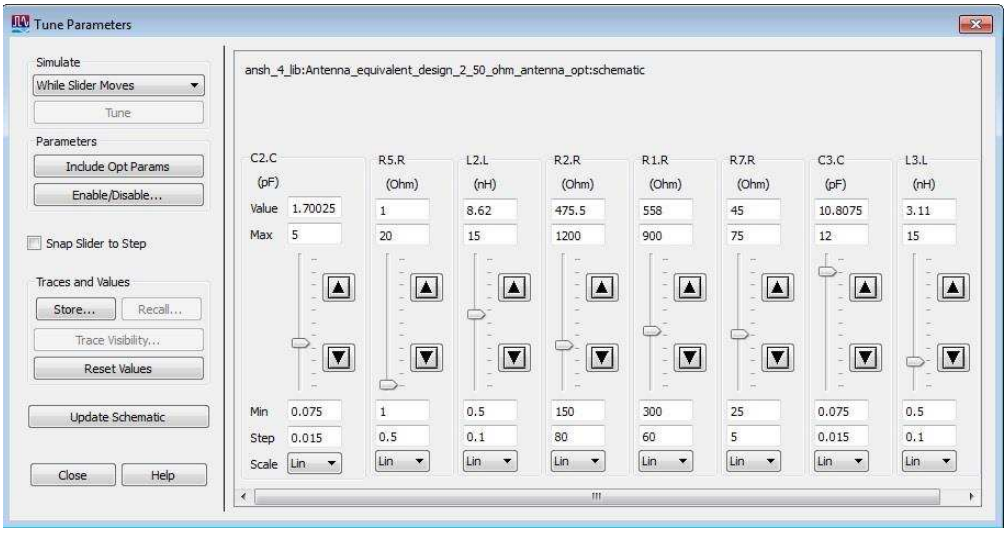

Fig. 8 Tuning parameter panel

By adjusting the tuning values in the panel, the variation in result was observed. Although a perfect matching was not obtained, the matchings were at the right place now in the design as it can be seen in Fig. 9a and 9b.

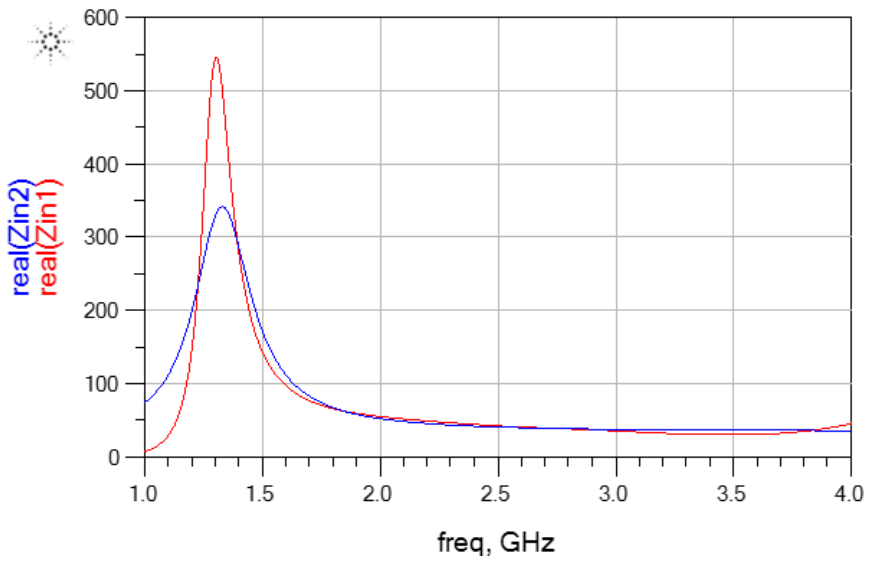

Fig. 9a Real part of impedances after tuning

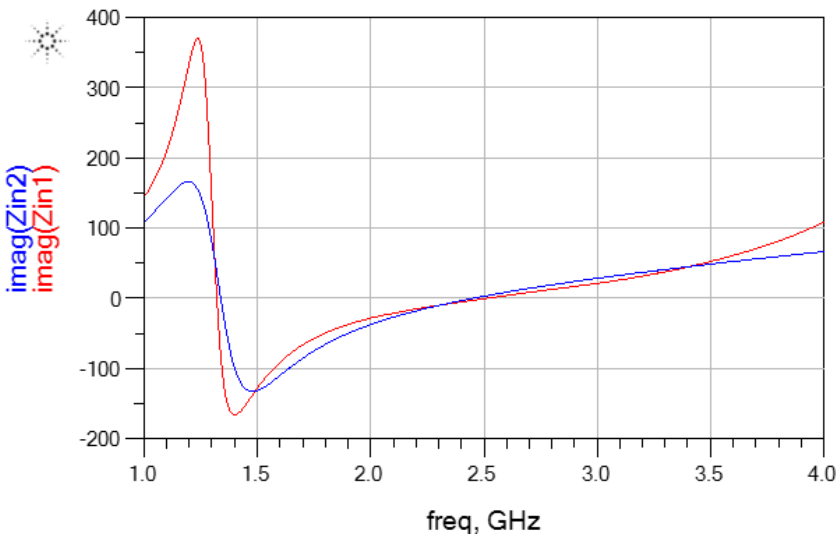

Fig. 9b Imaginary part impedances after tuning

The results after tuning although improved significantly from the initial stage as previously seen in Fig. 6a and 6b, the results were not satisfactory enough still to be considered as the equivalent design of the antenna[1]. The peaks of of the matching were not at a similar level and some further modifications were required with either the circuit or the values.

To Solve this issue, the componenets which were earlier put in the tuning mode were now switched to optimisation mode. Optimization in agilent ADS is an automated procedure of achieving the circuit performance in which ADS can modify the circuit component values in order to meet the specific optimization goals. It is worth noting that care should be taken while setting up the goals to be achieved and it should be practically possible else it will not be possible to meet the goals. Also the component values which are being optimized should be within the practical limits and this needs to be decided by designers considering the practical limitations[2].

To define the goals for optimisation, it was necessary to understand the needs and the objectives of those goals prior to their implementation. The main objective goals of the optimisation were to maximise the difference between the real parts of $S_{1,1}$ and $S_{2,2}$ along with equating the imaginary parts of $S_{1,1}$ and $S_{2,2}$ to zero(Fig. 10) . The goals were thus implemented for the frequency range of 1GHz to 4GHz.

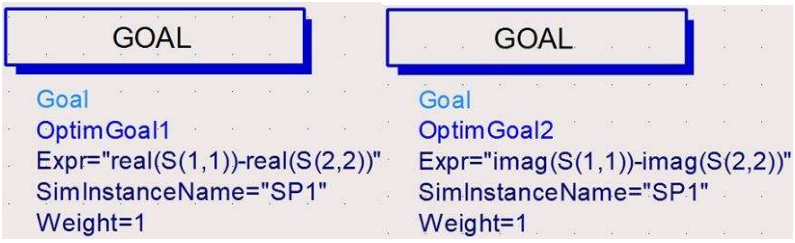

Fig. 10 The goals for the real and the imaginary parts in ADS

Once the goals were set, the optimisation was then run. The optimisation window can be seen in fig. 11. As the optimisation was run, it changed the values of the components within the permissible range and then changed the value to get either an equal or a result closest to the goals set. More often than not, the optimisation goals are met.

Fig. 11 The intermediate stage of optimisation window in ADS design

Once the optimisation was complete, the results were displayed. The fully optimised results of the equivalent circuit for the antenna can be seen in Fig. 12a and Fig. 12b. The results now have a near perfect match at the desired frequencies.

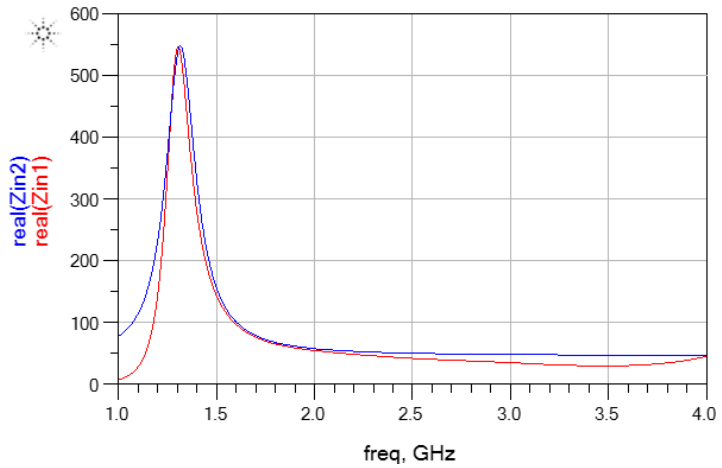

Fig. 12a. Fully optimised real part impedances

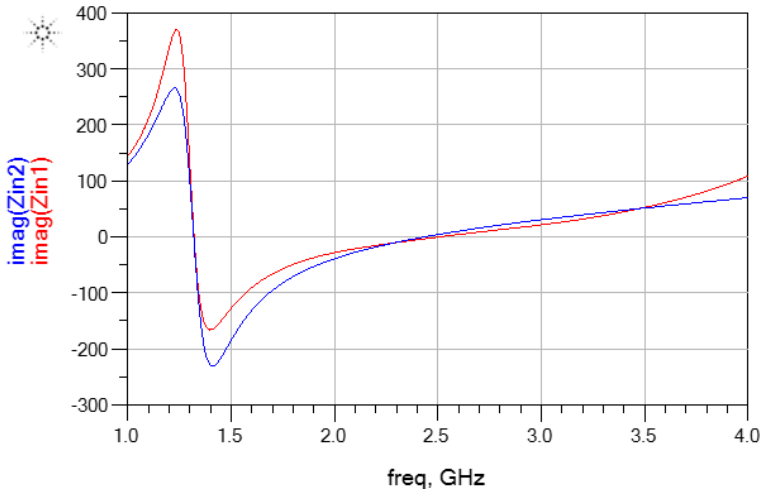

Fig. 12b. Fully optimised imaginary part impedances

As the optimisation presented satisfying results, the circuit was thus examined for the specific values of each component. The fully optimised hierarchy circuit component can be seen in Fig. 13.

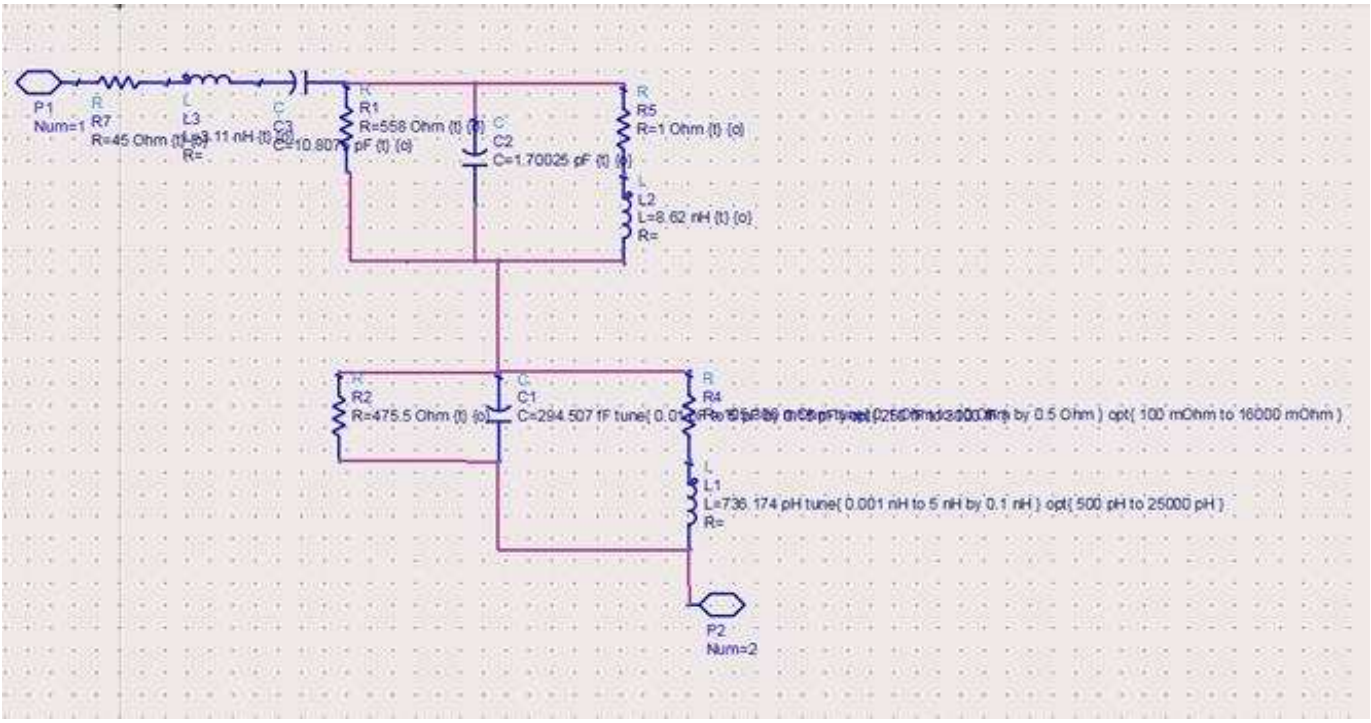

Fig. 13. The Hierarchy component with optimised component values

As the figure does not show all the values clearly, the values can be seen clearly in table 1 below. The values corresponded to the results obtained from the optimiser simulator.

Component	Value
Resistor R7	45-Ω
Inductor I3	11 nH
Capacitor C3	10.807 pF
Resistor R1	558-Ω
Capacitor C2	1.70025 pF
Resistor R5	1-Ω
Inductor I2	8.62 nH
Resistor R2	475.5-Ω
Capacitor C1	294.507 pF
Resistor R4	15-Ω
Inductor I1	736.174 pH

Table 1 Specific component values for the fully optimised circuit

5.4 Conclusion

This chapter dealt with exporting the CST design of the antenna and then calling it into ADS. The antenna this called was used as an ADS component and its real and imaginary impedances were compared in time domain. The antenna was to be made into an equivalent circuit using simple lumped components so that it can be implemented in further usage. A circuit was guessed which was estimated to obtain its peaks at 1.25 GHz and 4.75 GHz respectively. As the circuit was estimated, it was designed. To improve the functionality of the circuit, the lumped components were put into tuning and every component was individually tuned. The results thus provided were comparatively better. To create a fully optimised design, the lumped components were put into optimisation mode and the goals were define to maximise the difference between real-part of the input and the output impedances and to zero the resultant of the imaginary-part of the impedances. The equivalent circuit was fully optimised using optimiser and a block-component was created for the equivalent circuit to be used in the further stages of the design which are discussed in the chapters to follow.

References:

1. S. Madhu, (1988) *linear circuit analysis*. United Kingdom: Prentice-Hall.

2. *The RF and microwave circuit design cookbook* (1999) *Choice Reviews Online*, 36(06), pp. 36–3348–36–3348. doi: 10.5860/choice.36-3348.

3. B.B. Babani, (1974) *Handbook of integrated circuits: Equivalents and substitutes*. United Kingdom: Bernard Babani Publishing.

Chapter 6

ADS Simulations

6.1 ADS circuit design

In chapter 5, the Antenna equivalent circuit design was thus made as discussed in the earlier chapters. It is as shown below.

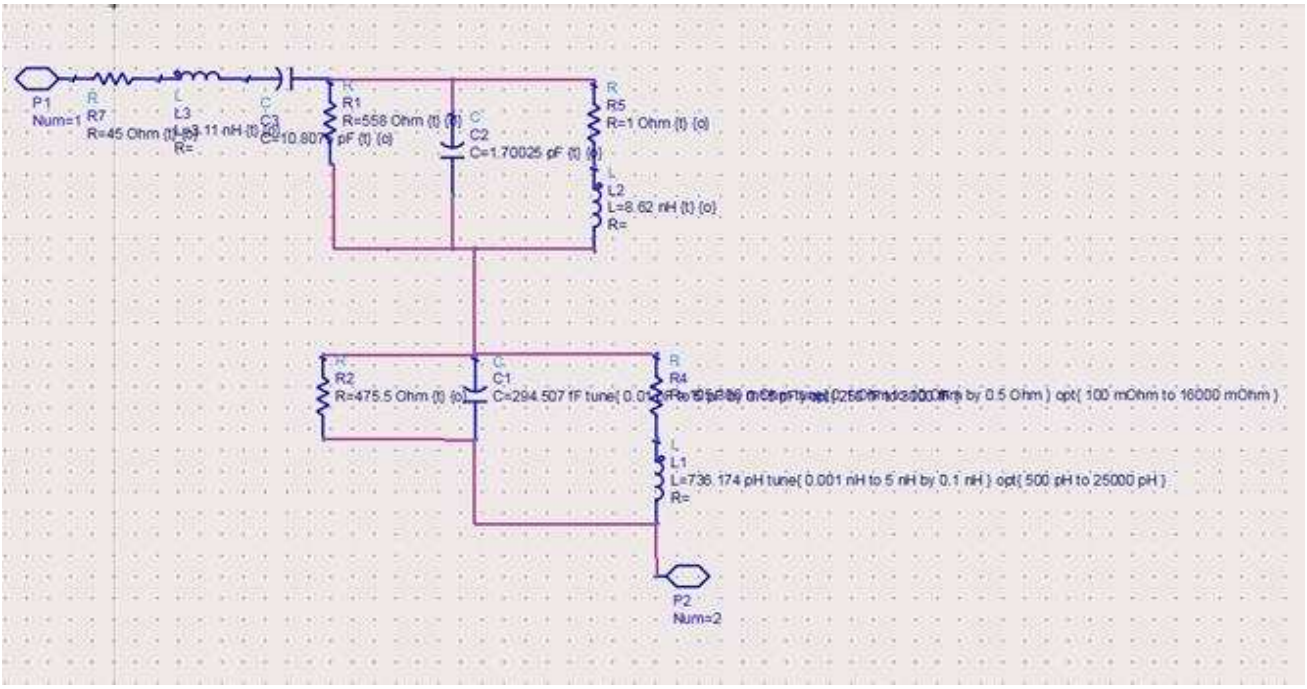

Fig.1 The equivalent circuit model for the antenna

As the purpose of the equivalent circuit was fulfilled, the circuit was now converted into an antenna component. The component was now to be placed in ADS and a matching network was to be designed to achieve the goals of power with higher voltage levels in an efficient way.

To obtain the most efficient output, it was necessary to implement a full wave rectifier to utilise the entire RF as well as AC input signals and converting those signals into DC with maximum effect.

An extensive search to find the suitable diode for energy harvesting purposes was run and after comparing the vital aspects of the diodes (Section 3.4), HSMS 2860-079 diode was preferred for the purpose of rectification. The critical aspects of the diodes which were put into consideration in the process were its functionality at the high frequency of 2.4 GHz, turn on voltage which was preferred to be as low as possible, higher isolation, better thermal conductivity and higher power dissipation. The mentioned aspects of design have been widely discussed (section 3.4). After all the comparisons and considerations, the HSMS 2860-079 diode was preferred and was thus implemented into the design due to its finer response and better rectification credentials at the desired frequency.

Once the diode was finalised, a filter was to be added to the circuit after the diode in series to taper off the AC and the RF components on the input which has passed through the diode. Since the received signal at the antenna had RF power with AC components, it required a full wave rectifier to eradicate the RF and the AC component of power by converting it into DC. Once this procedure was done, it was required to have a low pass filter added after the diodes to smoothen the ripples which were left after the rectification. While considering the various types of filters, a 3rd order Butterworth filter was preferred.

A Butterworth filter has the maximally flat response in the pass-band. At the cut-off frequency, ω_c, the attenuation is -3dB. Above the -3dB point the attenuation is relatively steep with a roll-off level of -20dB/decade/pole. That was ideal for the purpose of eradicating the ripples and enhancing the received rectified input through the diodes. The idea behind preferring the 3rd order low pass Butterworth filter was to have a steep attenuation to obtain the perfect match at the desired frequency and in time domain, to obtain the a steeper, higher peak for maximum magnitude of received voltage.

To start off the ADS simulations, instead of using a full wave rectifier, a single diode was implemented initially for half wave rectification and the 3rd order low-pass Butterworth filter was added in the circuit after the implementation of the diode. The schematics can be seen in Fig. 2.

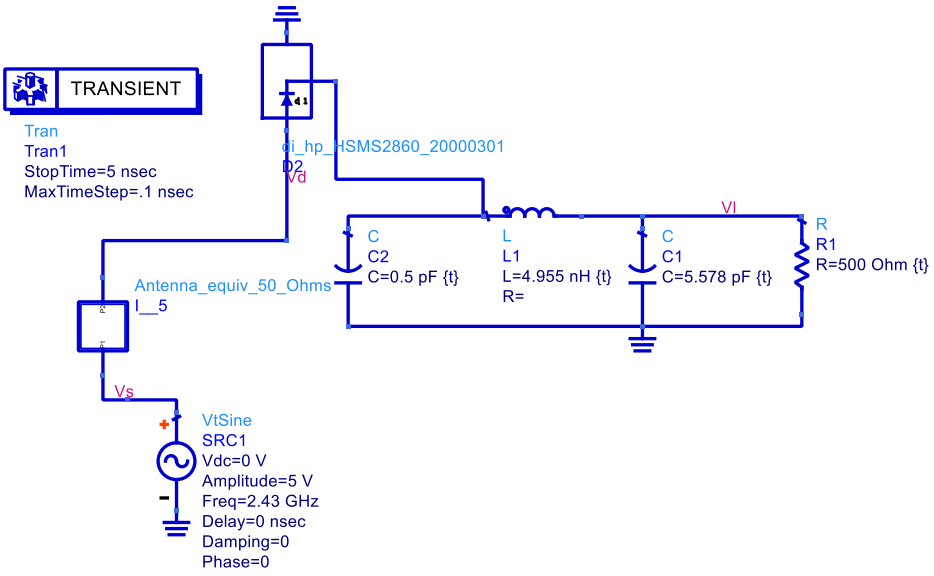

Fig. 2 Schematic of the 3rd order low pass filter with the diode and antenna component

The transient output was simulated after implementing a power source before the antenna component. The transient simulation results can be seen in Fig. 3.

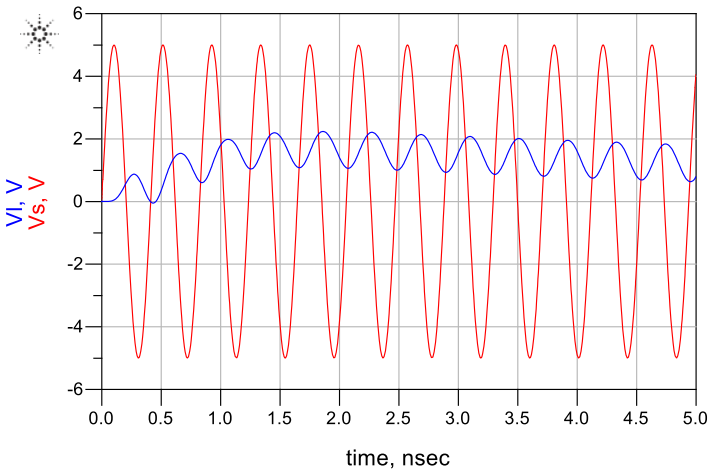

Fig.3. Transient simulation results of input voltage vs output voltage

As per the schematic (Fig.2), the Input voltage or the source voltage, namely V_s was the voltage measured between the input power source and the ADS antenna component. The output voltage, namely V_l was the voltage across the resistor in the Butterworth filter. The simulation plotted (Fig.3) the source voltage against the load voltage. As it can be seen in the graph, the maximum input

voltage V_{max} was randomly set at 5V peak-to-peak. The simulated output voltage showed a magnitude of 2.25V peak-to-peak. The value was significantly low as the real available voltage in a system would not be 5 Volts.

Since the need for absolute eradication of the RF and the AC-component ripple was there, the idea of microstrip lines was introduced into the design. A microstrip transmission line is a "top-grade" printed circuit design, featuring a track of copper or other conductor on an insulating substrate. There is a "back-plane" on the other side of the substrate, made-up of a similar conductor. At one end, there is a conductor, which is the track on the top, and another conductor, which is the backplane on the bottom. A microstrip is therefore a variant of a two-wire transmission line [1].

As the design majorly ignored the RF and the AC powers, only one side of the microstrip transmission line was preferred to be used for phase shifting processes. Phase shifters are devices used to adjust transmission phase in a system, they can be fixed phase digital phase shifters or analogue variable types. Microstrips have been popular for decades because they exhibit a low profile, small size, lightweight, low manufacturing cost, high efficiency, and an easy method of fabrication and installation.

As the requirement was to shift the phase of the input signal from the antenna to maximise the received signal post rectification and filter. A couple of microstrips were added to the schematic (Fig. 4) and their dimensions were put into tuning. The following pattern was observed when the design was simulated with an input signal of 2.23V peak-to-peak voltage.

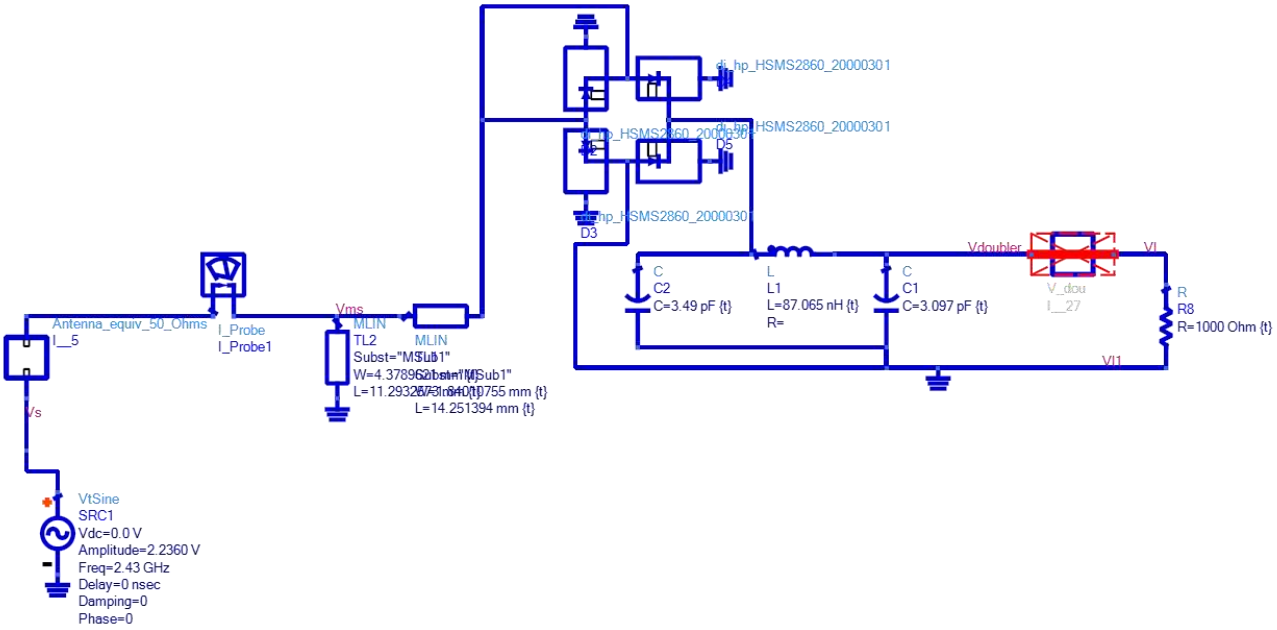

Fig. 4 Full-wave rectifier with microstrip lines

When the circuit was simulated with the amplitude voltage of 2.23V, the results were as they appear in Fig.5. The results show a plot between the voltages received at the microstrip lines vs the voltage received at the load resistor. It should be noted that for the 2.23V peak-to-peak voltage transmitted, only 0.87 Volts was available at the microstrips which were rectified to 1.27V at the load resistor.

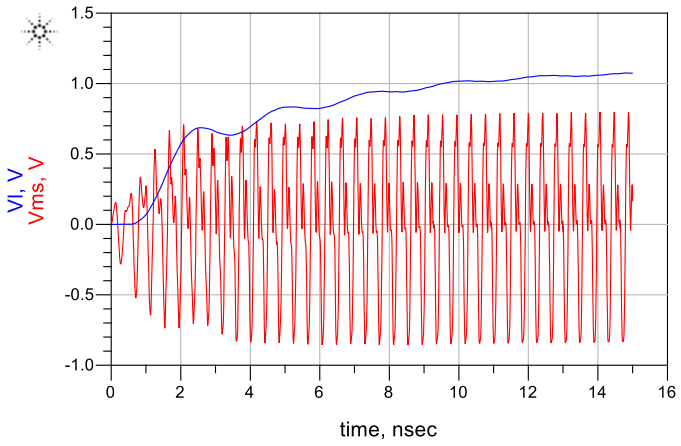

Fig.5 The simulation results of the full wave rectifier with microstrip line design

As the voltage received at the load resistor was effectively half of the transmitted voltage, the output power was correspondingly lower (Fig. 6).

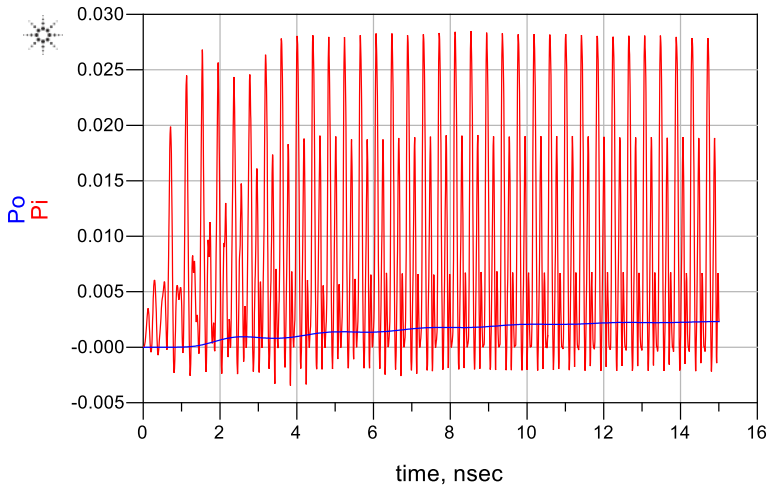

Fig.6. Plot between the input-power against the output power

As the full wave rectifier fetched significantly lower output voltage and power levels, it was required to design a phase shifter using microstrips and a set of diodes to accomplish the process of rectification. To successfully accomplish the full-wave positive rectification, it was essential to split the incoming RF signal from the transmitting antenna into two halves and phase shifting them as well as rectifying them in order to obtain two equal half-wave rectified waves whose phases were just enough so that their peaks didn't overlap or intersect. The two half-wave rectified signals were then to be merged before the filter.

The main concern thence was to find the suitable microstrips as well as the phase shifts to obtain the improved output and better rectification. A preliminary test was conducted to determine the need of the type of microstrip line or an array of microstrip lines in the design.
For the preliminary tests, 2 standardised diodes were placed in parallel with a microstrip place before the second one as it can be seen in Fig. 7. The remaining part of the circuit remained the same as Fig.4.

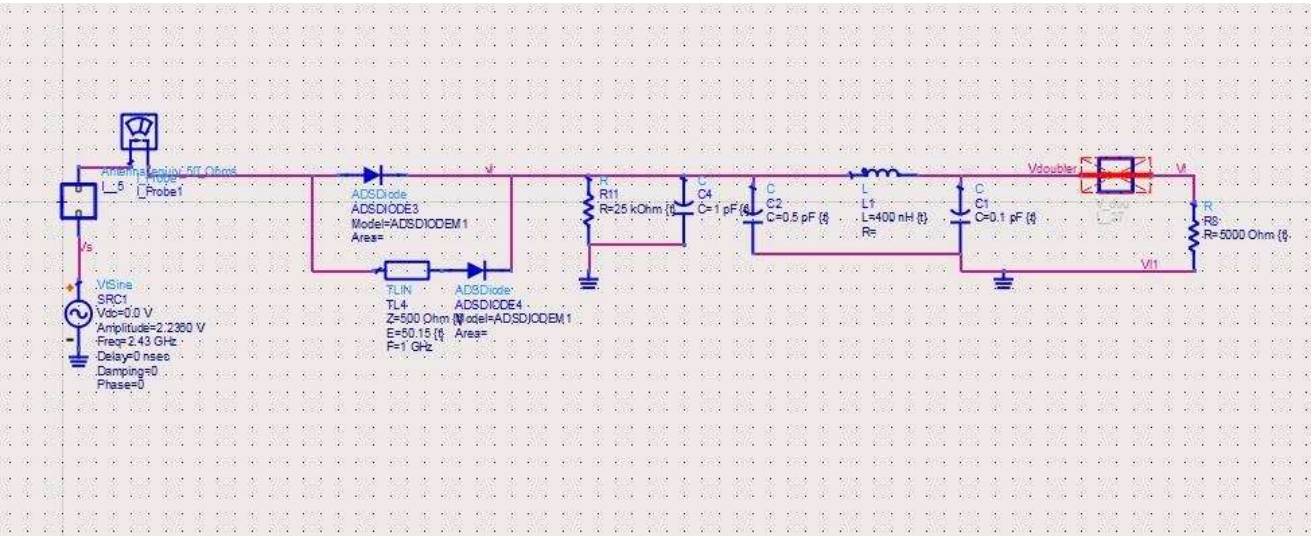

Fig. 7 Schematic design of the preliminary microstrip test

The results of the simulation can be seen below. What is worth mentioning in the simulation results as they can be seen in Fig. 8 is that the output power, namely V_l attains its peak at a value greater than the now pre-set input voltage value of 2.23V and peaks at 2.37V although the peak is attained for only a very small fraction of time. The amplitude of the output power however gradually declines and goes way below 2V in time.

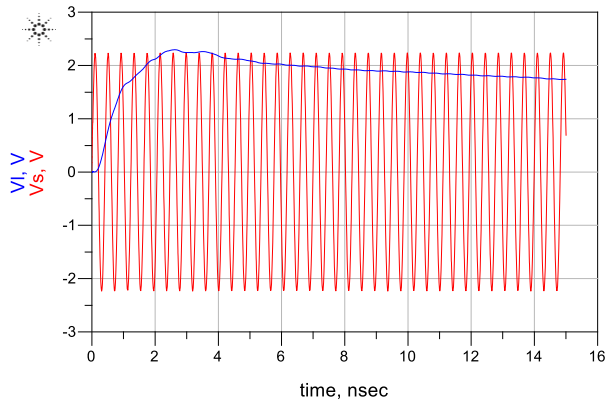

Fig. 8 Simulation results for the preliminary circuit design

Since the requirement was of a consistent output voltage with an output as high and as consistent as possible with minimalistic ripples, the preliminary design was rejected.

A requirement thus arose to find the suitable phase shift and hence the suitable microstrip combination to facilitate that phase shift. To begin with a preliminary search for a suitable phase shifting microstrip array composition, a phase shifter of 270° phase shift was implemented and the chips were matched at the 1 GHz frequency in the preliminary tests. The schematics can be seen in Fig.9.

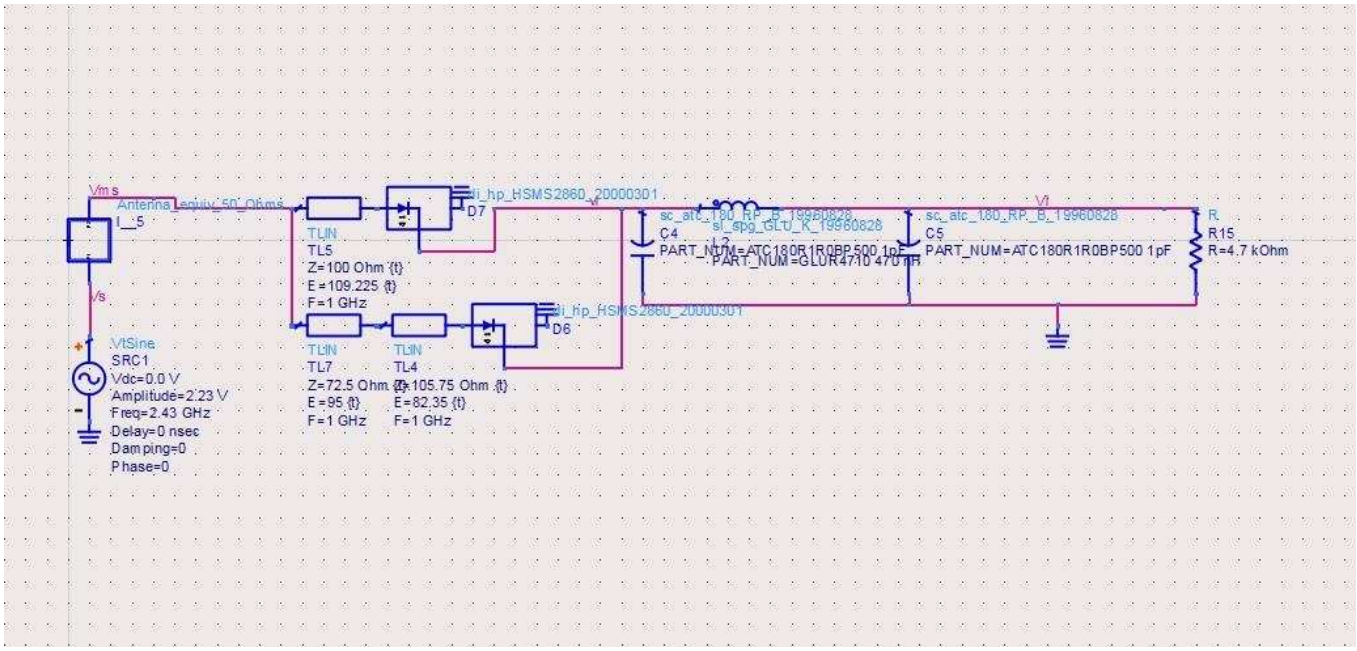

Fig. 9 270^0 phase-shift microstrip array design schematics

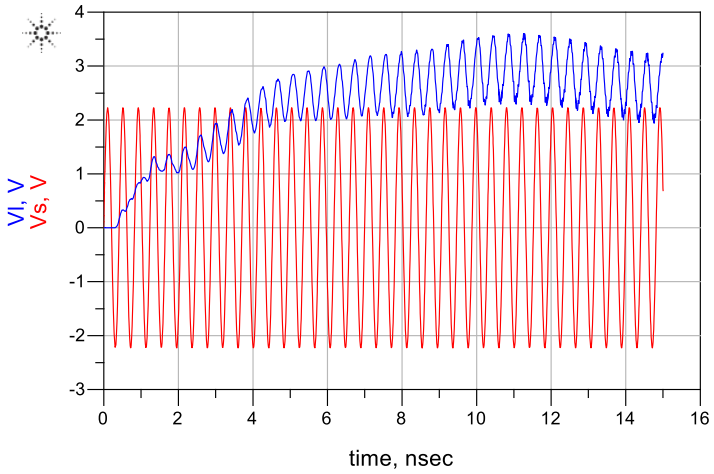

Fig. 10 270^0 phase-shift microstrip array design simulation results

As it can be seen in Fig.10, although the output voltage gradually increased in magnitude and was relatively higher than the previous simulation results (Fig. 8), some significant ripple was present of the RF-voltage with AC component which gradually increased with increasing time and amplitude.

Despite the presence of a ripple, the 270^{o} phase-shift layout yielded some satisfactory results. This phase-shift design was hence fine-tuned using tuning parameters to eradicate the ripple and also improve the results in the due process. The matching was kept the same at 1GHz. The antenna component was disabled to evaluate the effects of the antenna. The schematic and the results can be seen in Fig.11 and 12.

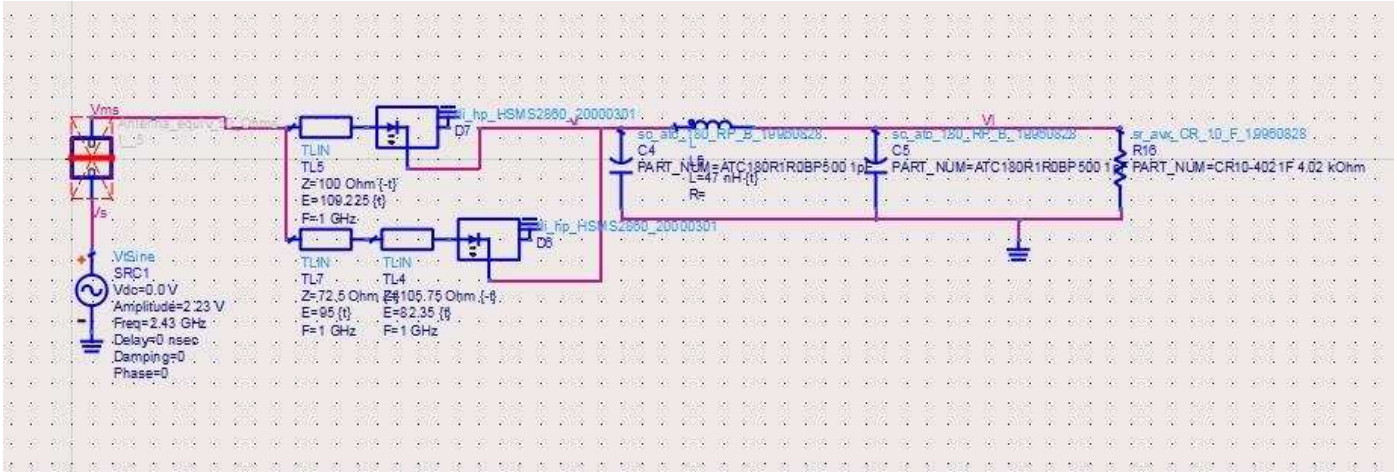

Fig.11 Schematic with disabled antenna component and tuned microstrips

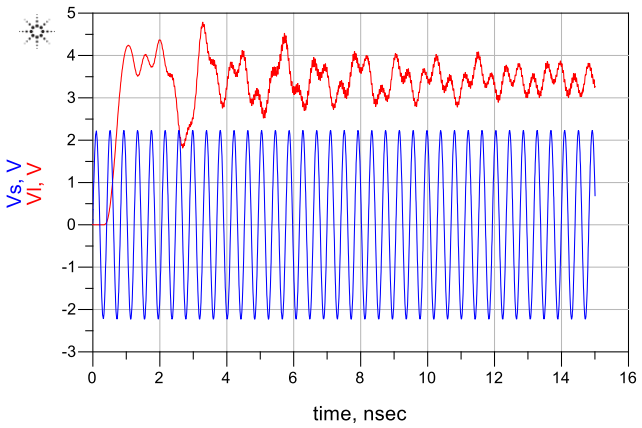

Fig. 12 Simulation results for the schematic with disabled antenna component and tuned microstrips

The ripple and the distortion goes from bad to worse when the antenna component is disabled. When the antenna component was enabled, the results appeared to be more settled with minimalistic ripples.

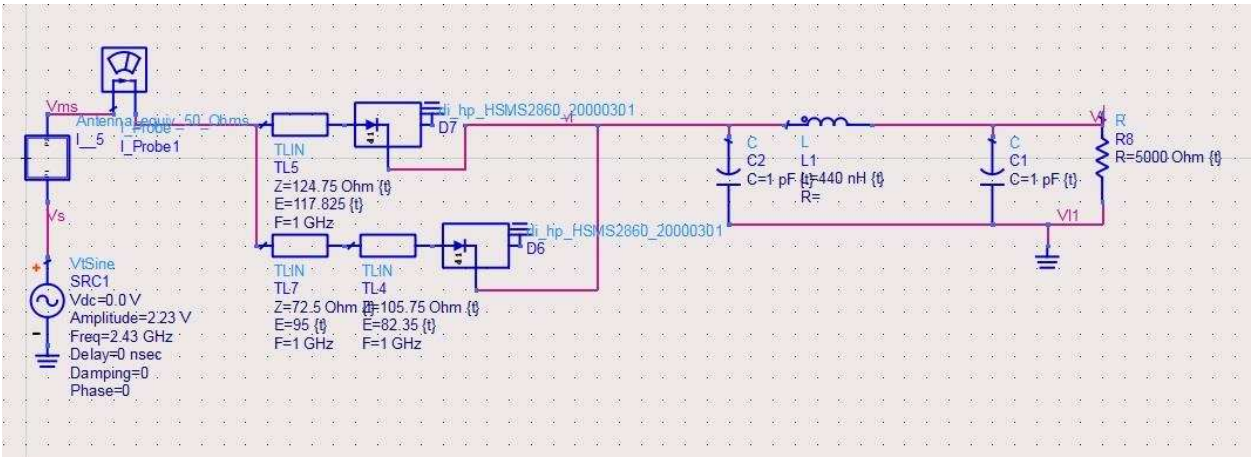

Fig. 13 Tuned microstrip design with enabled antenna component

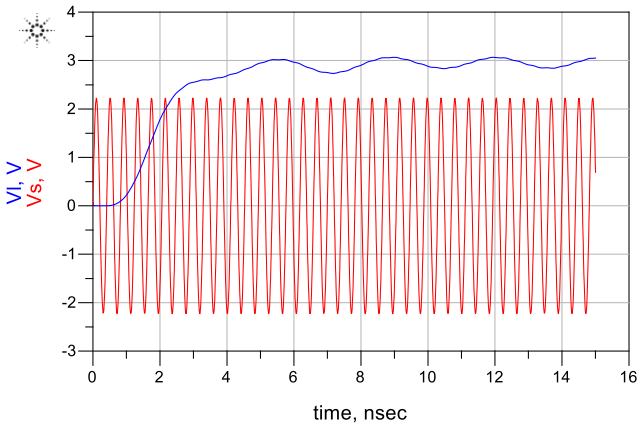

Fig. 14 Simulations results for the tuned microstrip design with enabled antenna component

With the antenna component enabled, the wayward ripples of AC and RF component were drastically reduced. The output voltage displayed a peak voltage at 3V against the standard input voltage of 2.23V. The consistency of peak voltage value was also significantly higher and minimal ripples were present. But, since in the preliminary tests the microstrips were matched at 1 GHz over a signal which had a frequency of 2.43 GHz, this design could not have been used.

Microstrips of the design were then designed to match at 2.43 GHz. The critical parameters of the microstrip, such as its effective impedance, its matching frequency and its electrical length were put into tuning to improvise the results. The design and the results can be seen in Fig. 15 and 16.

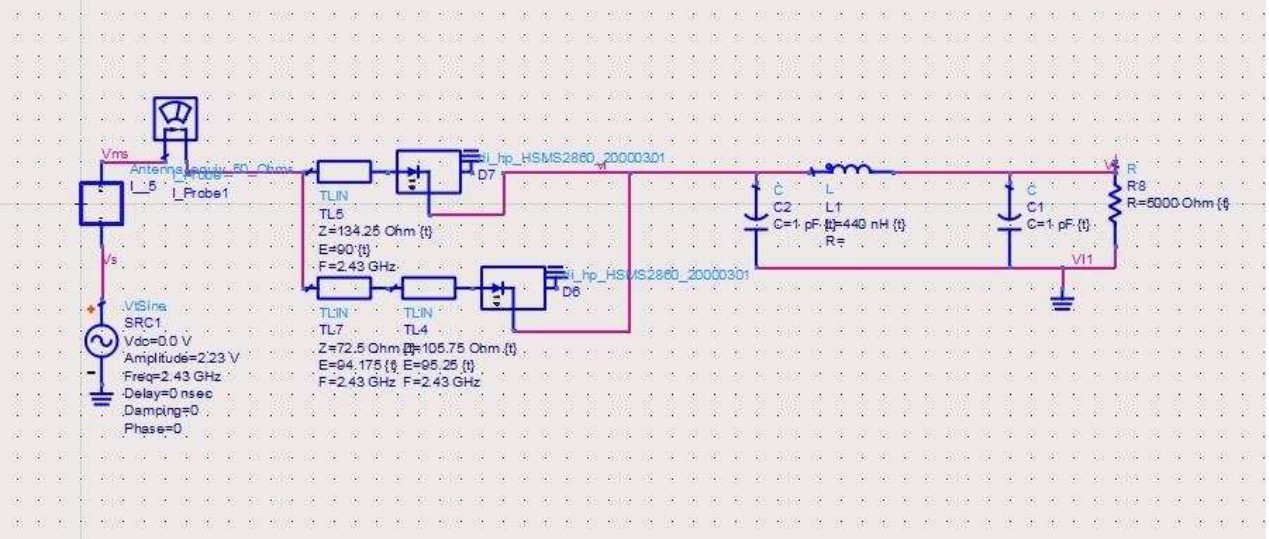

Fig. 15 Schematic design with microstrips matched at 2.43 GHz

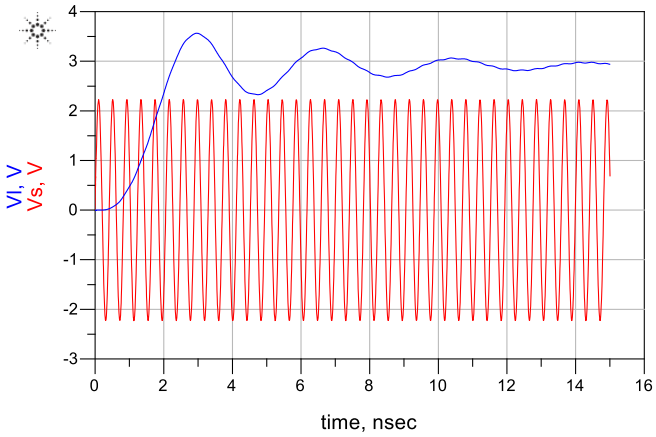

Fig. 16 Simulations results for the design with microstrips matched at 2.43 GHz

As it could be seen in Fig. 16, the peak output voltage value was significantly higher than the one obtained with the microstrips matched at 1 GHz in the preliminary tests with the output-voltage peaking at 3.62V and becoming consistent at the 3V mark. As there were some minor concerns such the ripple in the initial stages were higher which got better in time, the design was then to be optimised to get the best possible result.

For optimisation, all the components were put in the optimisation mode and the goals were defined. The goals that were required were to maximise the output voltage and to minimise the ripples. Once the goals were defined, all the parameters were assigned some practically and realistically feasible ranges. Once the goals were set, the optimisation was then run. The functioning of optimisation

window as discussed in chapter 5, was implemented in the design here. The results can be seen in Fig. 17.

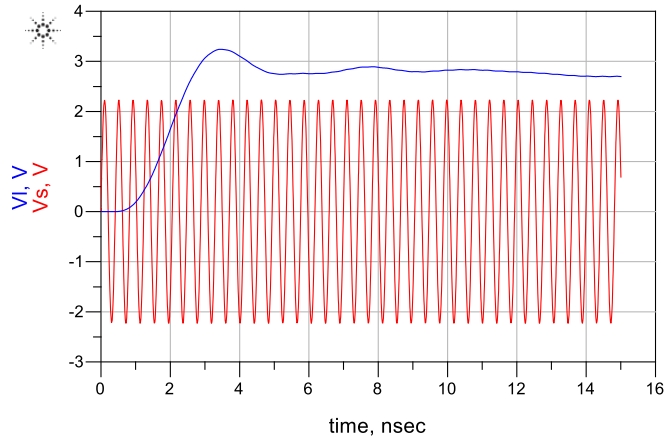

Fig. 17 The simulation results of the design after optimisation

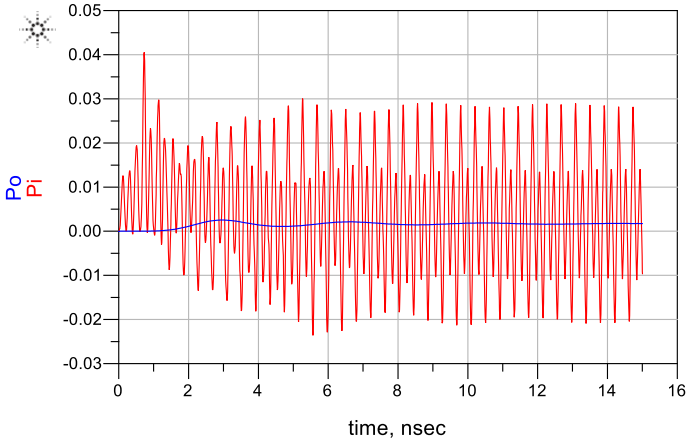

Fig. 18 Power input vs Power output graphs for the optimised design

As eminent from the figure, the ripples were minimized and the output voltage peaked at 3.4V with the average value in time normalising at 2.85V. The power levels (Fig. 18) also go significantly higher from the design which featured diodes for rectification (Fig. 6). The output power levels also attained consistency once they reach a certain level. Table 1 shows the values of the components via optimisation.

Component	Value
Resistor R7	45 Ω
Inductor I3	11 nH
Capacitor C3	10.807 pF
Resistor R1	558 Ω

Capacitor C2	1.70025 pF
Resistor R5	1 Ω
Inductor I2	8.62 nH
Resistor R2	475.5 Ω
Capacitor C1	294.507 pF
Resistor R4	15 Ω
Inductor I1	736.174 pH
Resistor R8	5k-Ω

Table 1 Optimised values for the schematic

Table 1 provides some crucial data worth observing. In order to optimise the schematic, the optimiser also includes the equivalent antenna component values to optimise the components to obtain the best possible results. The results shown in Fig. 17 and 18 were without implementing those changes into the equivalent antenna design but they were implemented in the schematic. The table for the changes which took place can be seen below (Table 2).

Component	Value
Capacitor C1	1 pF
Capacitor C2	1 pF
Inductor I1	440 nH
Resistor R8	5k-Ω

Table 2 Updated schematic values

As the values were within the theoretically and practically realisable range, the values were finalised and the design was now to be constructed in the layout.

6.2 layout exportation and designing

layout in ADS is the 3D representation and realisation of the schematic design. As a 3D visualisation mask is necessary to create a design out of schematics, we use the layout technique to create the simulation replica of the physical design. To create the layout, the lumped component were

required to be swapped with some certain components by makers which were also the layout component along with being the lumped component. Once the component were changed, the biggest issue which arose was that certain layout component did not possess the same component value as desired. For such instances, the components which complied with the attribute and had a value as close to the desired value as possible. Once the values were updated, a layout was then created with the schematic.

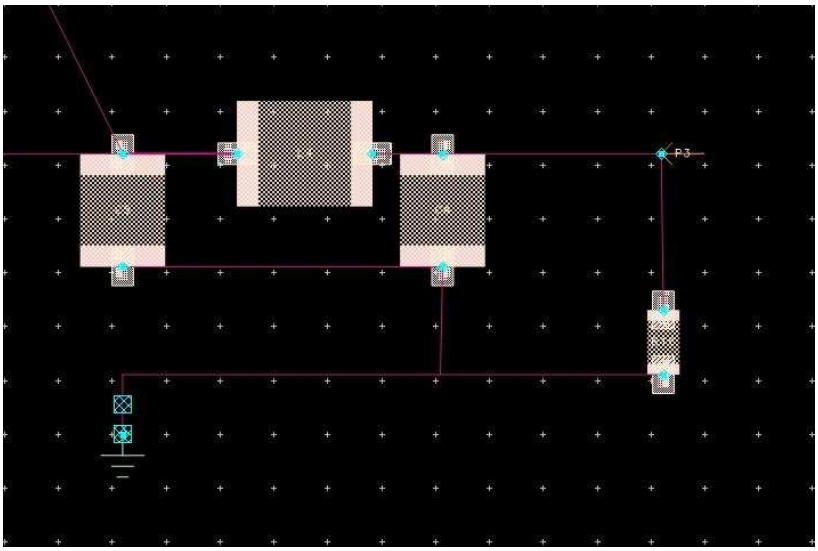

Fig. 19 the layout generated from the schematic

In Fig. 19, the layout generated from the schematic showing the filters can be seen. What is visible in the figure are the lumped components of the 3rd order low pass Butterworth filter. The next task now was to create the connections using the layout and define the substrate properties.

The substrate used in the process of designing the layout was a duroid manufactured by ROGERS. The name of the duroid was ROGERS RO3010. The substrate had a thickness of 0.6 millimetres.

In ADS layout, the substrate had to be defined. The assigning of the substrate was completed using the substrate editor and the substrate definition in ADS can be seen in Fig. 21.

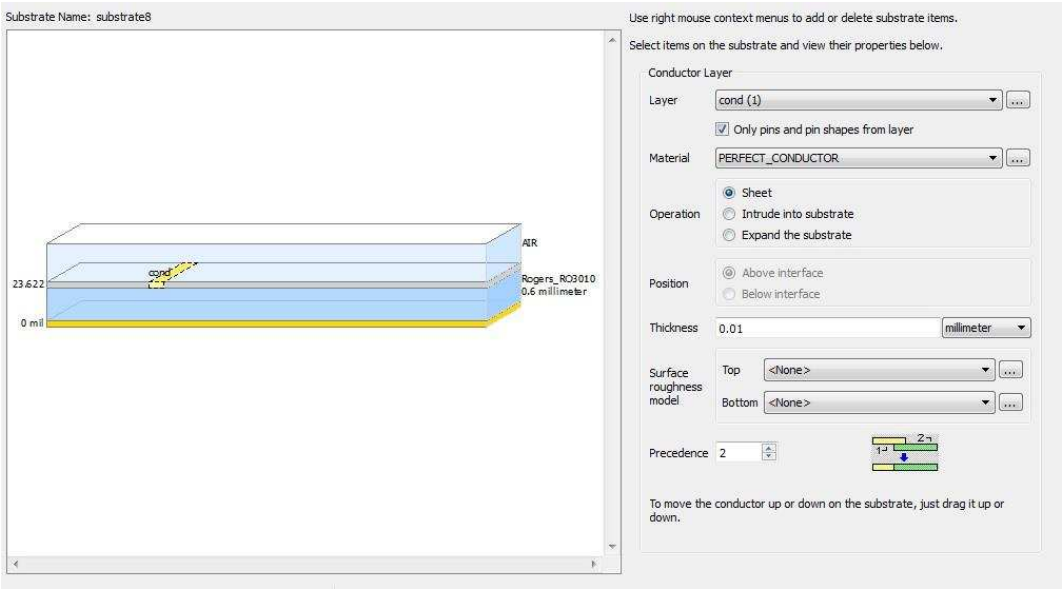

Fig. 21 The ADS substrate definition for ROGERS RO3010 duroid substrate

Once the substrate was assigned, the next task in line was to create the microstrip layout. The microstrip realisation, as defined by the schematic optimisation, can be seen below.

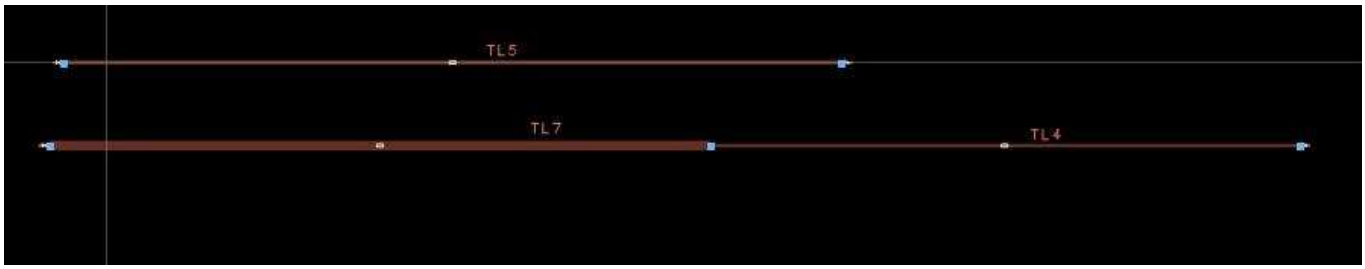

Fig. 22 Realisation of microstrips in the layout using RO3010 duroid substrate

Going back to the schematic design shown in Fig. 15 and collecting the microstrip data from the microstrip components, the dimensions of the Microstrip transmission lines are as follows:

- TI5 Microstrip

  Dimensions: 0.399mm X 70.763mm

- TI7 Microstrip

  Dimensions: 0.877mm X 60.076mm

- TI4 Microstrip

  Dimensions: 0.335mm X 53.571mm

Once the microstrip layout was created, it was required to create the connections and design the necessary tracks for those connections. To create the connections, it was essential to create the track which were nothing but the wiring connections realised on the duroid substrate in the layout design.

To generate the tracks in layout, it was important to understand their usage. The tracks were to be created and the layout component was then to be called in the schematics for final simulations. The tracks were to be made up of the same substrate as the microstrips and have to be used for connections. To create that, there were certain connections and junctions which were important in generating a layout. Fig. 23 shows a few types of connections implemented. There were certain connection points and for those connection points, 2-way, 3-way and 4-way connections to complete the connections on the substrate. To denote the grounded connections, VIAs were put as seen in Fig. 23 as P6, P8 and P10. The tracks and the components, as they were relatively smaller in size, it was necessary to optimise space and the total area covered by the duroid chip. To optimise the space, the microstrips were placed in the vertical orientation in simulation in place of horizontal orientation. Fig. 24 shows the total layout realisation of microstrips and connection tracks.

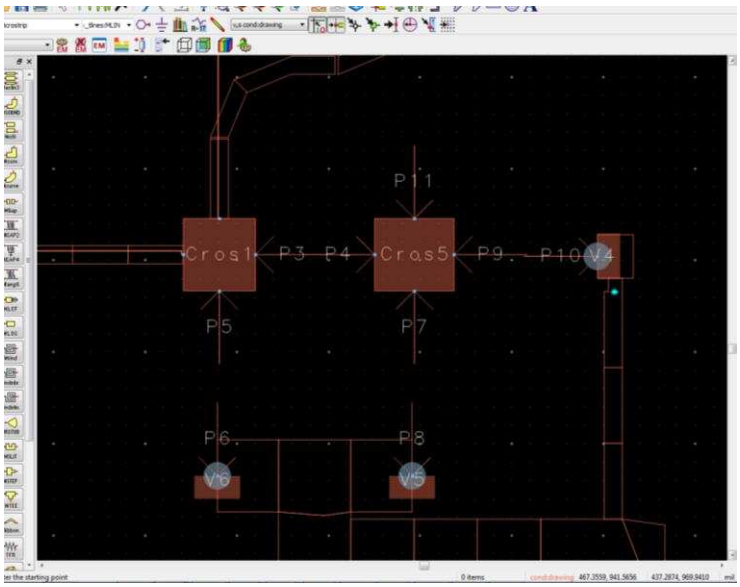

Fig. 23 layout showing 2 4-way MCROSO microstrip connection components

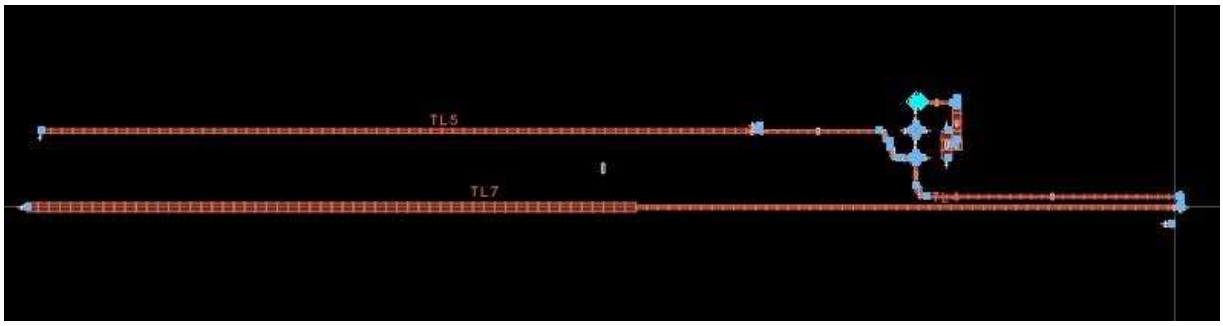

Fig. 24 layout realisation of the microstrips and the connection tracks

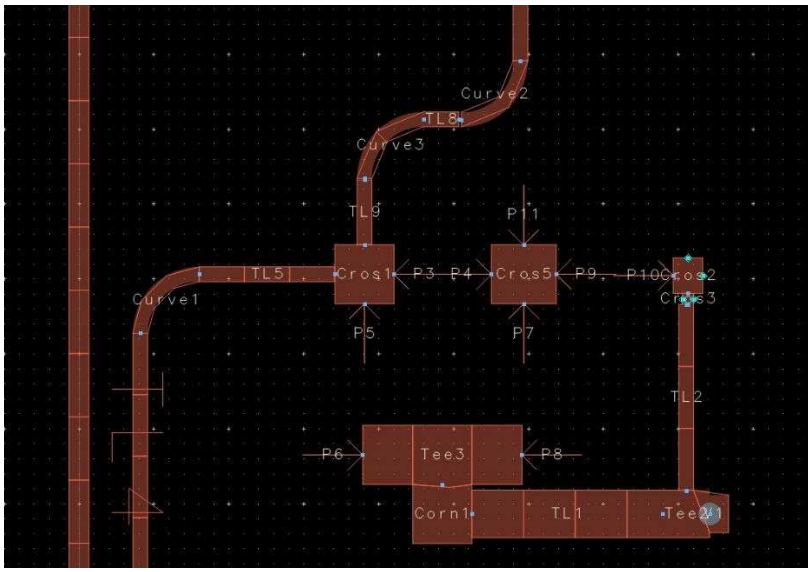

Fig. 25 Zoomed in layout tracks depicting tracks for the filter

Fig. 25 shows the tracks built for the filter merging the microstrips. The layout created was then to be recalled into a schematic and the connections were to be completed by fitting the components at their respective places. The connections were then to be completed by putting the components in the space in between.

The lumped components which were purchase-wise feasible and were decided earlier were placed after calling the layout designed in the schematics to analyse the final simulation results using actual

components. Fig. 26 denoted the schematic importation of the layout and since it looks unclear, a clearer view of the same has been given in Fig. 27.

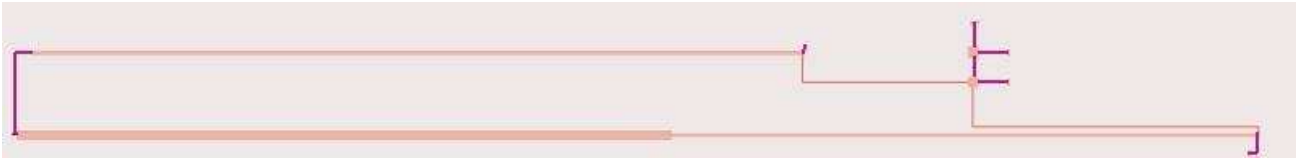

Fig. 26 The schematic importation of the layout with components

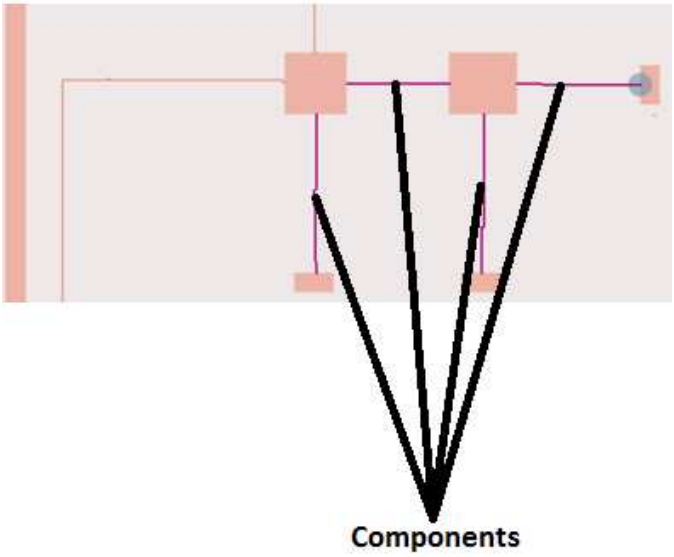

Fig. 27 A magnified view of the schematic denoting the filter circuit with wired tracks.

With the layout and the schematic both now complete with the substrate defined and all the components tuned and optimised to the nearest commercially available value, the design was simulated. The simulation results can be seen in the figures below (Fig. 28).

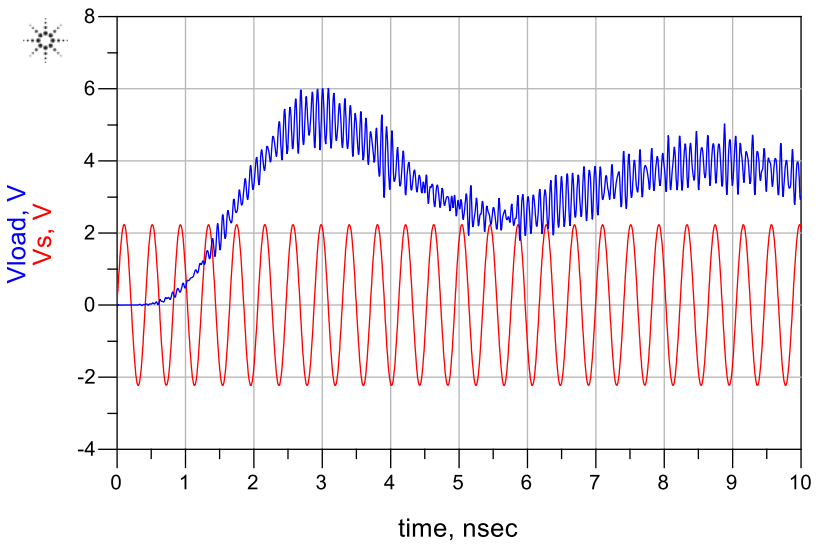

Fig. 28 Simulation results with antenna and the original values

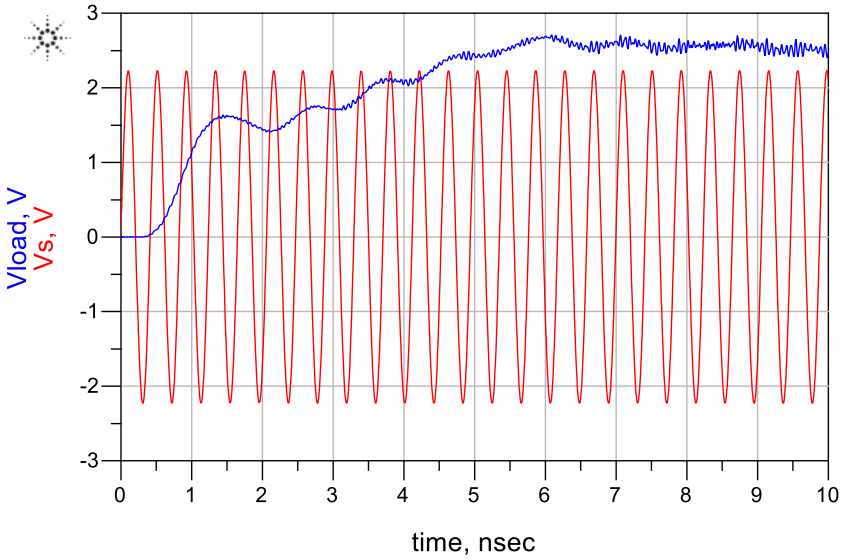

Fig. 29 Simulation results when doubling the filter lumped-component values

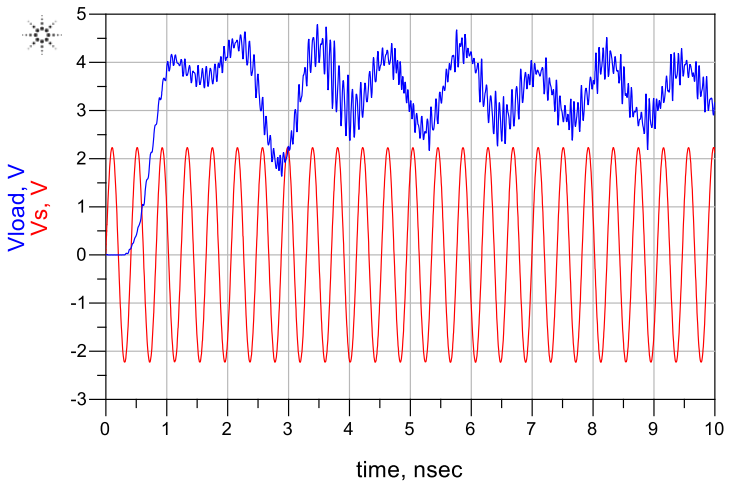

Fig. 30 Simulation results from changing the capacitor value from 1pF to 5pF

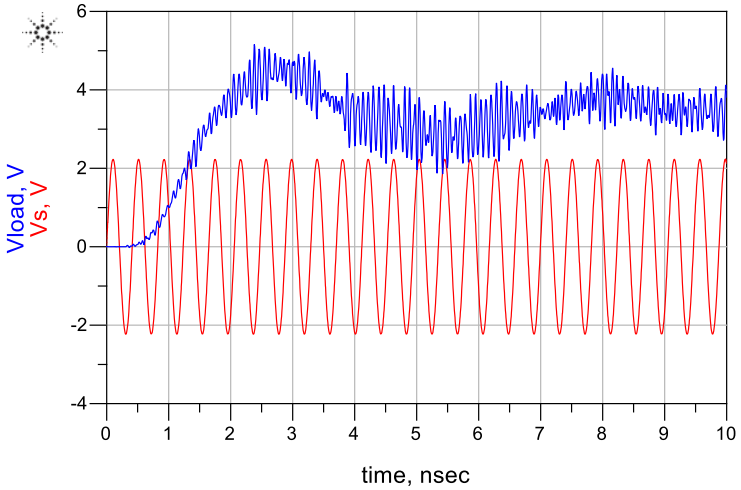

Fig. 31 Simulation results after varying the inductor value from 440nH to 100nH

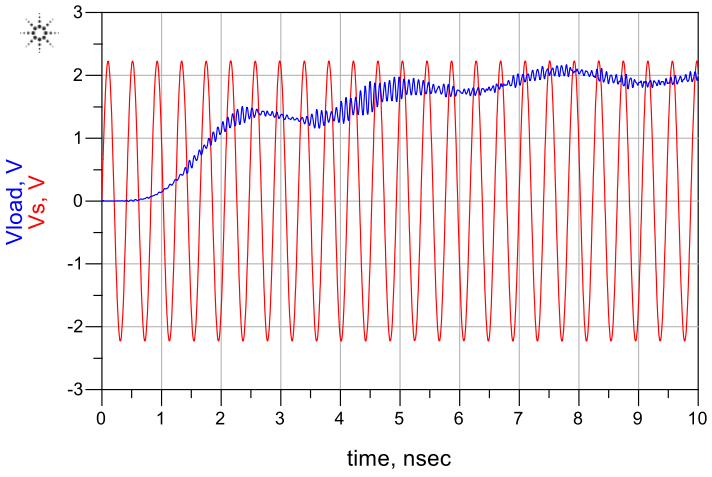

Fig. 32 Simulation results after varying the resistor value from 5k-Ω to 1k-Ω

As it is visible in Fig. 28 and Fig. 29, the original values displayed significantly higher ripple than the graph when the values of the components were doubled. However, the peak and the average voltage value was relatively higher for the design with original values (Fig. 28). Changes in the values of the capacitor, resistor and the inductor were made to eradicate the ripple available in the original simulation. The effect of the changes can be seen in the figures 30-32.

The increase in the capacitor value from 1pF to 5pF added another layer of ripples to the output which had some more delay than the normal one along with the presence of the original ripple (Fig. 30). The voltage peaked just below 4.5V and averaged at 3.47V.

Reduction in the value of the inductor from 440nH to 100nH reduced the amplitude of the ripple significantly although the ripple's presence was clearly visible. (Fig. 31). There was a little segment where the ripple becomes very high but it reduces in time. The voltage with the change in inductor value peaked at 4.8V and averaged at 3.92V.

Reducing the value of the resistor from 5k-Ω to 1k-Ω although nearly eradicated the ripple present, in spite of that it reduced the output load voltage by a great deal (Fig. 32). Despite having minimalistic ripples, the voltage peaked at 2.1V and averaged at 1.78V.

Figure 33 shows the matching network strip. The two microstrip lines but without all the lumped components can clearly be seen in the figure. The design was then used for testing, realisation and simulation. Fig. 34 shows the design after completion.

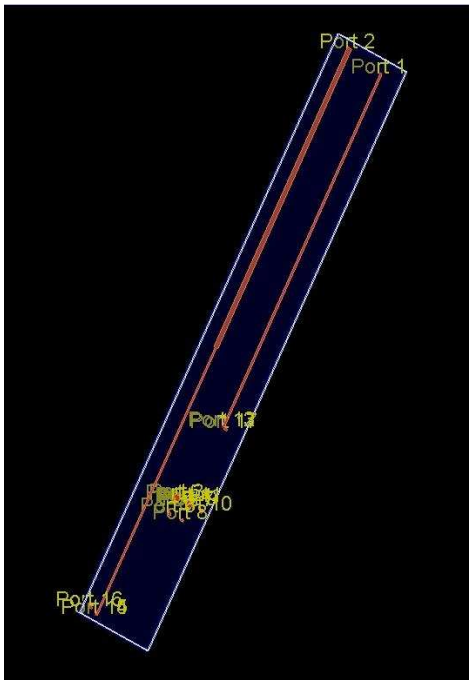

Fig. 33 ADS visualisation of the microstrip with connections and without tracks

Fig. 34 The matching network chip consisting of microstrip phase shifters and the low-pass filter

Conclusion:

This chapter dealt with a major portion of designing and simulation in ADS. The chapter started off with the implementation of the antenna equivalent circuit which was dealt in chapter 5 and continued the design of the matching network. The primary goal of the matching network was to rectify the incoming RF and AC voltage and convert it into DC. A 3rd order low pass Butterworth filter was implemented for its flat response in the pass-band and steep attenuation at the cut-off frequency. The rectification was done using 3 microstrip lines to obtain a 270^{o} phase shift and a duroid substrate named RO3010 Mfd. By Roger was selected to mount the matching network. The schematic was simulated and after tuning and optimizing the values, the circuit was finalised.

The finalised values were then adjusted to their nearest commercially available values and the design was thus put into layout mode. A layout was generated by ADS. The tracks and connection points were then created after readjusting the positioning of the microstrips and the filter components.

As the tracks were completed and the available space was optimised, the layout was then recalled in the schematics. The components were placed in their relevant places and the final simulation was done. The results were analysed and the simulation results were then to be compared with the practical measured ones. The next chapter deals with all the experimental measurements.

References:

1. A. B. Gnilenko, "Microstrip transmission line with complex conductor shape," Electronics Letters, vol. 33, no. 9, p. 786, 1997.

2. C. Shafai, S.K. Sharma, and J. Yip, (2008) *Microstrip delay line phase shifter by actuating integrated ground plane membranes*. Available at: http://ieeexplore.ieee.org/stamp/stamp.jsp?arnumber=4471912 (Accessed: 25 April 2016)

3. A. A. Eldek, "WIDEBAND 180 DEGREE PHASE SHIFTER USING MICROSTRIP-CPW-MICROSTRIP TRANSITION," *Progress In Electromagnetics Research B*, vol. 2, pp. 177–187, 2008.

4. R. duroid, (no date) *RO3000® Series Circuit Materials RO3003™, RO3006™, RO3010™ and RO3035™ High Frequency laminates*. Available at: https://www.rogerscorp.com/documents/722/acs/RO3000-laminate-Data-Sheet-RO3003-RO3006-RO3010-RO3035.pdf

Chapter 7

Power available in a typical office environment

7.1 Introduction

The amount of RF energy can be measured in many different ways. For solely the purpose of this research, what was expected of the indoor measurements was to find out the power available in a typical office environment. To obtain the simplified results, the department building of the School of Engineering and Digital Arts namely the Jennison building was chosen as the subject environment area for the measurement for the sheer ease and accessibility of the building. Some 50 arbitrary places in the department were selected across the department while varying their distances from the WiFi-routers. A Rhode & Schwartz spectrum analyser namely R&S© ZVI6 was used to obtain the readings from the experiment [1].

To opt for the best designed antenna and the maximum obtainable power, three different antennas namely the slot antenna, the UWB antenna and the slot antenna with the bent coaxial cable were selected to determine the variation in results and also determine the antenna which provided those results.

The antennas mentioned here were designed and fabricated as part of this research work. The full description and characteristics of these antennas have already been discussed in chapter 4. The details of these antennas are as follows:

1. Slot antenna

   Dimensions: 98mm X 60mm

Fig. 1 Slot antenna

2. UWB antenna

   Dimensions: 50mm X 48mm

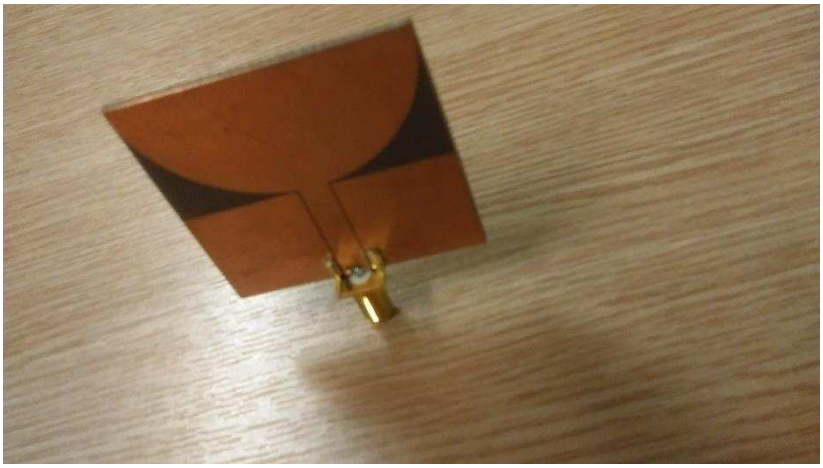

Fig. 2 UWB antenna

3. Bent coaxial cable slot antenna

   Dimensions: 98mm X 60mm , length of the cable= 100mm

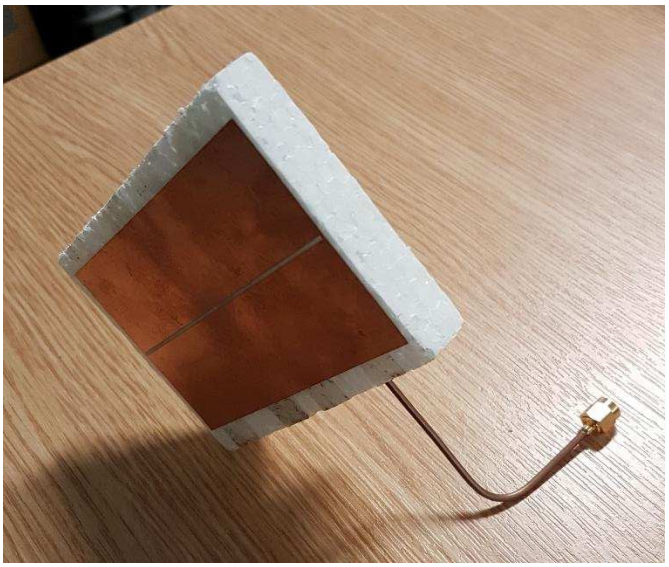

Fig.3 bent coaxial cable slot antenna

7.2 Departmental guide

The Environment that was selected, namely the Jennison building for future references, has 3 different floors which are referred as section. Section 1 was the ground floor of the main building, section 2 was the first floor of the main building and section 3 was the adjoining connected building floor. The floor plans can be seen in the figures below.

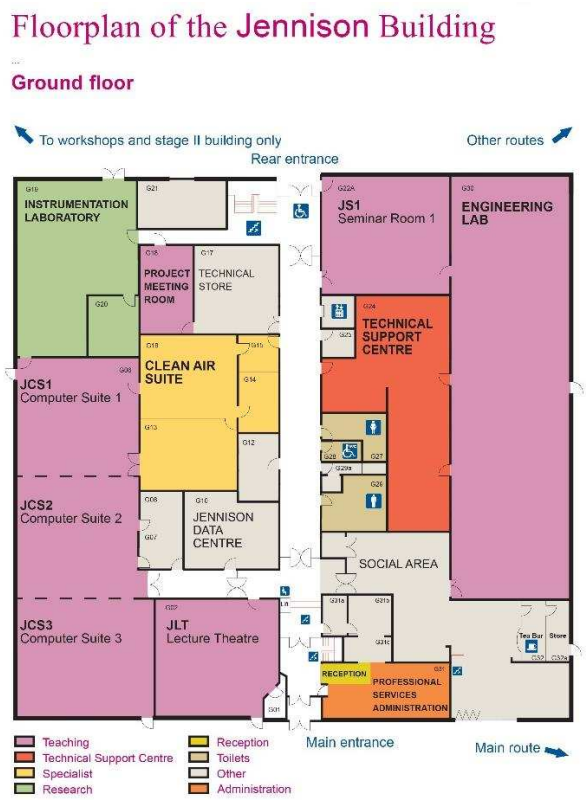

Fig. 4 Floorplan of the Jennison building Ground floor, section 1

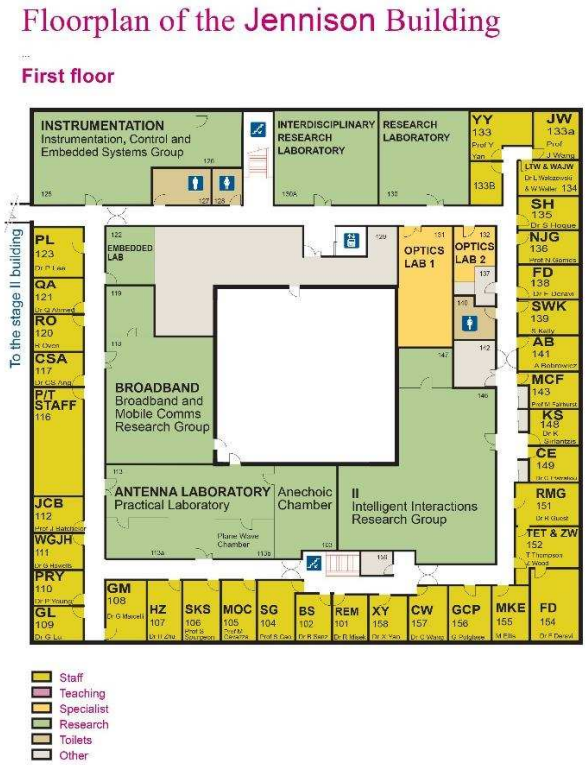

Fig.5 Floorplan of the Jennison building first floor, Section 2

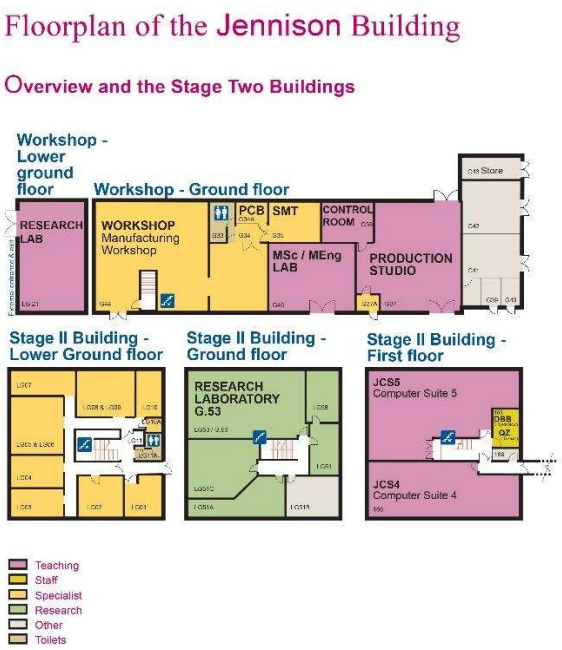

Fig. 6 Floorplan of the Jennison building, section 3

Floorplan of the Jennison Building

Ground floor

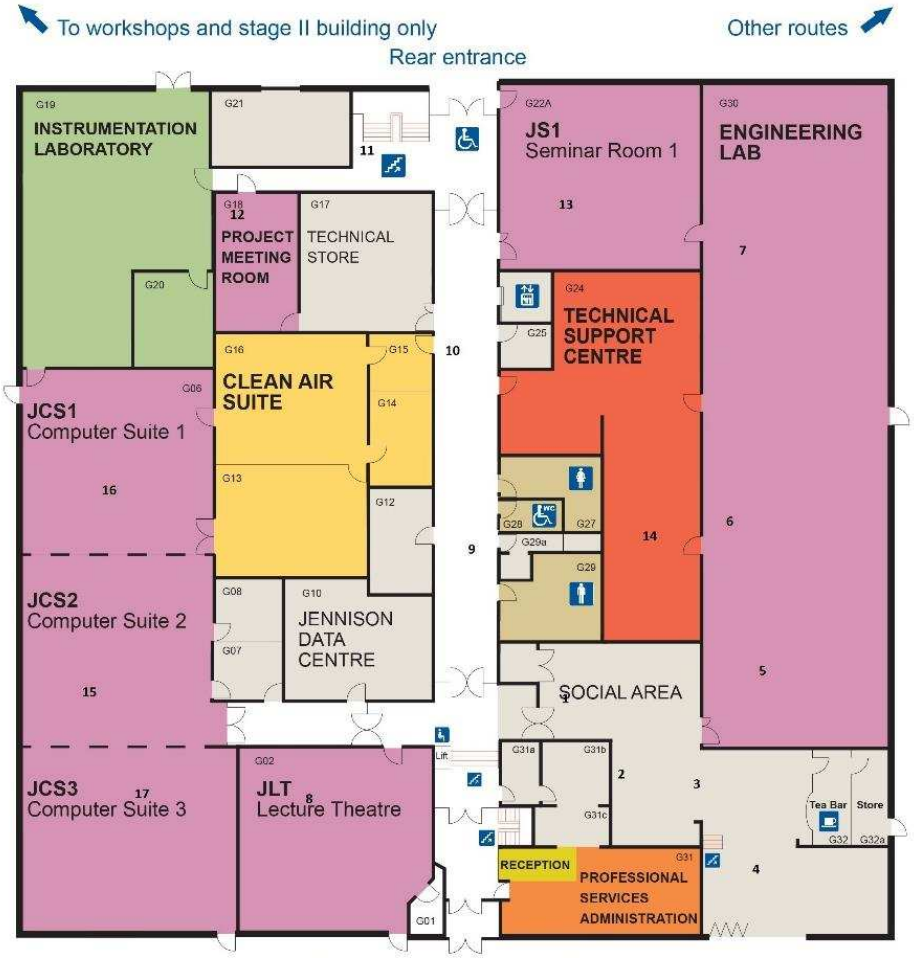

Fig. 7 Ground Floor-plan with marked locations

Floorplan of the Jennison Building

...

First floor

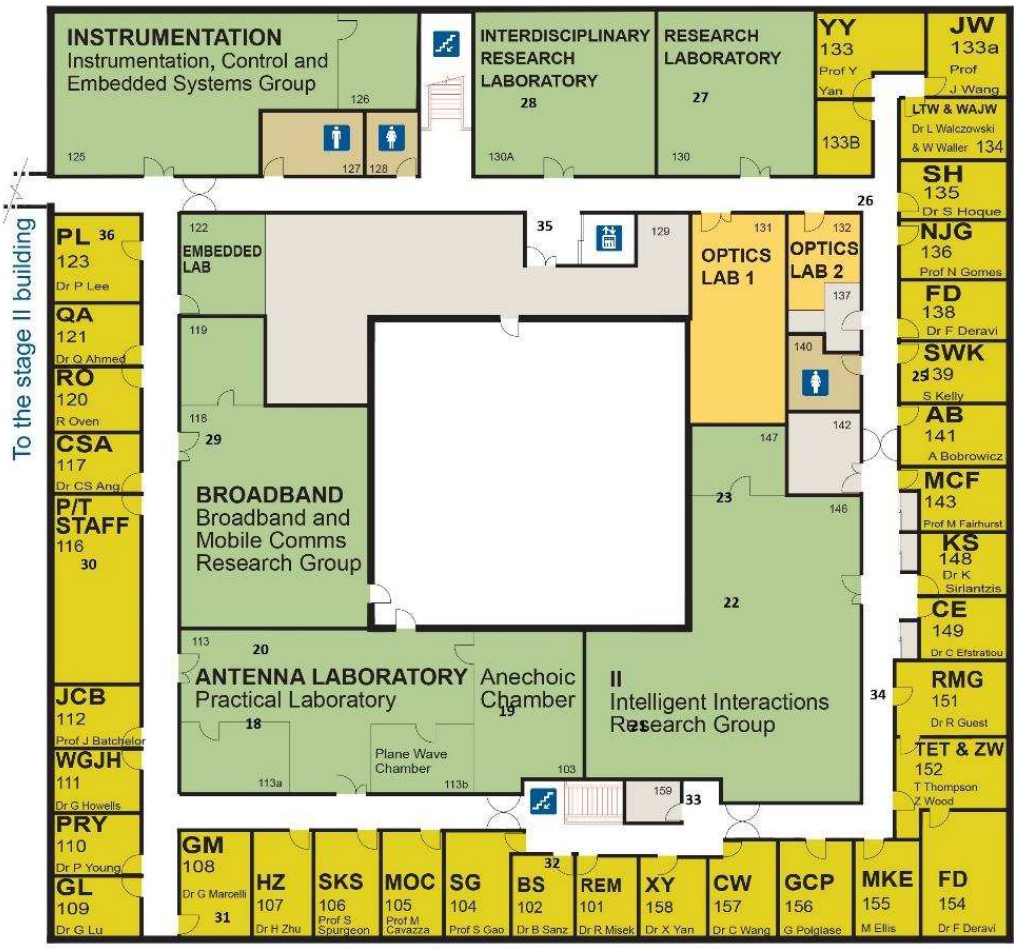

Fig. 8 First floor-plan of Jennison building with marked locations

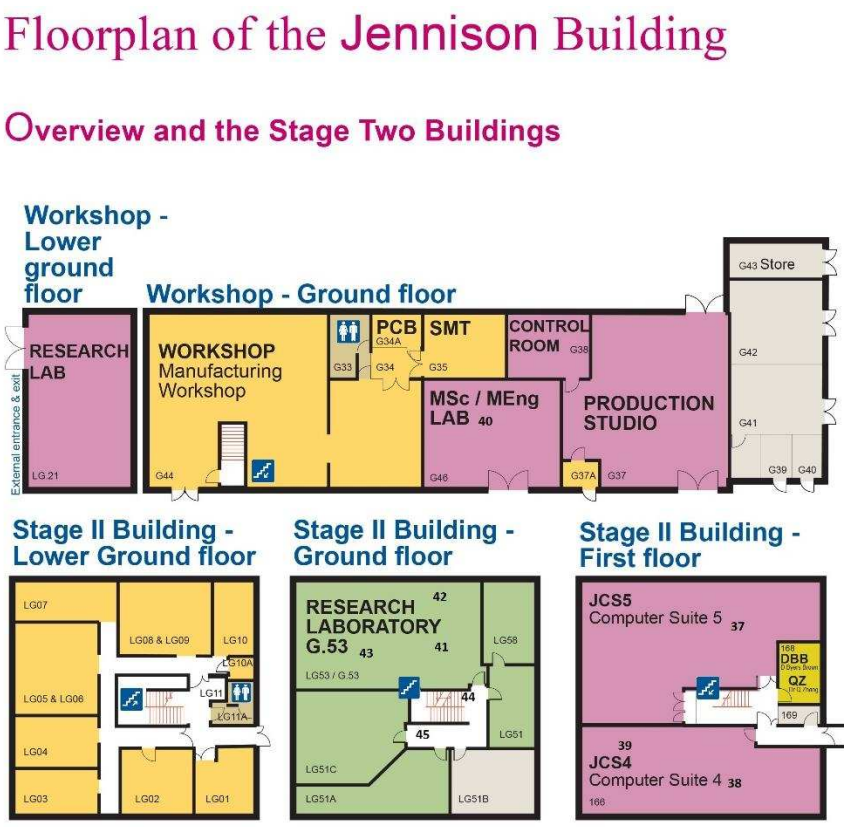

Fig. 9 Stage two buildings floor-plan with marked locations

The different layouts of the Jennison building can be seen above (Fig. 4-6). The arbitrary points were then assumed going from the main entrance of the building (Fig4) and the locations were assigned from thereon as seen in Fig. 7-9. The spectrum analyser was thus used to obtain the dBm value of the ambient RF power from the field at every arbitrary point. These points were taken at a maximum distance of 4 meters. Some points were to have better reception than the others due to their close proximity with the WiFi routers.

The arbitrary locations for the tests were picked and marked in the floor-plans which can be seen in Fig. 7-9. As the locations were selected, the measurements were started and the results were presented in the tables. Photographs of the CISCO WIAN access point can be found in Fig.10.

Fig. 10 1) CISCO WIAN access point router in rooms and 2) CISCO WIAN access point rounter in social areas

CISCO 3602i indoor WIAN access points routers have following characteristics:

1. Max transmitted power at 2.4GHz: 23dBm (200 mW)
2. Available power settings 2-23 dBm (1.56-200 mW)
3. The access point router (Fig. 10.2) consists of 4x4 MIMO antenna with 3 spatial antennas
4. 20- and 40-MHz channels supported
5. 802.11 dynamic frequency selection (DFS)
6. The router (Fig. 10.1) has an omnidirectional patch antenna

7.3 Measurement results

Once the assumptions were made, the measurements were conducted across the department. The results can be seen in Fig. 11 below.

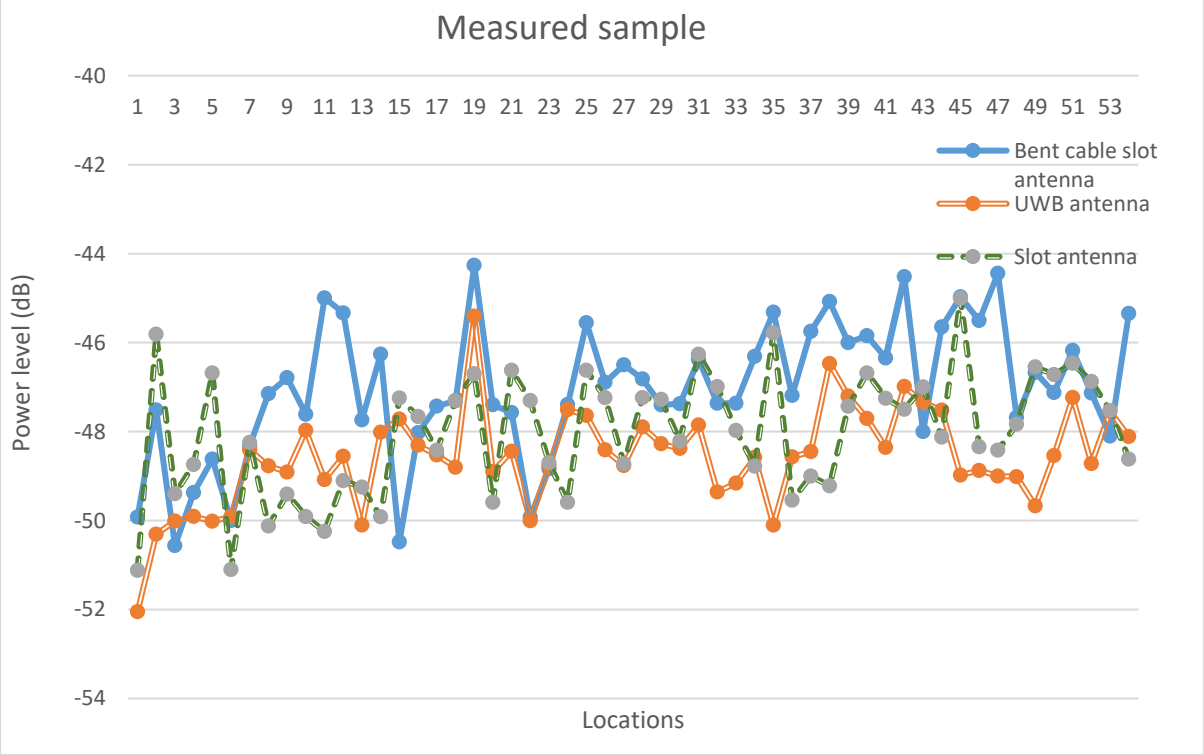

Fig. 11 Field measurement graph

The graph shows the various trends of antennas across the experiment. As it can be seen in Fig. 11, the characteristics of the antennas vary in different environments and they are never exactly same at any two points despite being adjacent to one another. The average field-strength value for the slot antenna was -48.0264 dBW which equates to -18.0624 dBm and 0.0156 mW. The UWB antenna had an average field value of -48.5765 dBW which equates to -18.5765 dBm and 0.0138 mW. The slot antenna with bent coaxial cable had an average RF field value of -47.0302 dBW that equates to -17.0302 dBm and 0.0198 mW.

The standard deviation of the slot antenna was 1.353373. For UWB antenna it was 1.0703 and for the bent coaxial cable slot antenna it was 1.5019.

Conclusion:

This chapter dealt with the RF-field measurement in a typical indoor environment. The objective of this chapter was to determine the amount of RF powers which are typically available in the domestic environments. 3 antennas were used out of which one was a UWB antenna and the other two were slot antenna with a minute difference that the coaxial cable in one of those was bent at the end. The antennas were then connected to a network analyser for RF field-strength measurements across the Jennison building in University of Kent.

The power received was initially measured in dBW which was then converted into dBm and mWatts. As per the observations, the maximum power received at the was 0.0304 mW at one specific point whereas in terms of average, the received power for the SIot antenna was 0.0156 mW, for the UWB antenna, the levels went down slightly to 0.0138 mW and for the antenna with the bent cable, the levels went the highest at 0.0198 mW which we can assume as 0.02 mW.

What can be concluded from the results is that the power levels across the department displayed consistency within a range. The received power levels were highest for the slot antenna with the bent coaxial cable as the bent cable gave room to the reduction in interference in reception of signals. As the experiments were conducted as longer distances, the general levels of received power were significantly lower but as the receptor went closer to the WiFi access point router, the results increased drastically which will be observed further in chapter 8.

These experiments of field-strength measurement gave an idea of the amount of powers which were available across a common indoor working environment. The results were therefore considered as a comparison for the upcoming results and were used to test the antenna design with the microstrip chip to do the tests in a common domestic environment which are discussed in the next chapter.

References:

1. H. Nakane, S. Omori, and I. Yokoshima, "Improving the frequency characteristics of RF standard magnetic-field generator employing loop antenna," *IEEE Transactions on Instrumentation and Measurement*, vol. 26, no. 1, pp. 25–28, 1977.
2. R. Thiex, O. Schwartz, T. Krings, and V. Rohde, "ID: 145 minor edema formation after DSPA-induced clot Lysis of experimental Intracerebral hemorrhages," *Journal of Thrombosis and Haemostasis*, vol. 4, no. s1, pp. 118–118, Oct. 2006.

Chapter 8

Experimental results

8.1 Fabrication

The first set of antennas were fabricated using the techniques of wet etching. Wet etching is a process which involves numerous chemical reactions to dissolve initial reactants to form the new, desired reactant in the desired shape. liquid chemicals are used to remove the materials from wafers. The etching can be divided into two part- isotropic wet etching and anisotropic wet etching. The process which was used initially was isotropic wet etching. This process involves a mixture of HFI, HNO_3 and acetic acid. In this method, the material is removed laterally with the etching process functioning downward [1]. A mask is generated for the desired shape and structure and the unwanted material is etched out of the surface area of the mask to generate the desired shape and structure.

The substrate used in etching the slot antennas was double sided Mylar which was then etched into desired slot antenna design generated over a mask on a transparent sheet.

In the last sections of this chapter, inkjet printing of nano-particle silver inks were employed.

8.2 Measurement

The measurements were conducted for all the experiments with the basic concept of measuring the received power, or voltage levels for a given load resistance. Initially, those experiments were done with varying frequencies, transmitted power levels, distances and even the width of the slot antennas. The details and the results of each of these experiment will be discussed in the coming sections.

The measurement setup consisted of network analysers, spectrum analysers and multimeter depending on the experiment. They were then connected to the antenna which was placed at the receiver end to retrieve the RF power. The linear distances between the antenna and the transmitter

were kept consistently measured and were varied methodically to establish the relation between them. Other tests included varying the strength of the input signal, varying the frequencies and varying the slot width all of whom, were conducted in similar environments in a plane-wave chamber. The details of each one of these will be discussed in the subsequent sections.

8.3 Slot antenna and a rectifier connected directly to the antenna

Preliminary test where the input impedance of the antenna was not fully matched to the impedance of the rectifier are described here. These tests were carried out solely for practical understanding purposes and as initial assessment of the system. Results for optimized rectenna network are described in the upcoming sections.

The first tests which were conducted by measuring the voltage levels in a chamber typically used for plane-wave measurements. These tests were conducted to understand the functioning of the slot antennas with varying factors such as distance from the source, intensity of power transmitted, variation in frequencies and variation in slot sizes etc. The tests are described below with the description and the results.

8.3.1 Measurement while varying the frequency of transmission

The fabricated antenna with the rectifier can be seen in Fig. 1a-b. A λ-wavelength slot was employed in this first experiment. The rectenna consisted of a double layer copper clad Mylar substrate of thickness of 0.05mm, with the slot etched on one side (Fig.1a) and the tracks for the diodes on the other side (Fig.1b). The dimensions of the antenna were 140mmX70mm. The total length of the slot was 120mm. The diode used in the design was the surface mount Schottky diode by skyworks SMS7630-079IF with an inductance of 0.7 nH and input resistance of 20-Ω. The typical diode circuit can be seen in figure 1c. The details about the diode such as its characteristics and its specifications have been discussed in chapter 3.4.

In this experiment, the apparatus was setup in the chamber as seen in Fig.2 and the frequency of transmission was varied and the received voltage at the receiver end were measured and noted.

Fig. 1a ModeI antenna for experimentation (Front side)

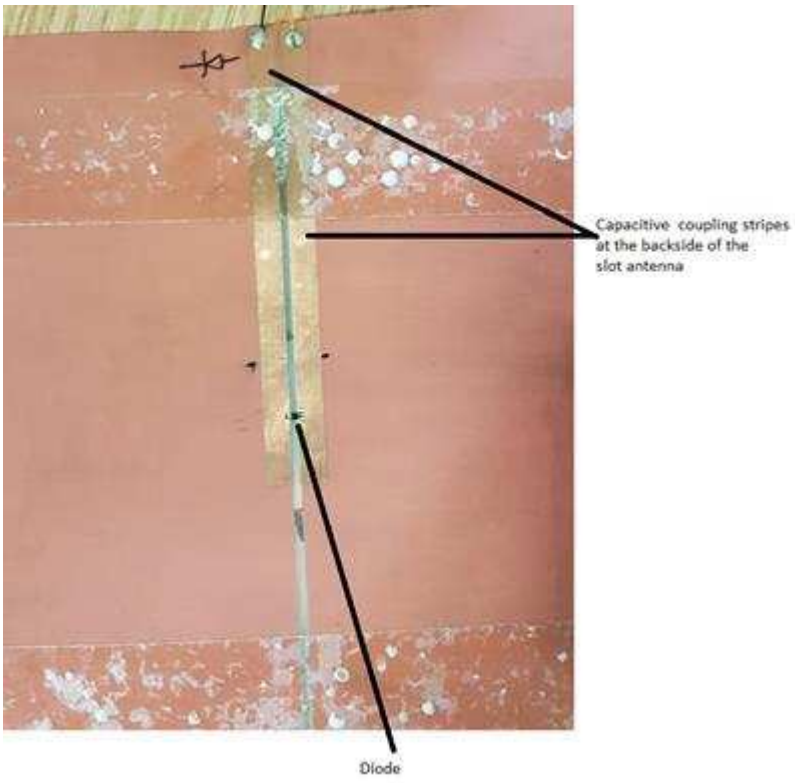

Fig. 1bModeI antenna for experimentation (Backside)

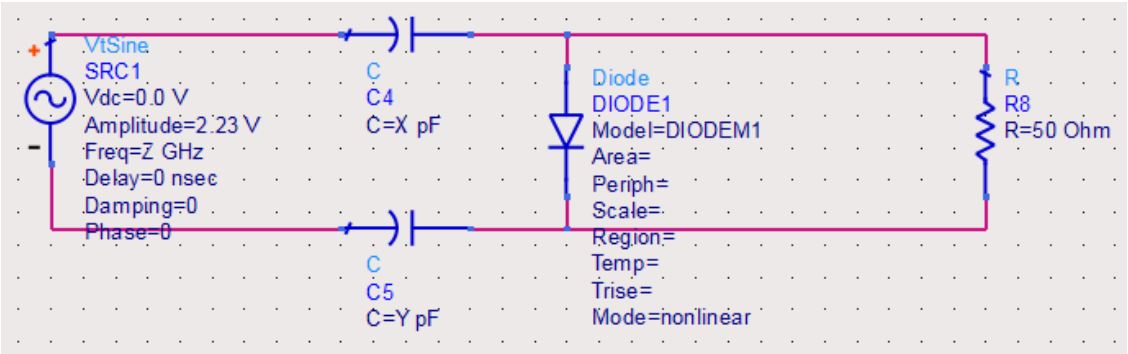

Fig. 1c Equivalent circuit model of the antenna showing the capacitive coupling

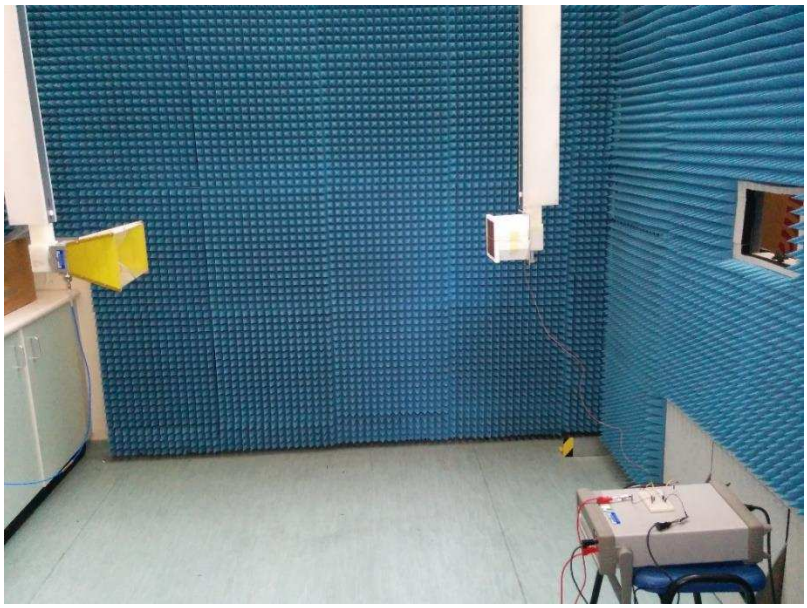

Fig. 2 The experimentation apparatus

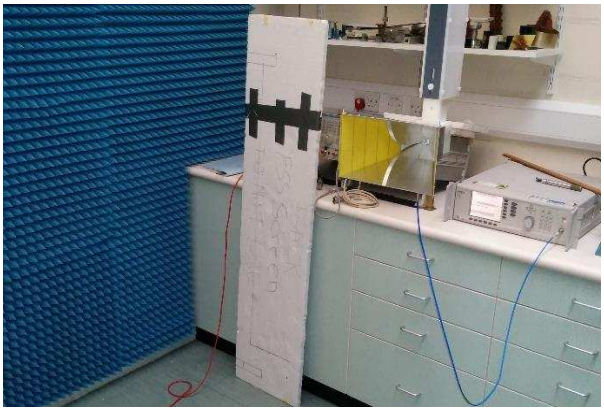

Fig. 3a Showing the apparatus from the transmitter end and Fig. 3b showing the apparatus from the receiver end

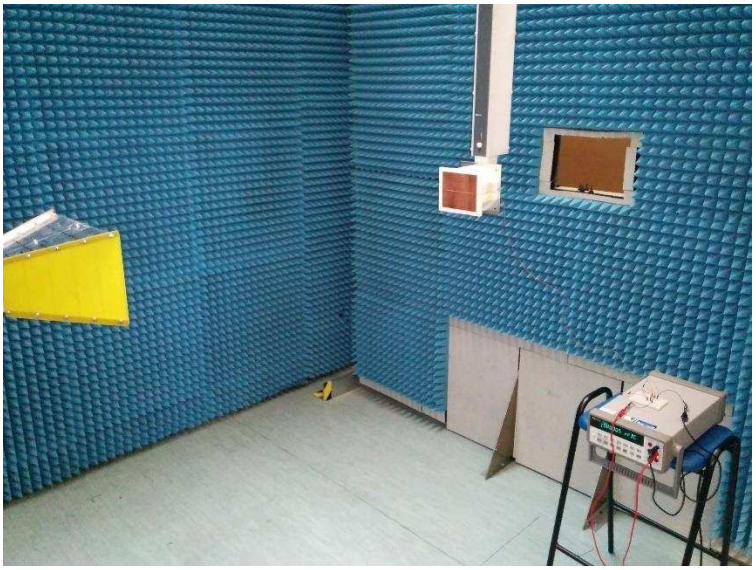

Fig. 4 Apparatus showing the measurement being underway

As the desired frequency was assumed to be within the bluetooth band, only the frequencies in the 2.4 GHz region were first examined. . The results (Fig.5) show that the maximum voltage is obtained at 2.43 GHz, demonstrating that the slot is best matched at desired frequency.

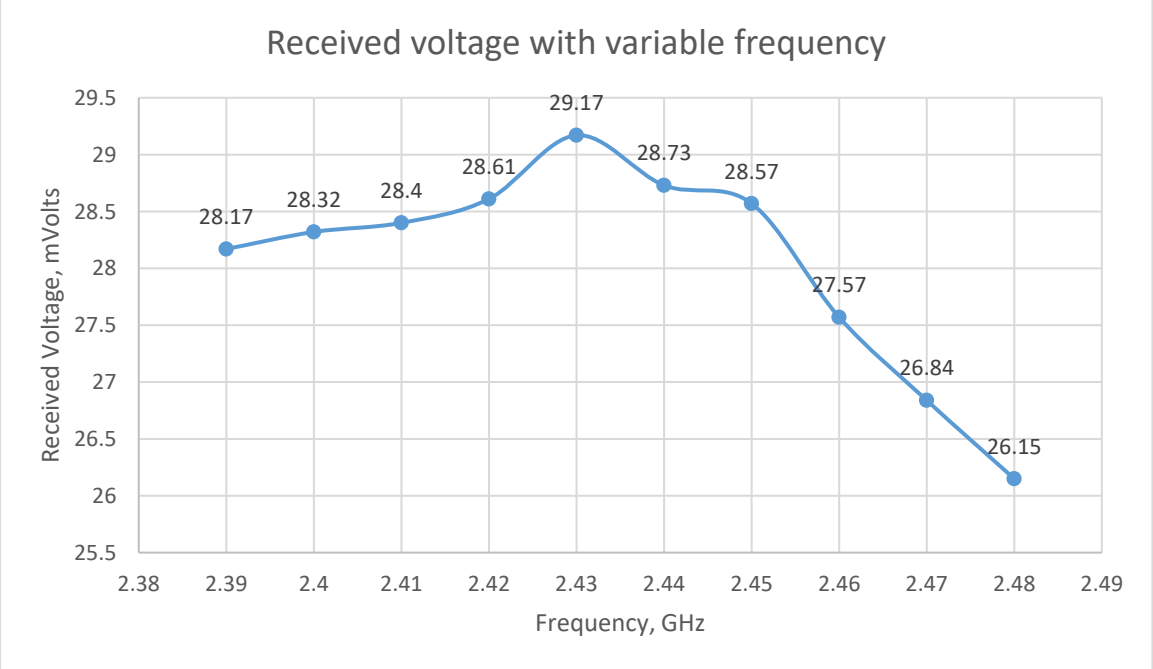

Fig. 5 Graph showing the trend of Received voltage vs the variable transmission frequency

8.3.2 Measurement while varying the power of transmission

The next test in the line was to assess if the rectified power was due to the input power, and the effectiveness of the harvesting process. In this experiment, the frequency was kept consistent at 2.43 GHz and at a distance of 1 meter, and the input power levels were varied and the results were measured. As it can be seen in Fig.6, the levels of the received voltages expectedly increase as the input voltage, proving the effectiveness of the rectenna.

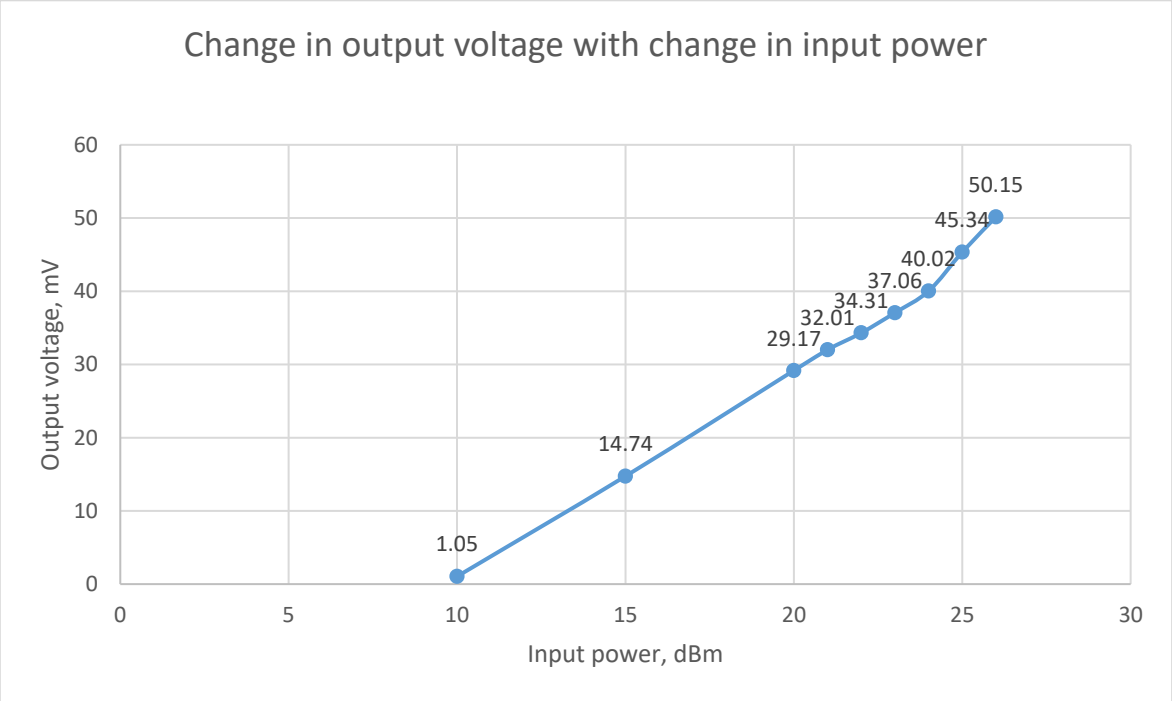

Fig. 6 Graph showing the change in output voltage vs the change in input power

8.3.3 Measurement while changing the value of the resistance

In this experiment, the frequency levels were varied with the power being kept constant at +20dBm and a load resistor was varied from 25Ω to 100-Ω was added after the antenna. The output voltages were measured for a wider band of frequencies and the results were noted. The same test was

conducted using the 25, 50 and 75Ωresistors respectively. The results and the graph can be seen in Fig.7.

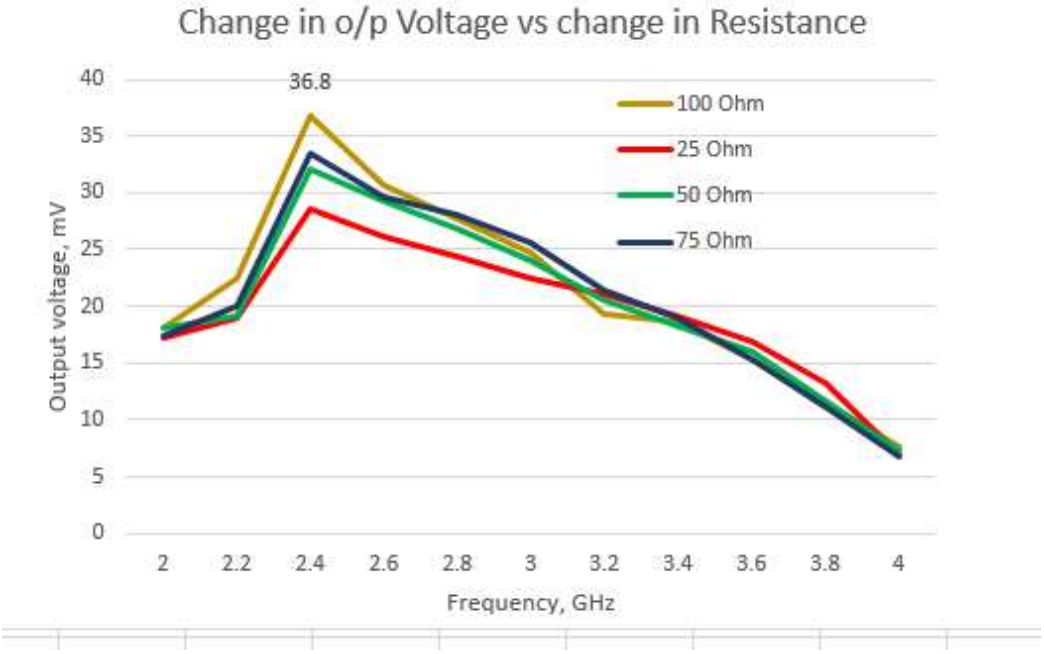

Fig. 7 Graph showing the output voltage levels vs the varying frequency of transmission

As the graph in Fig. 7 suggests, the output voltage was at its peak at 2.4 GHz for all the resistor values, with the best result obtained for 100Ω. The output voltage levels gradually increased as we proceeded from 2 to 2.4 GHz and decrease slightly from 2.4 to 3.2 GHz. The output voltage levels dropped drastically from thereon. That was due to the matching of the designed model antenna at 2.4 GHz.

8.3.4 Measurement while varying the length of the slot

In this experiment, the total length of the slot was varied by adding patches which decreased the width by 2mm at a time. The change in patch was then used and measured using the experiment. The results were then observed and analysed. The results can be seen below.

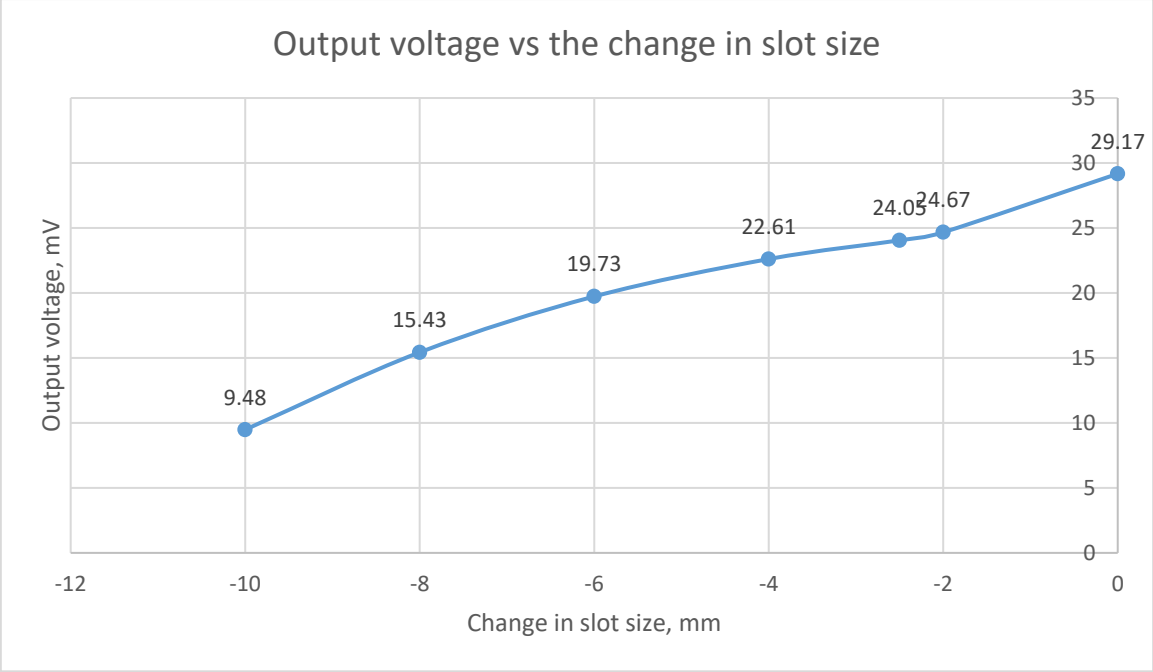

Fig. 8 Change in output voltage vs the change in slot size.

The Fig. 8 shows the results for the change in output voltage when the slot size is changed. It can be seen that the voltage levels drop drastically with the reduction in the size of the slot. The change in the slot size changes the matching of the antenna and thus causing the antenna to lose its ability to have a match at the desired 2.43 GHz. The reduction wasn't possible beyong the 10mm mark and it was certainly not possible to hetch the design to increase the slot size in any way hence, only the permissible reduction was conducted in the experiment.

8.4 Measurements with antenna and the matching circuit

As the matching circuit was designed and thus fabricated as seen in chapter 6, the design was thus tested using the antennas and the matching circuit. For these tests, the main criteria of testing was to use the receiver apparatus in the plane-wave chamber to access the power levels harnessed at the particular levels. The chip and the antenna together can be seen in Fig. 9a-b below.

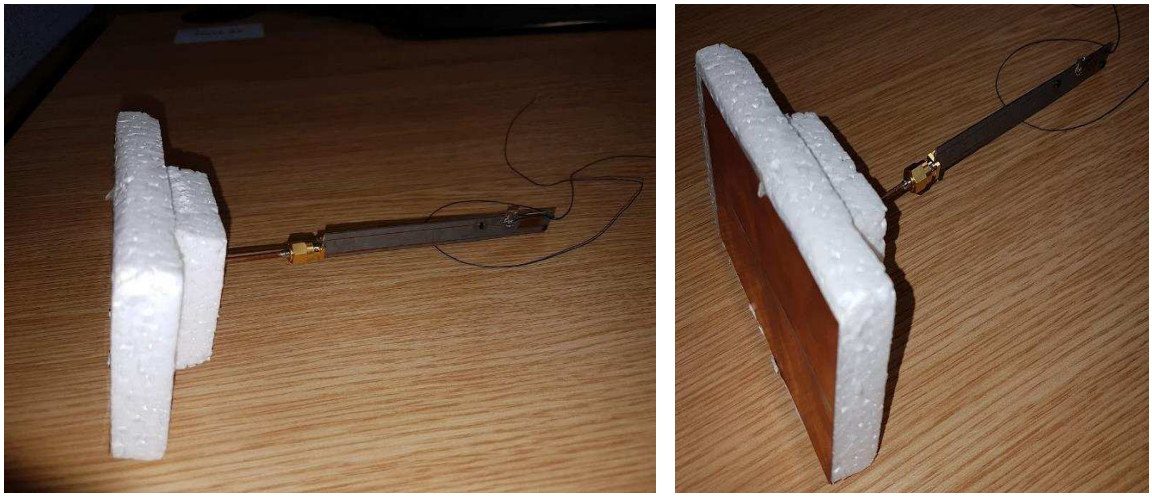

Fig. 9a. Antenna with the rectifier chip side view and 9b. diogonal view

For this particular test, the techniques anf the specifictaions for the measurements which we retreived from earlier sections of this chapter. As it was observed through the graphs in Fig. 5-8, the model antenna provided the best readings at 2.43 GHz at +20dBm power level. 2 different slot antennas were designed using the same configuration but the dimensions of the antennas were changed so that to reduced the size of the surface area of the antennas and make them more efficient and less bulky.The newly designed antennas were discussed in Chapter 5 which demonstrated their radiation patterns, S-parameters, surface currents and parametric analysis simulation results which were then used to fabricate the antennas.

The antennas that were used in the final tests were the slot antenna with an SMA, the slot antenna with a coaxial cable and an SMA and UWB antenna.The antennas can be seen in the figures below. The diode used for these experiments was different from the one used for the previous experiments. The diode used here was HSMS 2862-SOT-23 which is usually manufactured by Avago.

Fig. 9c SIot antenna with anSMA connector

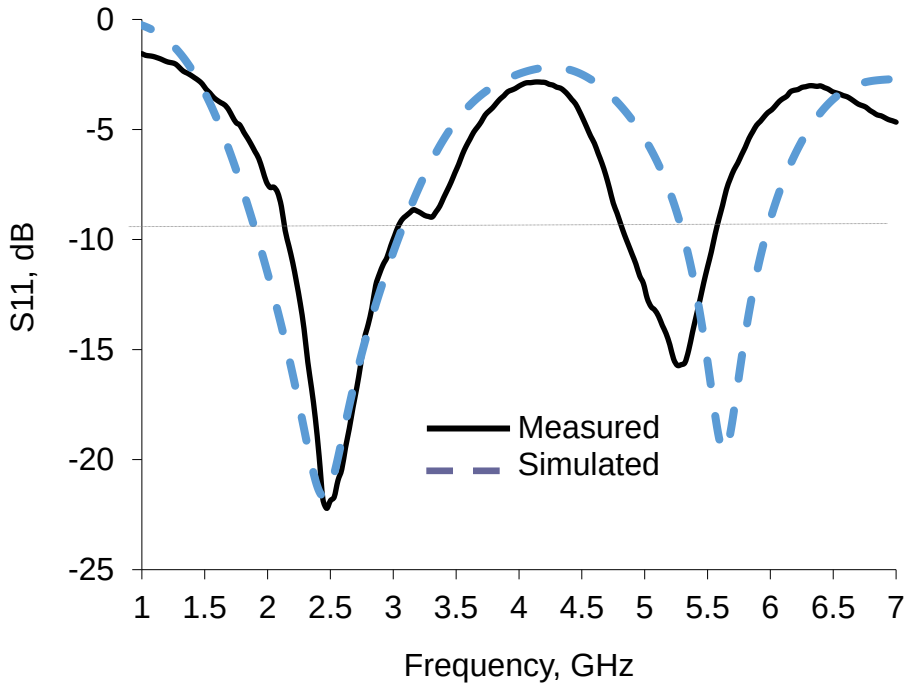

Fig. 10 Simulation vs result graph for the slot antenna with an SMA connector

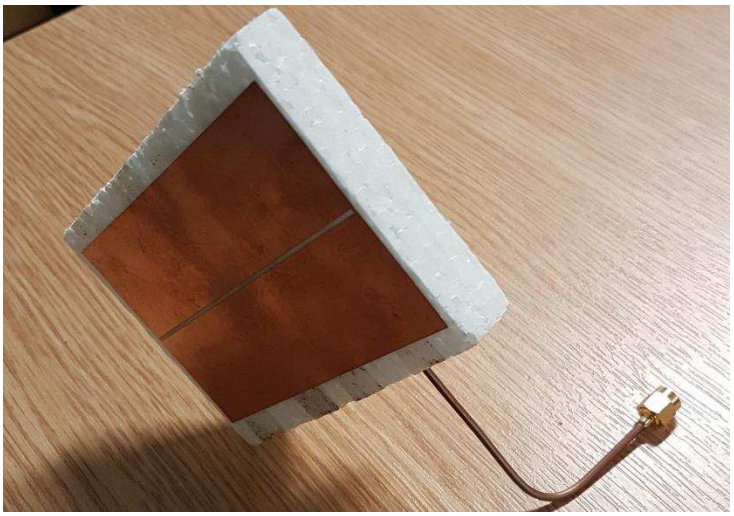

Fig. 11 SIot antenna with a coaxial cable and an SMA connector

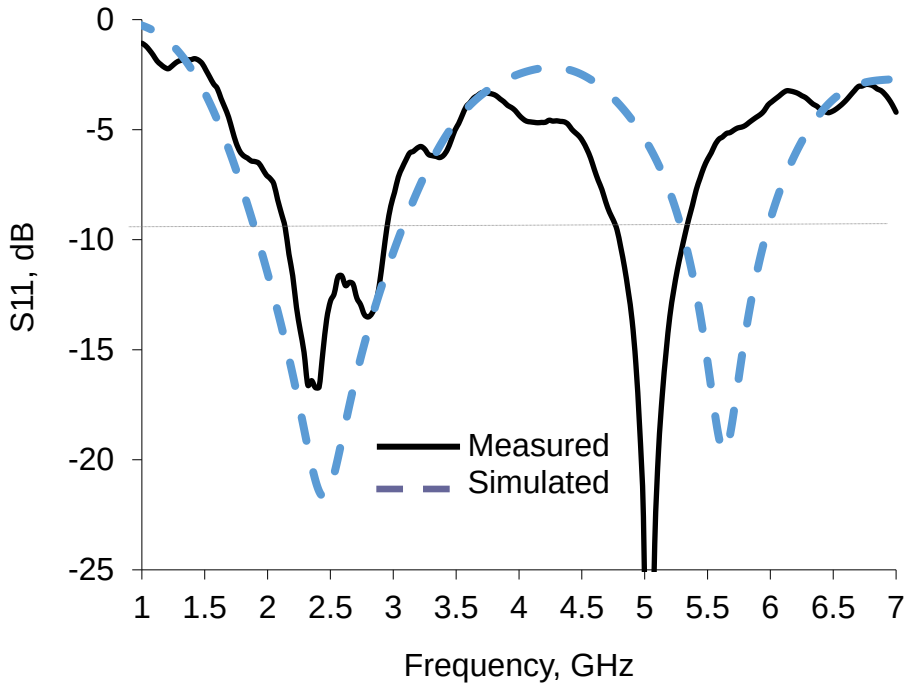

Fig. 12 Simulation vs result graph for the slot antenna with a coaxial cable and an SMA connector

The fabricated slot antennas, as they were seen earlier in this chapter in Fig. 9 and 11, were then tested for results. Coming onto the SIot antenna with just an SMA connector, the simulation were plotted with the measurement results and the compared reasonably well, as shown in Fig.10. Both the graphs were perfectly matched at -21.27 dB at the frequency of 2.43 GHz with the measured antenna depicting a narrower bandwidth. The measurements showed a shift in the matching at the

higher frequency. That was probably due to fabrication errors, particularly were the antenna was connected.

Fig.12 show the results for the slot antenna with a coaxial cable and an SMA connector. Again, It can be seen some variation in the simulations from CST and the measurements. The variations and the nature of matching in the design was due to the fact that the addition of the SMA connector and the coaxial cable weren't under consideration during the CST simulations and despite the variation from the simulation results, the measurements results showed a very good match of -17 dB at the frequency of 2.41 GHz.

Fig. 13 the UWB antenna

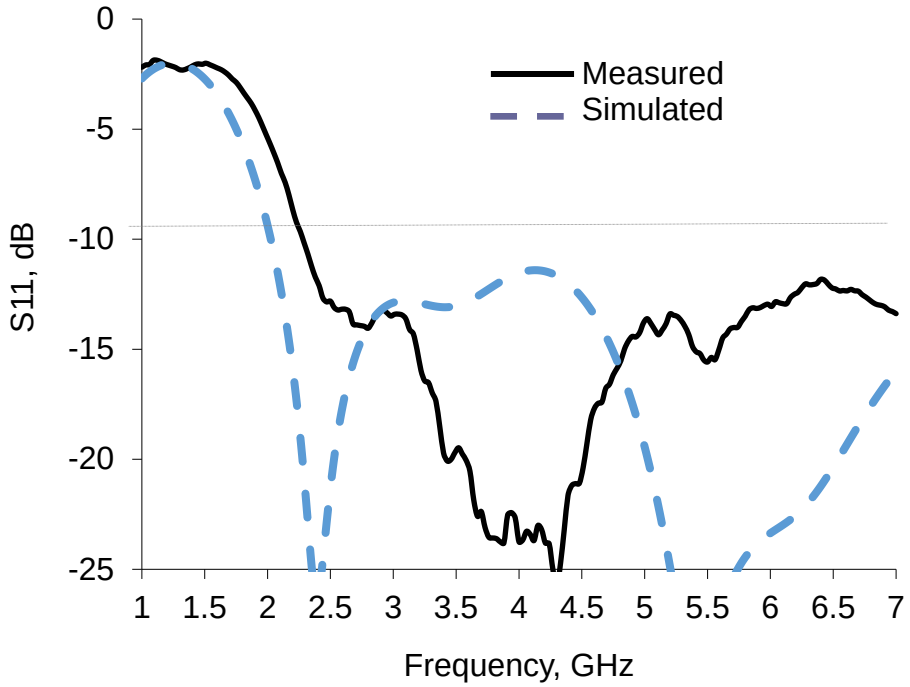

Fig. 14 The comparison between the simulation and experiment result of the UWB antenna

Figure 14 shows the simulation versus experiment results for the UWB antenna. UWB antenna, as the name suggests shows a wider band of operational frequencies and despite having a well below -10 dB matching at the desired frequency of 2.43 GHz, the measured and the simulated results appear to be matching at different frequencies with a lot of ripples present in the measurement. The ripple in the experimental values can be observed due to the minute manufacturing defects and multiple fluctuating RF signals present in the ambient environment within the plane-wave chamber. The variation in matching however, was due to the fact that the connection of SMA and the implications of the strands of the connector on the ground planes of the antenna were not considered during the CST simulations.

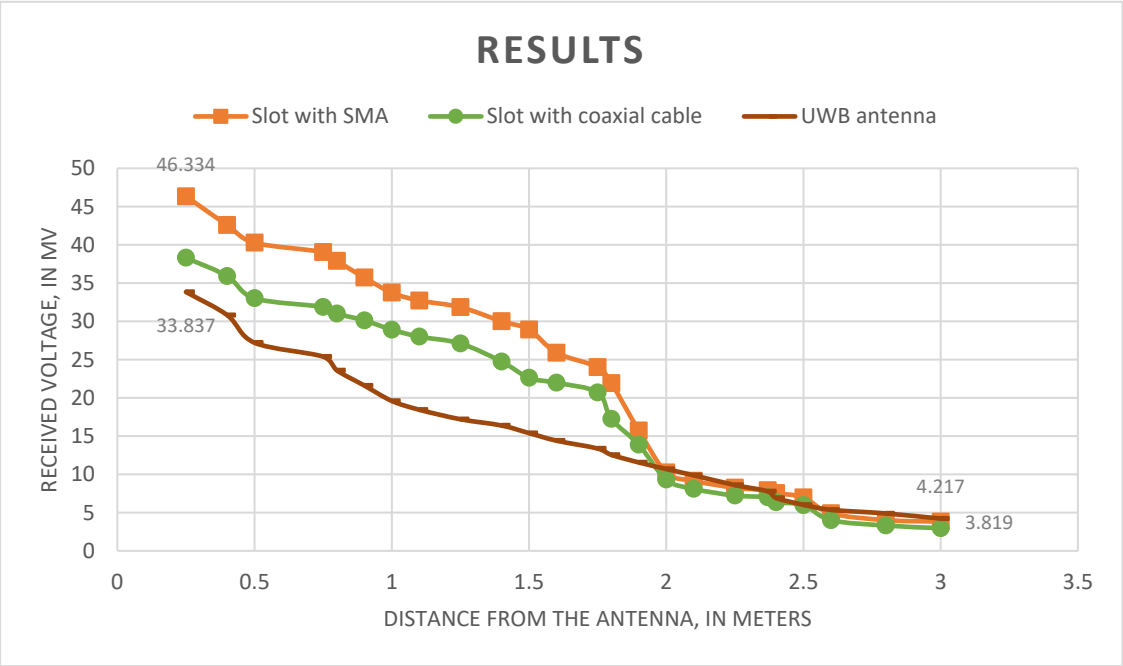

Fig. 15 Measured received voltage at various distances for different antennas

Orange: Slot antenna with only SMA, Green: Slot antenna with coaxial cable and Brown: UWB antenna

The next measurement that was conducted was to compare the antennas for the maximum distance up to which they could transmit. The test was conducted in the plane-wave chamber and the antennas were fed with the signal from the transmitter horn antenna and their received voltage values were measured while changing the distance between the transmitter and the receiver. The graph in Fig. 15 shows the trend of the voltage received versus the distance from the transmitter antenna. The trends show that the maximum distance attained for the reception of RF power signals was beyond 3 meters. It can also be observed that no two antennas showed the same characteristic pattern when it was placed close to the transmitter. The slot antenna with the SMA connector showed the maximum reception of 46.334 mV at a distance of 25 centimeters from the transmitter. The UWB antenna was the least responsive at 25 centimeters with a reception of 33.837 mV. The reason behind the low reception of the UWB antenna despite its ability to receive wider frequency band is the relatively lower gain as compared to the Frequency selective slot antenna with the SMA connector along with the other frequency selective slot antennas. As the reception band of the UWB antennas, going by the name are significantly wider than those of the slot antennas as seen during simulations in Chapter 4. Due to this reason, the functioning of slot antennas at the given frequency of 2.43 GHz was better

than that of the UWB antennas. The variations in the results of various slot antennas were observed due to the losses caused in the system due to the presence of various physical and RF related factors. Physical factors, as the name implies were the presence of the coaxial cable and the losses attached with the addition of the cable. RF implications, such as the presence of various frequency bands and interactions among different signals is also a deciding factor in the amount of losses present within a system. The efficiency of the system for these tests, conducted in controlled environment was conducted using the Friis power equations (As discussed in Chapter 3, section 3.6) using the information available and obtained through the system. The controlled environment tests using a single slot yielded a maximum efficiency of 65.52% with the slot antenna with just the SMA connector under the considerations that the entire system and component worked at its peak performance and every component was assumed to be working perfectly. The efficiency was calculated putting the total received power which included the rectified DC power along with the RF distortions which couldn't be eradicated against the total transmitted power from the signal generator.

The interesting pattern which needs to be observed is the similarity in the characteristics of the antennas. In Fig. 15, the output characteristics of all the antennas beyond the 2 meter mark show identical patterns for all the antennas and the values for the output voltages become nearly equal at that point. To verify these results, the same apparatus was then used in the field measurement setup and was tested at a particular indoor environment for comparison purposes.

8.5 Field measurement tests using antenna and the matching circuit

In this test, the same apparatus which was used for the tests in section 8.4 was used. The apparatus consisting of namely the antennas and the matching circuit was thus used to be tested in an ideal domestic environment setup. For that, the test was conducted at an arbitrary place chosen at random and the same tests which were conducted in the plain-wave chamber were repeated using a WIAN access point routers. The main objective of the test was to compare the results of the tests conducted in the plain-wave chamber to those of the open area. The test was conducted. The apparatus and the results can be seen in the figures 16-18 and the graph below.

Fig. 16 Test setup

Fig. 17 Testing setup 2

Fig. 18 WiFi access point router

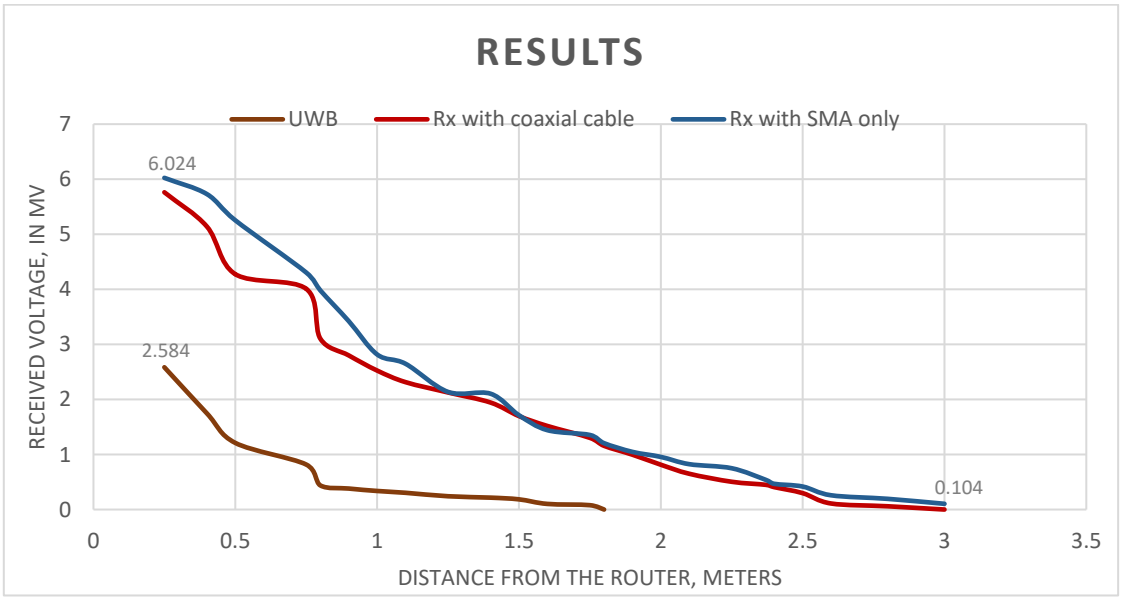

Fig. 19 Graph showing the received voltage vs the distance from the router

The results of the field measurements can be seen in Fig. 19. As expected, the received voltage decreases in a near exponential manner and it becomes zero after attaining a certain peak distance from the access router. As it can be seen, the slot antenna with only the SMA attached to it displayed the best results out of the antennas that were tested.

The results as denoted in Fig. 19 show that the antenna with the SMA connector has the best result with the voltage at a distance of 25 cm being 6.024 mV and showing some minor reception of 0.104 mV till the 3 meter mark.

The UWB antenna, as it was in the case of the tests in the plane-wave chamber was the least responsive again due to the difference in gains between the slot and the UWB antennas as well as due to the difference in the matching with the microstrip chip. The maximum distance attained by UWB antenna was also significantly lower at 1.8 meters only. The efficiency for the field measurement tests along with the rectifier microstrip chip was calculated by not just using the Friis equation formula but it also required the usage of the simpler formulas such as $P=\frac{V}{I}$ as well as $\eta= V_o^2/V_i^2$ along with the available power levels for a transmitting WiFi access router for every distance to obtain the available power at every point. The power levels were higher as the measurements moved closer to the router. The peak in the efficiency was obtained at a distance of 25 cm as expected with the efficiency value reaching at 33.95% which were significantly lower due to the absence of available high power levels and the power losses to the ambient environment. The losses were present because of the omnidirectional properties of the transmitting patch antenna. The available power, was scattered in all the directions and due to the small surface area of the antenna used for this experiment, only a fraction of that power could be harvested. Usage of an antenna array for the same purpose would result in a drastic increase of the received power but that was deemed the work to be implemented in the design in the future.

8.6 Evaluation of a low-Cost Inkjet Printed Slot Antenna for Energy Harvesting Applications

This section presents the paper which arose during this research which presents a study of the effectiveness of fabricating slot antennas using low-cost inkjet printing techniques for use in energy harvesting applications. A slot antenna has been fabricated using commercially available nanoparticle silver ink and an inkjet printer suitable for home or office use. A second identically antenna has been fabricated using standard etching methods on a double sided copper Mylar substrate. The reflection coefficient characteristics of both antennas have been measured and compared. The antennas were

then tested in an indoor environment using PowerCast radio frequency (RF) power transfer and energy harvesting system [14]. The performance of the antennas in the energy harvesting configuration are evaluated and discussed.

A. **Antenna Design**

A slot antenna is a well-known resonator with many useful properties. Its complementary form is a wire or strip and the impedance and data pattern of this form can be used to predict the behaviour of the slot antenna [15]. The large amount of metal used in the slot antenna makes it an attractive solution for inkjet printing technology. This is particularly true if the conductivity of the deposited metallic layers is not very high compared with other fabrication methods. A half wavelength slot antenna was designed to operate at the 915MHz ISM band. The dimensions of the antennas are shown in Fig.20 and table 1. As described in [15], the feeding of the slot have to be placed in one side in order to achieve 50Ω input patch. The substrate used was a polyethylene terephthalate (PET) film of thickness 135μm, permittivity, ε_r , of 3 and loss tangent of about 0.02. In order to be able to connect the inkjet printed antenna without damaging the printed tracks, capacitive coupling pads were placed at the back of the antenna (Fig.20b). The dimensions of the metallic pads was 5mm x 5mm. This pads can also work as decoupling capacitors for the RF energy harvesting circuit, though this was not the primary use in the design.

Fig.21 presents the simulated reflection coefficient (S_{11}) of the antenna when the port was connected directly to the slot, and also when the port was connected to the capacitive coupling pads. As can be seen from the figure, the pads have a very minor effect in the S_{11} of the antenna. The resonant frequency decreased by less than 1%. In both cases, the antenna resonated at about 915 MHz with -10dB bandwidth of about 9%.

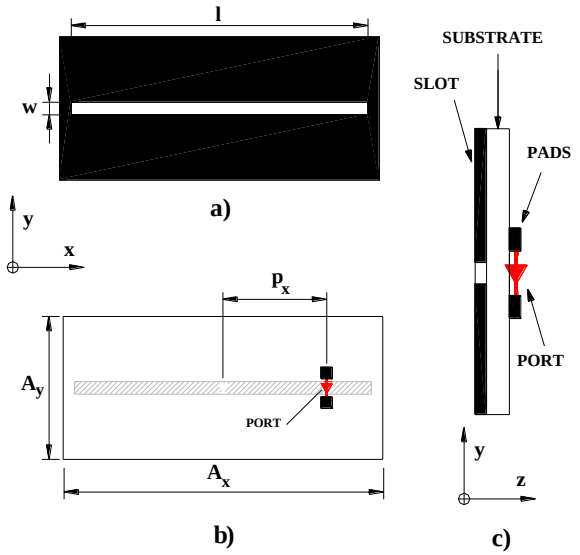

Fig. 20 SIot antenna dimensions: (a) front view, (b) back view, (c) side view

TABIE 1 Antenna dimensions

	l	*w*	A_x	*Ay*	P_x
Dimensions (mm)	158	1	188	96	1.3

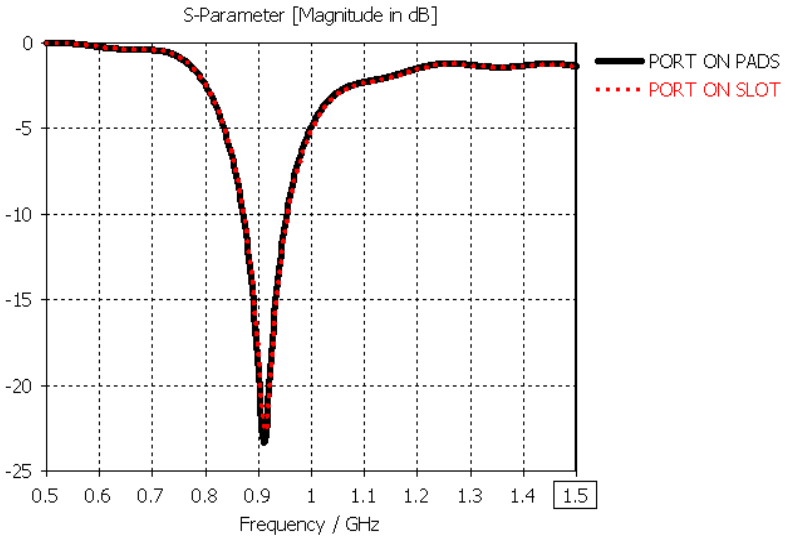

Fig. 21 Simulated reflection coefficient (S_{11})

Fabrication and Measurements

The antenna design was exported to a .gbr file and then converted to a .pdf file for printing. A Brother MFC-J5910DW inkjet printer was employed together with the AgIC-CP01A4 paper and AgIC-AN01 Silver Nano Ink [16]. Fig. 22 shows the fabricated antenna on the paper substrate. The substrate had a thickness of 135µm. The sheet resistance of the printed metallic layers is about 0.2Ω/sq [16]. The resistance between any two ends of the antenna was found to be less than 1Ω. The two capacitive coupling pads were fabricated using adhesive copper tape and were attached to the back of the PET film in the location described in Fig.20 b. The pads were connected to a semi rigid coaxial cable which had a 50 Ω SMA connector in the other end. A piece of Polyurethane was used as support for the antenna and connector. In order to assess the performance of the inkjet printed antenna, the same model was fabricated by etching the patterns on the metallic layers of a double-sided copper clad Mylar substrate (Fig.23).

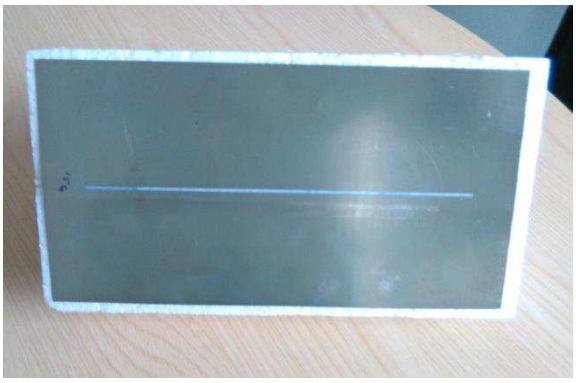

Fig. 22 Inkjet printed slot antenna

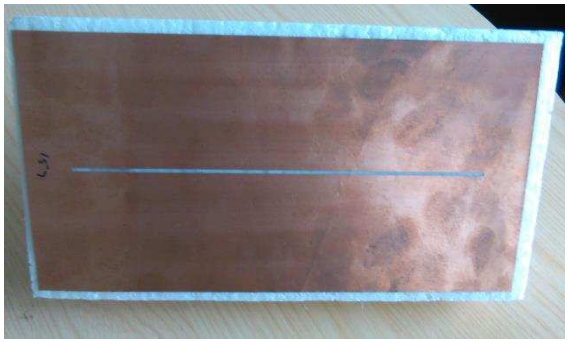

Fig.23 Copper etched slot antenna

The measured reflection coefficients (S_{11}) of the inkjet printed and copper etched antennas are shown in Fig.24. The simulated reflection coefficient is included for comparison. The copper etched antenna

resonated at about 900MHz, while the inkjet printed antenna at slightly lower frequency. The two antennas covered the 902-928Mz required for the PowerCast power transfer and energy harvesting system.

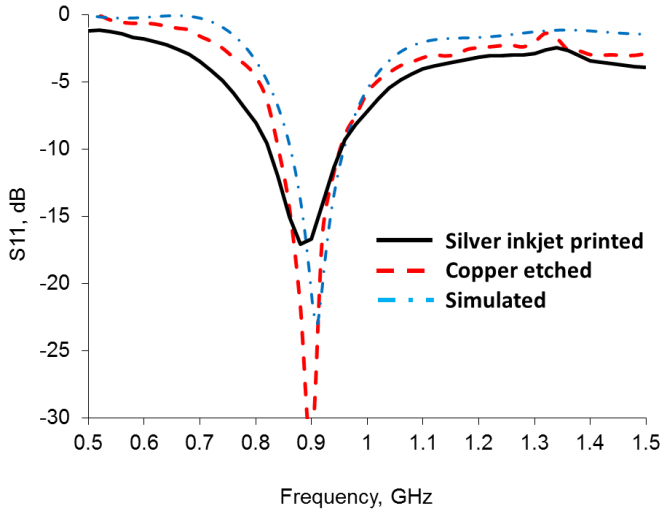

Fig.24. Reflection coefficients (S_{11})

The computed radiation patterns of the antenna at 915MHz are shown in Fig. 25. As expected, patterns were those a slot antenna, and were not affected by the inclusion of the capacitive coupling pads. The gain of the antenna was 4.9 dB.

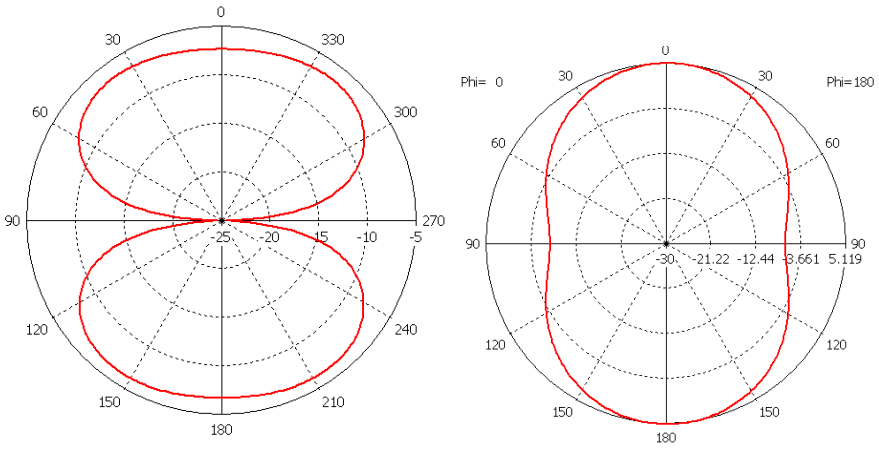

(a) x-y plane (b) x-z plane

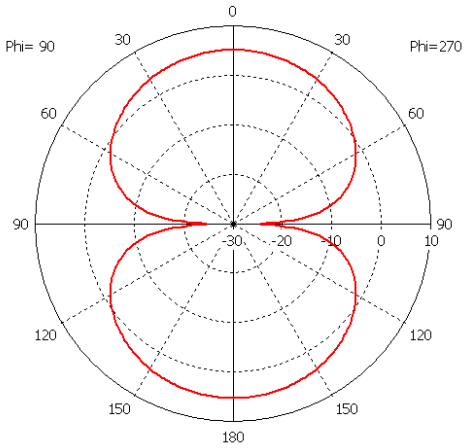

(c) y-z plane

Fig. 25 Computed radiation patterns

B. **Evaluation of the Antennas using PowerCast Energy Harvesting System**

The lifetime Power® Energy Harvesting Development Kit [14] was used for the assessment of the slot antenna in an energy harvesting system. In this development kit, the source of RF energy was the TX91501 transmitter (Fig.26 (a)) which sends radio waves at 915 MHz. The power output of the TX91501 is a factory fixed (not user adjustable) and equals to a maximum of 3 watts. Besides this frequency, other RF energy sources that operate within a range of 850-950 MHz can also be used to harvest energy from. The harvesting module with the wireless sensor board and an antenna supplied by the manufacturer is shown in Fig.26 (b). The board is equipped with an SMA connector which is used connect the antenna under test. The module uses the PowerCast P2110 power harvester receiver, which has all the RF circuitry necessary to convert ambient RF signals to DC. It also has capacitors as storage devices to power the wireless sensor board without using batteries. The P2110 converts RF energy into DC power and it charges the capacitor until a threshold is reached. When the capacitor is charged, regulated output of Power harvester Receiver is used to power the wireless sensor board until the low-voltage threshold on the capacitor is reached or until the operation is completed by the wireless sensor board.

The TX91501 transmitter is designed to transmit power and data to target devices equipped with the PowerCast power harvester receivers (P2110 or P1110). This is done by transmitting radio frequency power in the form of Direct Sequence Spread Spectrum (DSSS) at a centre frequency of

915MHz. The beam of the radiation pattern is 60 degrees wide, 60 degrees high and vertically polarizes to enhance transmission.

The main operation of the system is as follows. When one of the test antennas is connected to the board, it feeds the power harvester receiver. The power harvester receiver converts the RF energy into DC power which is used to charge a super capacitor on the main board. The super capacitor accumulates energy until a threshold of 1.2 V is reached, it then discharges its energy to a voltage booster. Then, the voltage booster increases voltage level from 1.2 V to 3.3 V which is enough to power a wireless sensor node.

The wireless sensor board is equipped with 2.4 GHz IEEE std. 802.15.4 RF transceiver, 12-pin module and a general purpose 16-bit flash microcontroller. It contains three different sensors mounted on its circuit, one for humidity, another one for light intensity and a third one for temperature. When the wireless sensor board receives power from the super capacitor, it wakes up its microcontroller to perform measurements using the mentioned sensors, then sends gathered data to the sink node in a form of data packet. The wireless sensor board also transmit data related to the RF power received, and DC power converted.

The configuration for the measurements of the power transfer and energy harvesting system is shown in Fig.8. Measurements were carried out in an indoor environment with a fixed transmitter and a movable harvesting receiver

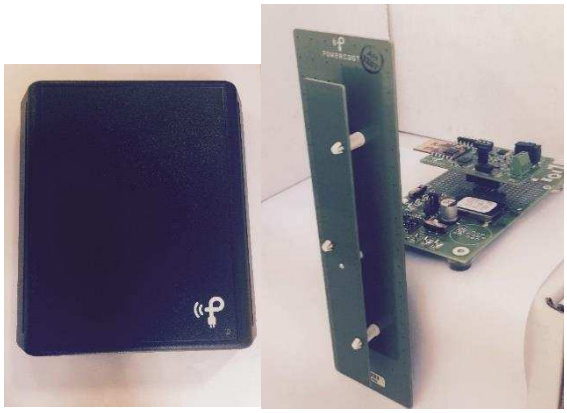

Fig. 26 Main units of the lifetime Power® Energy Harvesting Development Kit: (a) TX91501 transmitter (b) receiving energy harvesting and wireless sensor module

Fig.27. Power transfer and energy harvesting set up

Fig.28 shows the RF power harvested and DC power converted by the module from 1 to 8.5m. In general, the graph of power versus distance follow an exponential decay, with some fluctuations due to the nature of the indoor environment. The average RF power received and DC power converted by the silver ink antenna was about 25% lower than the copper antenna. The maximum distance of operation was about the same for both antennas (8.5m). The available RF power at the receiver antenna was 0.15mW for silver ink and 0.19 mW for copper antenna at maximum operational range. The harvested DC power at the maximum range of operation was 0.07 mW for the silver and 0.09 mW for the copper antenna. The wireless sensing board was still able to activate the sensors and send the corresponding data at 8.5m.

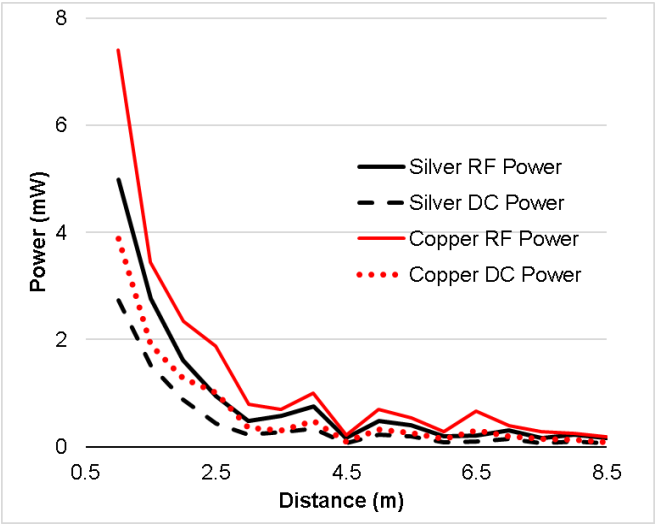

Fig. 28 Harvested RF and converted DC power for the Inkjet printed, and copper antennas

Conclusion:

This chapter dealt with the measurements conducted in the labs and in which the results of the simulation were compared with the results of the simulation results and the explanation and a justification for the variations were given for every experiment.

The chapter initially dealt with the experiment involving the measurement of received voltage using a powered signal generator and the apparatus was set up in the plain-wave chamber. The various factors were then varied and the output voltages were then measured to analyse the effect of the variation on the output voltage. The first test which was primarily done to examine the amount of voltage received was conducted in which the antenna and the RF signal generator were placed to form a system and the distance between the signal generator horn antenna and the receiver slot antenna were varied to determine the effect of distance on the antenna output. The test concluded that the received voltage reduced when the distance was increased as expected.

When the frequency was varied, the output voltage showed mixed results. The output voltage kept on increase as the frequency was increased. It attained a peak at 2.43 GHz and from thereon, the voltage gradually started decreasing showing a match at the frequency.

Varying the input power through the RF signal generator gave rather simple and expected output. The output voltage increased with the increase in the input power in nearly a linear way.

Measurements with an added 100-Ω resistor showed the same pattern as the test with varying the frequency. The peak value however increased slightly at the matching frequency.

Changing the width of the slot resulted in a decrease in matching as the slot size was reduced due to the change in the actual matching of the slot. This showed that the current size of the slot was the optimum one to obtain the best results. Increasing the size was not possible due to the fabrication being done beforehand.

Experiments with the matching network were done in two parts: as field measurements and as the tests in the plain-wave chamber. The field measurement tests revealed that slot antenna with coaxial cable yielded the best output voltage. The received voltage curve showed a gradual non-linear decline as the distance from the transmitter WiFi access source router increased. The maximum distance attained to receive the voltage was up until the 3-meter mark.

When the same test was conducted in the plane-wave chamber with a controlled RF power signal generator, the antenna with an SMA connector yielded the best results. The received voltage was significantly higher than that of the field-measurement tests due to the reason that the transmitted

power in this test was higher. Although the maximum distance attained was more than 3 meters, all the antennas, despite showing dissimilar patterns till the 2.5-meter distance mark, showed rather similar and nearly equal results from thereon till the 3-meter mark and even beyond. The results will thus be discussed with minute details in the coming chapter which deals with the conclusion of the whole thesis.

Inkjet printing using inexpensive printers with silver nanoparticle ink cartridges can be employed to fabricate planar slot antennas. The characteristics of these antennas allow for resistance values on the surface of the metallic layers to be relatively low. Capacitive coupling pads permit the feeding of the antenna without damaging the printed metallic layers. These types of antennas are able to operate in an indoor power transfer and energy harvesting environment. The maximum distance achieved for this application is about the same than it is for a copper antenna fabricated using standard etching methods. However, the RF power harvested and DC power converted is about 25% lower than for the copper antenna. The main advantage of the silver ink printed slot antennas is that they can be fabricated easily, and are still able to operate reasonably in an energy harvesting environment.

References:

[1] V. J. Logeeswaran, et al., "Harvesting and Transferring Vertical Pillar Arrays of Single-Crystal Semiconductor Devices to Arbitrary Substrates," Electron Devices, IEEE Transactions on, vol. 57, pp. 1856-1864, 2010.

[2] T. Le, K. Mayaram and T. Fiez, "Efficient Far-Field Radio Frequency Energy Harvesting for Passively Powered Sensor Networks", IEEE J. Solid-State Circuits, vol. 43, no. 5, pp. 1287-1302, 2008.

[3] M. Pinuela, P. Mitcheson and S. Lucyszyn, "Ambient RF Energy Harvesting in Urban and Semi-Urban Environments", IEEE Transactions on Microwave Theory and Techniques, vol. 61, no. 7, pp. 2715-2726, 2013.

[4] H. Jabbar, Y. Song and T. Jeong, "RF energy harvesting system and circuits for charging of mobile devices", IEEE Transactions on Consumer Electronics, vol. 56, no. 1, pp. 247-253, 2010.

[5] Y. Kawahara , “Instant Inkjet Circuits: lab-Based Inkjet Printing to Support Rapid Prototyping of UbiComp Devices,” Proc. 2013 ACM Int’l Joint Conf. Ubiquitous Computing (UbiComp 13), pp. 363–372, 2013.

[6] R. Vyas et al., “Paper-based RFID-enabled wireless platforms for sensing applications,” IEEE Trans. Microw. Theory Tech., vol. 57, no. 5, pp. 1370–1382, May 2009.

[7] S. Khan, I. Iorenzelli and R. Dahiya, "Technologies for Printing Sensors and Electronics Over large Flexible Substrates: A Review", IEEE Sensors J., vol. 15, no. 6, pp. 3164-3185, 2015.

[8] S. Kim, R. Vyas, A. Georgiadis, A. Collado, M. M. Tentzeris, “Inkjet-printed RF energy harvesting and wireless power trasmission devices on paper substrate,” Digest of EuMC, pp. 983-986, Oct. 2013.

[9] J. C. Batchelor, E. A. Parker, J. A. Miller, V. Sanchez-Romaguera, and S. G. Yeates, “Ink jet printing of frequency selective surfaces,” Electron. lett., vol. 45, no. 1, pp. 7–8, Jan. 2009.

[10] Sangkil Kim, Yu-Jiun Ren, Hoseon lee, A. Rida, S. Nikolaou and M. Tentzeris, "Monopole Antenna With Inkjet-Printed EBG Array on Paper Substrate for Wearable Applications", IEEE Antennas Wirel. Propag. lett., vol. 11, pp. 663-666, 2012.

[11] G. Shaker, S. Safavi-Naeini, N. Sangary and M. Tentzeris, "Inkjet Printing of Ultrawideband (UWB) Antennas on Paper-Based Substrates", IEEE Antennas Wirel. Propag. lett., vol. 10, pp. 111-114, 2011.

[12] W. Whittow, A. Chauraya, J. Vardaxoglou, Yi li, R. Torah, Kai Yang, S. Beeby and J. Tudor, "Inkjet-Printed Microstrip Patch Antennas Realized on Textile for Wearable Applications", IEEE Antennas Wirel. Propag. lett., vol. 13, pp. 71-74, 2014.

[13] A. Chauraya, J. Tudor, J. Vardaxoglou, R. Torah, Y. li, W. Whittow, S. Beeby and K. Yang, "Inkjet printed dipole antennas on textiles for wearable communications", IET Microwaves, Antennas & Propagation, vol. 7, no. 9, pp. 760-767, 2013.

[14] Y. Kawahara, S. Hodges, N. Gong, S. Olberding and J. Steimle, "Building Functional Prototypes Using Conductive Inkjet Printing", IEEE Pervasive Comput., vol. 13, no. 3, pp. 30-38, 2014.

[15] Powercast Corp., http://www.powercastro.com (Accessed 13/06/2016)

[16] J. Kraus and R. Marhefka, Antennas for all applications. New York: McGraw-Hill, 2002.

Chapter 9

Conclusion

In this thesis, the modelling of an energy harvesting system for domestic environment was presented. The description of the research and the steps taken during the work were presented along with the theoretical and literature background to back the assumptions and considerations made. Along with the simulation as well as the experimentations, the designing required an estimation process for the selection of the equivalent circuit designing of the antenna.

The research began with the literature survey which was primarily focused on finding out the suitable antennas for the purpose of energy harvesting. The critical factors for picking the antennas such as the matching frequency, the bandwidth, the harvested power, the aperture size, design complexity and properties of the material used in fabrication to name a few. The antennas which demonstrated the best results in the criteria above were slot antenna, UWB antenna and dipole antenna. All the three antenna showed a very good match at the 2.4 GHz frequency. That frequency was selected due to the fact that the 2.4GHz band of frequency was available in abundance for the purpose of energy harvesting and field measurement analysis tests. Although the bandwidth of the dipole antenna was relatively lower than that of the slot antenna and the UWB antenna for the energy harvesting applications, the matching at the frequency was slightly more prominent than that of the UWB antenna. The materials that were most commonly used were copper mylar for etching and silver ink for inkjet printing.

As the antenna were finalised, the antennas matching at the desired frequency of 2.4 GHz were designed and simulated in CST and the design was then fine-tuned to improve the results. The S_{11} of the antenna was simulated by using 50-Ω impedance match. The S_{11} parameter results were then subject to a parametric analysis to find out the best and the most suitable dimensions for every design. The main criterion for a parametric analysis for the slot antenna were the variation in the length and the width of the aperture as well as the height of the slot along with its length. The various dimensions were varied by factors of millimetres and their variation were compared with another to pick the best

available dimensions for the antennas. For the UWB antennas, the width of the feedline and the height of the ground planes were varied and were compared in the same way.

The defined the goals which were set while exploring the antennas and the expectations which were present from every antenna which was evaluated. The requirements of a wideband antenna working at the WiFi frequency and with a very good matching at 2.4 GHz or nearest to that was discussed.

Dipole antennas were studied. A half-wave dipole antenna was designed and simulated. The S_{11} simulations results of the half-wavelength dipole antenna had a significantly good matching of -31.67 dB at 2.41 GHz. The 3D farfield radiation pattern demonstrated the omnidirectional properties of the antenna and the directive gain of the antenna was simulated to be 2.357 dBi. However, due to a very narrow bandwidth and balun properties of the antenna, it was not very suitable for the purpose of energy harvesting.

Then the Ultra-Wide-Band (UWB) antennas were discussed. The main advantage of using a UWB antenna as the name suggests, was a very wide band of below -10dB across the frequency band. The matching was -27.14 dB at 2.4 GHz and went as low as -33 dB for higher frequencies. The surface currents distributions at 2.4 GHz and 5.4 GHz were demonstrated. The distribution patterns at 2.4 GHz were more even and uniform across the inner edges of the feedline and the ground planes. At 5.4 GHz however, the distribution wasn't as even and uniform as it was for 2.4 GHz due to more interactions within the frequencies. The 3D farfield results denoted the directional properties of the antenna with a directive gain of 2.723 dBi achieved. The omnidirectional properties along the XZ plane radiation pattern were observed with a lobe magnitude of 2.82 dBi.

The third type of design dealt with was the slot antenna. A λ/2 wavelength slot antenna and λ-wavelength slot antenna were considered. Two λ/2 antenna were compared which were same in dimensions but the positioning of the port was different. In the first design, the port was placed in the middle of the slot and in the second one, the port was moved to the side of the slot. The design in which the port was displaced by 25.55 mm from the center of the slot depicted a matching of -21.18 dB at 2.415 GHz. The middle positioning of the slot gave lower match at the desired frequency. A parametric analysis was performed for the antenna and the main criteria, the length of the aperture and the height of the antenna aperture were varied and the results were thus examined which were on display. The variation in matchings and positioning of a match with changes followed a familiar pattern. Reducing the height reduced the quality of the match and shifted the matching to the left and the right of the desired frequency. Increasing the height shifted the match to the right of the desired frequency hence giving a match at a higher frequency and decreasing the height resulted in a

match shifting towards the left of the desired frequency at a lower frequency value. In case of length, the analysis followed the pattern of improved and unimproved match with the changes in frequency.

Chapter 5 dealt with the development of an equivalent circuit for the antenna. It first gave guidelines of how to export the CST results of the antenna and then calling it into ADS. The antenna called in ADS was used as an ADS component and its real and imaginary impedances were compared in time domain. The antenna was then turned into an equivalent circuit using simple lumped components so that it could be implemented in further usage. A circuit was assumed and refined which was estimated to obtain its peaks at 1.25 GHz and 4.75 GHz respectively according to the patterns revealed by the simulations of time domain. To improve the functionality of the circuit, the lumped components were put into tuning and every component was individually tuned. The results drastically improved and the designing of the equivalent circuit of the antenna with a fully optimised design, the lumped components were used in optimisation mode and the goals were define to maximise the difference between real-part of the input and the output impedances and to zero the resultant of the imaginary-part of the impedances. The equivalent circuit was fully optimised using optimiser and a block-component was created for the equivalent circuit to be used in the further stages of the design. Usage of an equivalent circuit was a novel work which arose and which was implemented in this thesis. The usage of the equivalent circuit design helped in obtaining the realistic outputs in ADS using the rectifier chip.

Designing of the rectifier microstrip chip and the realisation of the simulation into hardware was handled in the next chapter. The chapter started off with the implementation of the antenna equivalent circuit which was dealt in chapter before that one and continued to the designing of the matching network. The primary goal of the matching network was to rectify the incoming RF and AC voltage and convert it into DC. A 3rd order low pass Butterworth filter was implemented due to its characteristic features of flat response in the pass-band and steep attenuation at the cut-off frequency. The rectification was achieved using 3 microstrip lines in a combination to obtain a 270^{o} phase shift which were mounted on a duroid substrate named RO3010 manufactured By Roger® along with the designed filter. The schematic was simulated and after tuning and optimizing the values, the circuit was finalised.

The finalised values were then adjusted to their nearest commercially available values and the design was then put into layout mode. A layout was generated using ADS and the tracks and connection points were made after readjusting the positioning of the microstrips and the filter components. The design was then fabricated and the measurements were then conducted.

The 8th chapter dealt with the measurements conducted in the labs and in which the results of the simulation were compared with the results of the measurement and the explanation and a justification for the variations were given for every experiment.

The chapter initially describes the fabrication and the fabrication techniques used in this thesis. It then continued the experiment involving the measurement of received voltage using a powered signal generator and the apparatus was set up in the plane-wave chamber. The various factors were then varied and the output voltages were then measured to analyse the effect of the variation on the output voltage. The first test which was primarily done to examine the amount of voltage received was conducted in which the antenna and the RF signal generator were placed to form a system and the distance between the signal generator horn antenna and the receiver slot antenna were varied to determine the effect of distance on the antenna output. The test concluded that the received voltage reduced when the distance was increased as expected.

When the frequency was varied, the output voltage showed mixed results. The output voltage kept on increase as the frequency was increased. It attained a peak at 2.43 GHz and from thereon, the voltage gradually started decreasing showing a match at the frequency.

Varying the input power through the RF signal generator gave rather simple and expected output. The output voltage increased with the increase in the input power in nearly a linear way.

Measurements with an added 100-Ohm resistor showed the same pattern as the test with varying the frequency. The peak value however increased slightly at the matching frequency. The test was replicated for the 25, 50 and 75 Ω resistors and it was found that the maximum voltage was received with the 100Ωresistor.

Changing the width of the slot resulted in a decrease in matching as the slot size was reduced due to the change in the actual matching of the slot. This showed that the current size of the slot was the optimum one to obtain the best results. Increasing the size was not possible due to the fabrication being done beforehand.

The comparison between the simulation and the measurement results of the antennas was presented . The 3 major antennas were depicted along with their S_{11} simulation and measurement characteristics. The slot antenna with just the SMA connector gives nearly an inch perfect match at the frequency of 2.43 GHz. The matching distorts at higher frequencies due to interferences and various noises available in the system. The slot antenna with the coaxial cable along with the SMA connector displayed a -17 dB match at the frequency as compared to the -21 dB match in the simulation. The matching also showed some significantly drastic improvement and a shift towards the

lower frequency. This was due to the fact that the considerations of the coaxial cable along with the SMA connector could not be made in the CST simulations. The UWB antenna however showed more ripples and higher variations from the simulation results that was due to the fact that the connection and the soldering of the SMA connector on the ground planes as well as the feed line changed the dimensions of the conductive areas which were not taken into account while performing the simulations in CST.

Experiments with the matching network were done in two parts: as field measurements and as the tests in the plane-wave chamber. The field measurement tests revealed that slot antenna with coaxial cable yielded the best output voltage. The received voltage curve showed a gradual non-linear decline as the distance from the transmitter WiFi access source router increased. The maximum distance attained to receive the voltage was up until 3 meters.

When the same test was conducted in the plane-wave chamber with a controlled RF power signal generator, the antenna with an SMA connector yielded the best results. The received voltage was significantly higher than that of the field-measurement tests due to the reason that the transmitted power in this test was higher as well as the fact that this test was conducted in a much more controlled and protected environment. Although the maximum distance attained was more than 3 meters, all the antennas, despite showing dissimilar patterns till the 2.5 meter distance mark, showed rather similar and nearly equal results from thereon till the 3 meter mark and even beyond.

Inkjet printing using inexpensive printers with silver nanoparticle ink cartridges could be employed to fabricate planar slot antennas on which a paper arose which was presented at the end of the chapter. The characteristics of those antennas allowed for resistance values on the surface of the metallic layers to be relatively low. Capacitive coupling pads permitted the feeding of the antenna without damaging the printed metallic layers. These types of antennas were able to operate in an indoor power transfer and energy harvesting environment. The maximum distance achieved for this application was nearly the same as they were for a copper antenna fabricated using standard etching methods. However, the RF power harvested and DC power converted were about 25% lower than for the copper antenna. The main advantage of the silver ink printed slot antennas was that they could be fabricated easily, and were still able to operate reasonably in an energy harvesting environment.

In this thesis, the work on antennas and RF energy harvesting devices and chips for office or domestic environments was presented. The antenna design was simulated using CST microwave studio software and after conducting some preliminary parametric tests, the designs were fine tuned for the best simulation results. The equivalent circuit and the matching network for the antenna as well as the rectification chip were designed in the Agilent ADS software where the circuitry as well as the 3D

visualisation of the chip was conducted. Once the chip was designed in ADS, it was fabricated and was used with the antennas for the tests in a common domestic environment and the results with various antennas were compared for the magnitude they attained as well as the maximum distance up until which the harvesting of the transmitted power was feasible with a given antenna.

The research work may be further extended into harvesting and harnessing a single or an array of RF energy spectrum in the future. Introduction of an antenna array and designing of the matching circuit within the Mylar antenna with the matching network and microstrips on the backside of it. The design may also include various printing techniques such as 3D and Inkjet printing and can be tested to be used in a domestic environment patch-sheet for a consistent energy harvesting unit to evaluate the amount of powers received for further analysis.